

CALORIMETRIC POWER CALIBRATION AND SOURCE EFFECTS IN
THE KANSAS STATE UNIVERSITY TRIGA MARK II NUCLEAR REACTOR

by

EDWARD ALBERT HECKMAN, JR.

B.S., Pennsylvania State University, 1966

A MASTER'S THESIS

submitted in partial fulfillment of the
requirements for the degree

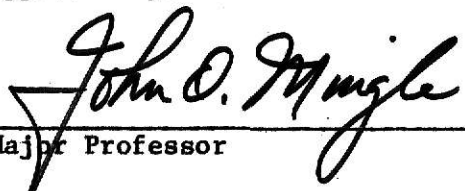
MASTER OF SCIENCE

Department of Nuclear Engineering

KANSAS STATE UNIVERSITY
Manhattan, Kansas

1973

Approved by:


Major Professor

LD
2668
T4
1973
H4
C.2
Doc.

TABLE OF CONTENTS

	Page
LIST OF TABLES	v
LIST OF FIGURES	vii
Chapter	
1.0 INTRODUCTION	1
2.0 DESCRIPTION OF THE TRIGA MARK II NUCLEAR REACTOR AT KANSAS STATE UNIVERSITY	3
3.0 TEMPERATURE DISTRIBUTION IN THE KANSAS STATE TRIGA REACTOR AS A FUNCTION OF SPACE AND TIME	12
3.1 TEMPERATURE DISTRIBUTION IN THE CORE	12
3.1.1 DISTRIBUTION OF POWER DENSITY IN THE FUEL	13
3.1.2 FUEL AND CLADDING TEMPERATURE DISTRIBUTION	14
3.1.3 THE COOLANT TEMPERATURE DISTRIBUTION	17
3.1.4 COMPUTER SOLUTION OF TEMPERATURES IN THE CORE	19
3.1.4.1 STEADY-STATE SOLUTION (CORTSS)	19
3.1.4.2 DETERMINATION OF EMPIRICAL PARAMETERS	20
3.1.4.3 TIME DEPENDENT SOLUTION (CORT)	29
3.2 TEMPERATURE DISTRIBUTION IN THE POOL	35
3.2.1 HEAT FLOW INTO THE POOL FROM THE CORE	37
3.2.2 A MODEL TO DETERMINE THE TEMPERATURE DISTRIBUTION IN THE POOL	38
3.2.2.1 HEAT SOURCE	38
3.2.2.2 FORMATION OF THE CHIMNEY	41
3.2.2.3 FLOW DOWN THE SIDES	42
3.2.2.4 FULLY ESTABLISHED FLOW	44
3.2.2.5 NUMERICAL SOLUTION TO THE POOL TEMPERATURE DISTRIBUTION (POOLT)	46

3.3	RESULTS AND CONCLUSIONS	48
4.0	CALORIMETRIC POWER CALIBRATION	52
4.1	MONITORING THE POWER LEVEL	52
4.2	CALORIMETRIC POWER CALIBRATION	53
4.3	MEASUREMENT OF THE TEMPERATURE GRADIENT	57
4.3.1	TECHNIQUES FOR MEASUREMENT	57
4.3.2	MEASUREMENT OF THE TEMPERATURE GRADIENT USING THERMISTORS	58
4.3.2.1	DESCRIPTION OF THE EQUIPMENT	60
4.3.2.2	EXPERIMENTAL PROCEDURE	60
4.3.2.3	ANALYSIS OF THE RESULTS	66
4.3.3	PROBE LOCATION	66
4.4	CONCLUSIONS	74
5.0	REACTIVITY OF REACTOR SOURCES	83
5.1	ANALOG SIMULATION OF THE REACTOR	83
5.2	EXPERIMENTAL DETERMINATION OF SOURCE PARAMETERS	91
5.2.1	STEADY-STATE DETERMINATION OF SOURCE WORTH	91
5.2.2	STEADY-STATE DETERMINATION OF SOURCE STRENGTH	92
5.2.3	SOURCE INSERTION EXPERIMENTS	100
5.3	DETERMINATION OF SOURCE EFFECTS USING ANALOG SIMULATION	113
5.3.1	STEADY-STATE OPERATION IN THE PRESENCE OF THE SOURCE	113
5.3.2	SOURCE INSERTION AND REMOVAL FROM A STEADY-STATE REACTOR	116
5.4	CONCLUSIONS	118
	ACKNOWLEDGEMENTS	118A

REFERENCES	119
----------------------	-----

APPENDICES

A. Analog Simulation of a Reactor	121
B. Least Squares Fitting of Data to a Straight Line	133
C. Numerical Solution of the Time and Space Dependent Temperature Distribution in the Fuel and Cladding	138
D. Natural Convection Heat Transfer from a Vertical Cylinder . . .	146
E. Experimental Temperature Distribution in the Pool	152
F. POWCAL	162

LIST OF TABLES

Table	Page
3.1 Radial Temperature Distribution across the Core for Various Heat Generation Distributions and Contact Resistances	21
3.2 Determination of an Improved Guess for the Heat Generation Distribution	23
3.3 Bulk Water Temperature out of the Core (from CORT and CORTSS)	39
3.4 Heat Flow out of the Core (from CORT and CORTSS)	40
4.1 Calculation of Equivalent Total Heat Capacity of the Reactor Vessel	56
4.2 Comparison of Electrical Temperature-Sensing Devices	59
4.3 Characteristics of the Thermistor Sensor and Probe	61
4.4 Characteristics of the Automatic Switchbox	62
4.5 Characteristics of the Temperature Indicator	62
4.6 Characteristics of the Recording Adapter	63
4.7 Typical Results from SLOPE	70
4.8 Results from STRAT	72, 73
4.9 Analysis of Reference Data	75
4.10 Comparison of Asymptotic Slopes and "True" Slopes	76
5.1 The Relationship between Potentiometer Setting and Reactivity for Potentiometer #1 (Rod Simulator)	90
5.2 The Relationship between Potentiometer Setting and Source Worth for Potentiometer #2	90
5.3 The Relationship between Potentiometer Setting and Source Strength for Potentiometer #3	90
5.4 Source Worth Data from Steady-State Experiments	93, 94
5.5 Analysis of Variance for Source Worth Data	96
5.6 Combined Source Worth Data from Steady-State Experiments	97

5.7	Source Strength Data from Steady-State Experiment at 0.01 Watt	99
5.8	Zero Power Source Insertion Data	99
5.9	Analysis of Variance for Source Strength Data	101
5.10	Results of Least Squares Fit of Source Insertion Data	107
5.11	Analysis of Variance for Source Worth Computations	111
5.12	Power Dependent Contribution to Source Strength	114
5.13	Reactivity Required to Achieve Steady-State Operation in the Presence of the Source	114
A.1	RC Values in Unit Type 2.457 Based on U-235	126
A.2	Options for Neutron Generation Time and Maximum Reactivity . . .	126
A.3	Relationship between Potentiometer Settings and Reactivity for Potentiometers #1 and #2	129
A.4	Relationship between External Voltage and Effective Neutron Density of the External Source	129
E.1	Parameters for the Pool Temperature Distribution Experiment . .	154
E.2	Typical Results from DATAFIX	156

LIST OF FIGURES

Figure		Page
2.1	The Reactor Pool and Equipment in the Pool	5
2.2	Cross-Section of the Lower Reactor Pool	6
2.3	Fuel Loading #11	8
2.4	The Reactor Core (Central Thimble Removed)	9
3.1	Radial Temperature Distribution across the Core	22
3.2	Interpolation of the Contact Resistance and Heat Generation Distribution from CORTSS Trial Data	24
3.3	Vertical Temperature Distributions in the Core (Results from CORTSS)	26
3.4	Film Thickness, Power Density and Heat Flow as a Function of Vertical Position (Results from CORTSS)	27
3.5	Radial Temperature Distributions in the Core (Results from CORTSS)	28
3.6	Computational Procedure for CORT	30
3.7	Temperature Profile in the Fuel, Cladding and Coolant Film (Results from CORT)	32
3.8	Temperatures at Various Locations in the Fuel, Cladding and Coolant Film as a Function of Time	33
3.9	Film Thickness and Heat Flow at Various Fuel Heights as a Function of Time	34
3.10	The Temperature Rise on the Center-Line of the Fuel in a B-Ring Element	36
3.11	Computational Procedure for POOLT	47
3.12	Results of POOLT Compared to Experimental Data (Short Times)	49
3.13	Results of POOLT Compared to Experimental Data (Long Times)	50
4.1	Experimental Set-Up for the Temperature Gradient Measurement	64
4.2	Temperature Rise at Various Locations During 100 kw Steady-State Operation	67

4.3	The Temperature Gradient During 100 kw Steady-State Operation (from SLOPE)	69
4.4	Cross-Section of the Reactor Vessel Showing the "Best" Region for Probe Location	77
4.5	Graphical Determination of the Power Level from Calorimetry Data	79
4.6	Determination of the Power Level from Calorimetry Data Using POWCAL	80-82
5.1	Analog Simulation of the KSUTM II Reactor	86
5.2	Comparison of Test Curves and Manufacturer's Data	88
5.3	Expanded Reg Rod Calibration Curve	95
5.4	Zero Power Source Insertion Data	104
5.5	Zero Power Source Insertion Data	105
5.6	Least Squares Fit of Zero Power Source Insertion Data	108
5.7	Least Squares Fit of Zero Power Source Insertion Data	109
5.8	Least Squares Fit of Zero Power Source Insertion Data	110
5.9	Reactivity Required to Maintain Steady-State Operation (Data from Analog Simulator)	115
5.10	Source Insertion and Removal from the Reactor at Steady-State (Data from Operational Tests on the KSUTM II Reactor)	117
A.1	Analog Simulation of a Reactor with a Removable Source	122
A.2	Operational Relays on the Reactor Simulator Unit	130
C.1	Typical Control Volumes for the Numerical Solution of Temperatures in the Fuel and Cladding	139
D.1	Typical Natural Convection Film around a Fuel Element	148
E.1	Grid Positions for the Temperature Distribution Experiment	153
E.2	Temperature Distribution in the Reactor Pool During 100 kw Steady-State Operation	157
E.3	Temperature Distribution in the Reactor Pool During 100 kw Steady-State Operation	158

E.4	Temperature Distribution in the Reactor Pool During 100 kw Steady-State Operation	159
-----	------------------------------------------------------------------------------------------------	-----

1.0 INTRODUCTION

The TRIGA reactor at Kansas State University first became critical in March 1962. Since that time many operations have been established as standard operating procedures. The impetus for this paper was derived from the need for improvement of two standard operating procedures.

The first improvement involves the procedure for power calibration of the reactor. Calibration of the ion chamber readouts in terms of thermal power output of the reactor has always been accomplished by a calorimetric technique. This technique involves the measurement of pool water temperature as a function of time. The procedure used to accomplish this measurement is awkward and slow and the results achieved have been of dubious precision. Unfortunatley, here at Kansas State University, no work has been done to establish the worth of this procedure in accomplishing its intended function, namely, indicating the operating power of the reactor. A new technique, utilizing solid state temperature sensing devices, has been established. The new operation is more easily accomplished and gives results with much higher precision than the old technique. With the aid of an analytic model the results from the calorimetric technique are shown to be indicative of the actual thermal power output of the reactor.

The second area of study involves source effects. Part of the standard start-up procedure for the Kansas State University TRIGA Mark II (KSUTMII) reactor has been to find zero power criticality at the beginning of each operating day. This has been done cognizant of some source effects on criticality but without the knowledge of how these effects manifest themselves. An experimental and theoretical study of the dynamic effects of the source in the KSUTMII reactor has been accomplished. As a result of this work

a technique for the determination of zero power criticality in the presence of the source is suggested.

2.0 DESCRIPTION OF THE TRIGA MARK II REACTOR AT KANSAS STATE UNIVERSITY

The nuclear reactor at Kansas State University is a TRIGA Mark II reactor manufactured by the General Atomics Corporation, now Gulf General Atomics Corporation. The TRIGA is a low power, experimental, swimming pool type reactor, designed primarily for training, research, and neutron irradiation. The complete reactor system is described in reference [12]. The components pertinent to the research described in this paper are described in detail here.

The reactor pool is a right circular cylinder approximately 6.5 feet in diameter by 20.5 feet deep. The pool walls are constructed of concrete shielding ranging from 3 to 8 feet thick. The inside surfaces of the pool are lined with a 0.25 inch aluminum liner. The water level of the pool is maintained at 20 feet with distilled water which acts as both coolant and moderator. In addition to this water, the core, reflector, ion chambers, and several irradiation facilities occupy portions of the volume of the pool. The total pool volume is 664 cubic feet. However the core (about 30% of the volume of the core is water), reflector, and other reactor components displace 47 cubic feet, leaving 617 cubic feet or 4620 gallons of water in the pool.

The primary water is cooled in a closed loop. The water leaves the pool through a 2.5 inch aluminum pipe with the intake 3 feet below the surface of the water in the pool. It then is pumped through a six-pass heat exchanger. The cooled water is returned to the pool through a 2.5 inch aluminum line with a diffuser on the open end such that the inlet water is distributed across the top of the core. The normal flow rate of the primary water is

120 gallons/minute. Of this primary flow 10 gallons/minute by-pass the heat exchanger and flow through a clean-up loop consisting of a particulate filter and an ion exchange column. Also in this clean-up loop is a water monitor box which contains instrumentation to monitor the temperature, conductivity, and activity of the primary water. The secondary water is softened city water. This secondary water passes once through the heat exchanger and is cooled in a small cooling tower.

A complete description of the position of the reactor components in the pool can be determined from Figures 2.1 and 2.2. The reactor core is a cylinder approximately 18 inches in diameter by 24 inches high. A concentric 12 inch thick graphite ring is used as a radial reflector. Top and bottom graphite reflectors are manufactured as an integral part of the fuel elements. The core is composed of individual fuel and graphite elements in a closely packed array. The elements are seated in the bottom grid plate which has 90 counter-sunk holes into which the bottom fixture of the elements sit. The elements are positioned at the top of the top grid plate which has 90 corresponding 1.505 inch holes through which elements can be loaded into, and unloaded from, the core. Both grid plates are supported by the reflector. The reflector in turn is bolted to a four legged aluminum table which positions the bottom of the core about 2 feet from the bottom of the pool.

The bottom grid plate is a 0.75 inch diameter aluminum plate. The plate is bolted to six L-shaped flanges welded to the bottom of the reflector. Besides the 90 seating holes, the bottom grid plate has one 1.51 inch hole in the center for positioning the central thimble and 36, 5/8 inch holes concentric with the seating holes to allow cool water to enter the core. However most of the water probably enters the core through the 2 inch gap between the bottom of the reflector and the top of the bottom grid plate.

**THIS BOOK
CONTAINS
NUMEROUS PAGES
WITH DIAGRAMS
THAT ARE CROOKED
COMPARED TO THE
REST OF THE
INFORMATION ON
THE PAGE.**

**THIS IS AS
RECEIVED FROM
CUSTOMER.**

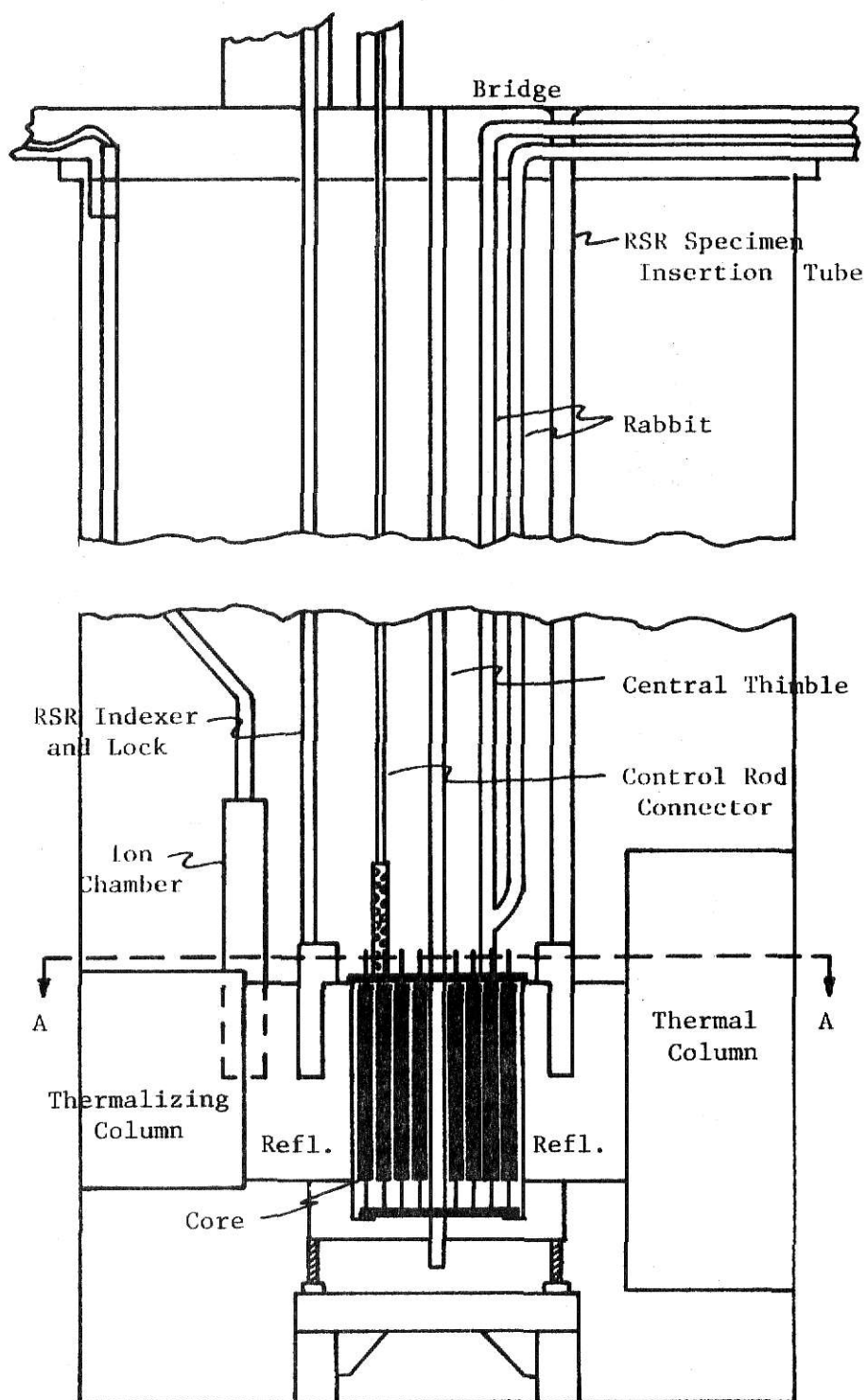


Figure 2.1 The Reactor Pool and Equipment in the Pool

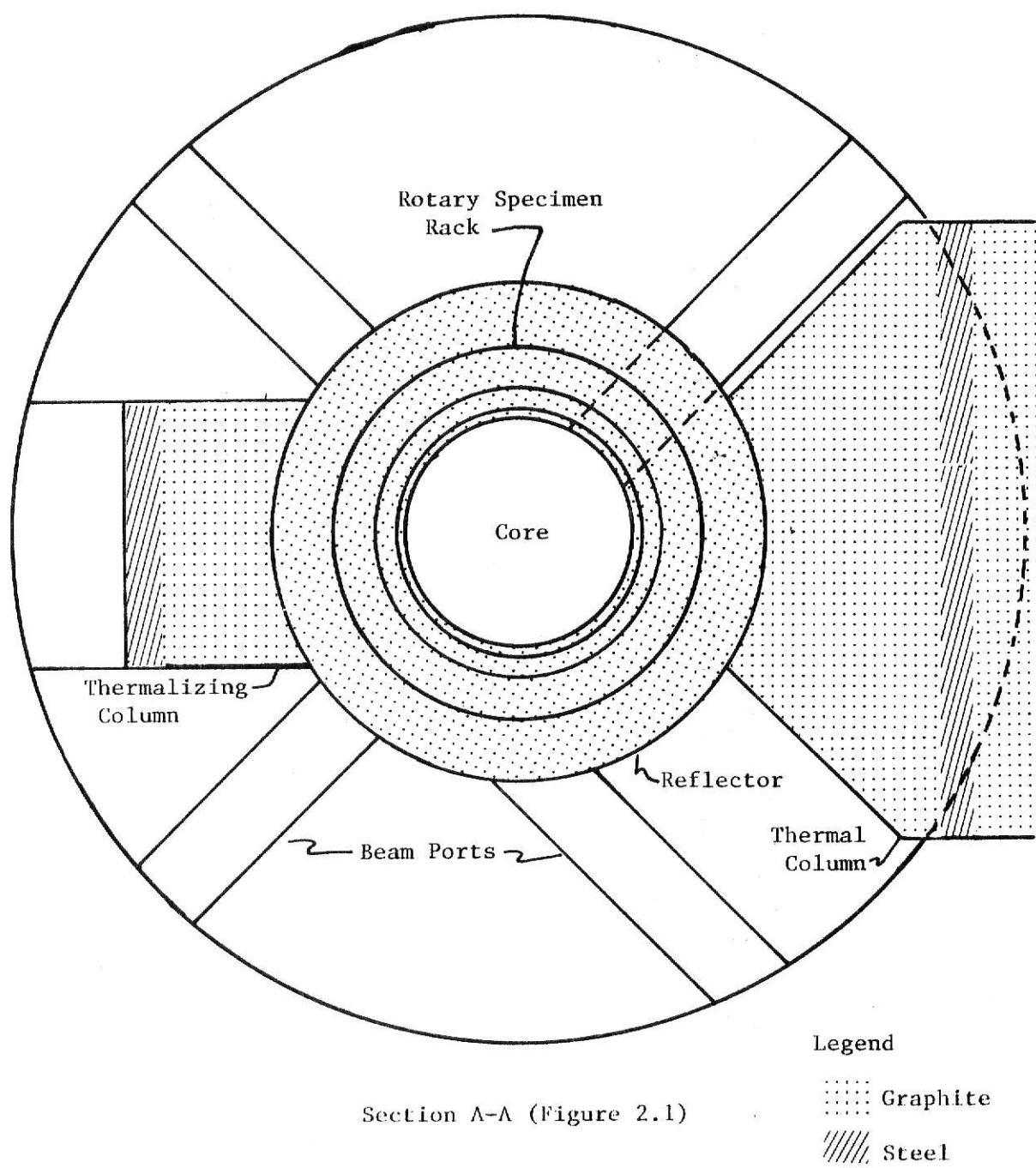


Figure 2.2 Cross Section of the Lower Reactor Pool

The top grid plate is a 0.75 inch thick, 19.44 inch diameter, aluminum plate. The plate is bolted firmly to the top of the reflector with no gaps as in the case of the bottom grid plate. The heated water leaves the top grid plate through the gaps between the 1.505 inch holes and the triangular spacers on the tops of the elements. The nominal clearance between the tips of the triangular spacer and the hole in the grid plate is 0.029 to 0.040 inches. Also a 1.515 inch hole for positioning the central thimble is provided in the center of the top grid plate.

The 91 locations in the core are loaded with either fuel elements, graphite dummy elements, control rods, the source, the central thimble, or the rabbit. All these components are movable and a record is kept of the position of each component. To facilitate bookkeeping each configuration is assigned a number. The configuration used in this work is designated as fuel loading #11. The location of all the components in fuel loading #11 appears in Figure 2.3.

The fuel elements are 28.37 inches tip to tip. The element is a 30 mil thick aluminum can 1.48 inches in diameter and about 22 inches long with fixtures at both ends. The fixture on the bottom is designed for seating the element while the top fixture is used to handle the element. Inside the can is a section composed of uranium, 20% enriched in U-235, intimately mixed with zirconium-hydride. This fuel-moderator section is in the form of a cylinder 1.42 inches in diameter and 14 inches long. Two 4 inch long sections of graphite sandwich the fuel-moderator section. The graphite element is identical to the fuel element except the entire can is filled with graphite. A more complete description of the internal core geometry appears in Figure 2.4.

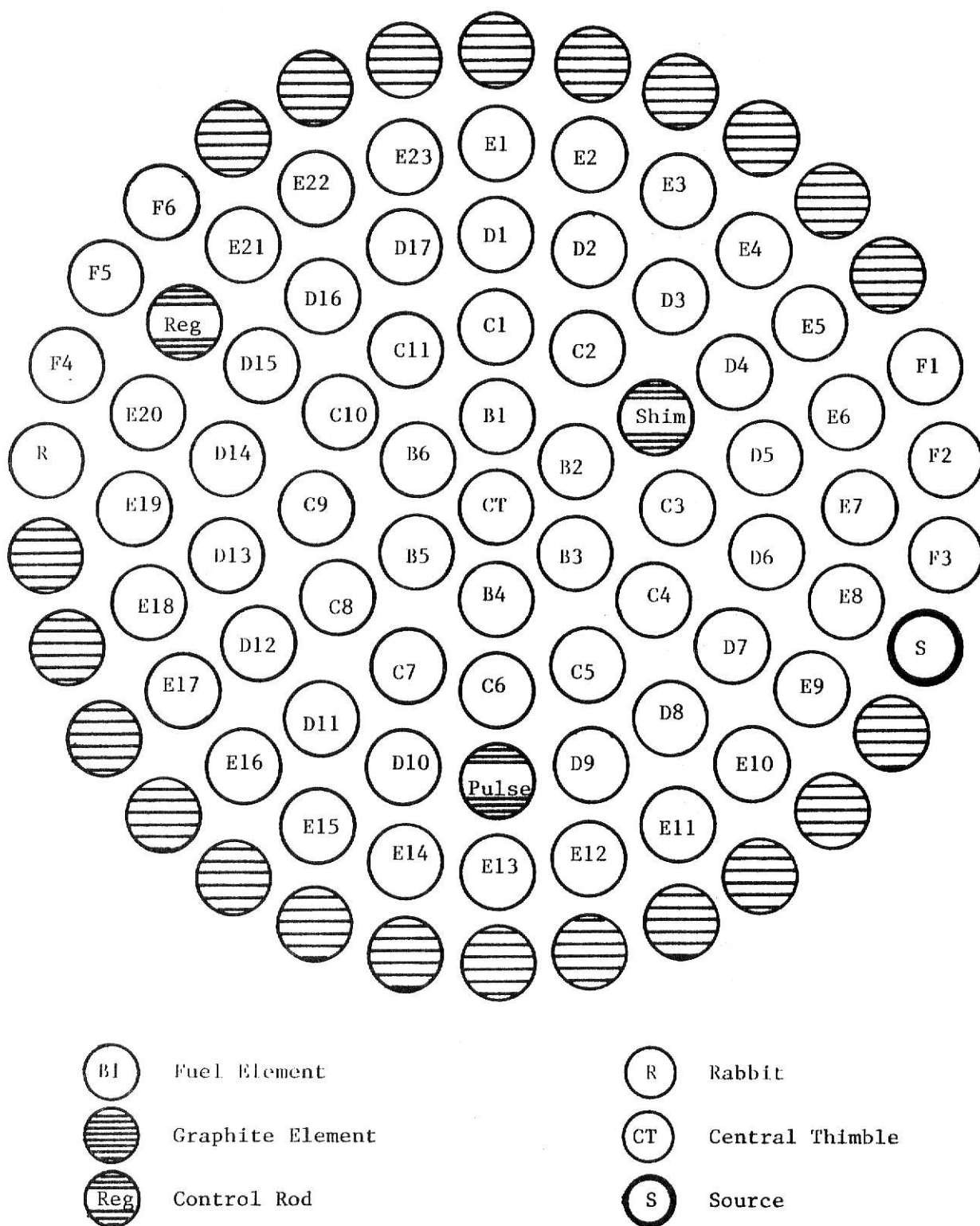


Figure 2.3 Fuel Loading #11

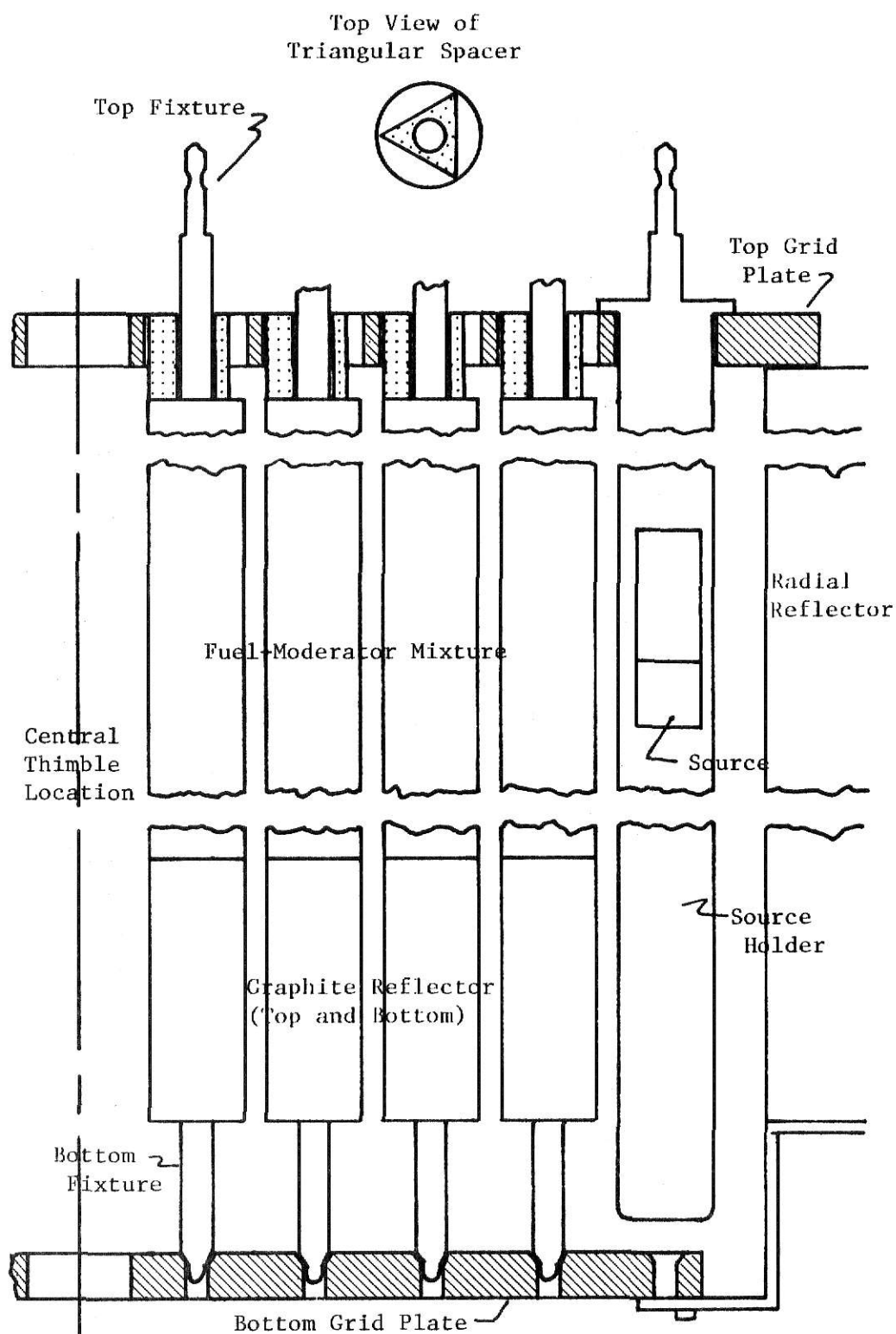


Figure 2.4 The Reactor Core (Central Thimble Removed)

There are three control rods: the reg, the shim, and the pulse or safety rod. Each rod is located in a different ring of the core and each is a different diameter. Accordingly the three rods do not have the same reactivity worth. For the core configuration corresponding to fuel loading #11 the reg rod is worth \$1.55, the pulse rod is worth \$2.06, and the shim rod is worth \$4.10. All these worths have been determined by the reactor staff using the differential positive period technique.

The rabbit is the pneumatic irradiation facility. The core terminus has an end fixture similar to that on an element therefore the rabbit can be seated in any core location but is usually positioned in the location shown in Figure 2.3. The rabbit is always filled with air and thus appears as an air void in the core.

The central thimble is an aluminum tube 1.5 inches in diameter and about 20 feet long. The tube is plugged at one end which terminates about 7-1/2 inches below the bottom grid plate. Because of vent holes in the tube near the top of the active lattice the central thimble is always filled with water.

The source holder is an aluminum rod 1.5 inches in diameter and about 25 inches long. The rod is supported in the core by a small shoulder on the upper end which rests on the upper grid plate. The lower end of the rod clears the bottom grid plate by 0.5 inch. On the top end of the source holder is a fixture similar to that on the fuel elements. In addition a wire has been placed through a hole in the top fixture and along with about 20 feet of nylon string, with one end attached to the wire and the other end fastened to the bridge, this facilitates handling of the source holder. The holder is made of two sections that are screwed together. The lower

section has a cylindrical cavity reportedly milled to nominally 1.12 inches in diameter and 3 inches deep in which the source sits. The cavity is positioned such that the source is located approximately in the vertical center of the core.

The source itself is an americium-beryllium neutron source. It contains 0.24 grams of americium and 5.0 grams of beryllium. The original source strength was 2.26×10^6 neutrons/second. The americium and beryllium are contained in a stainless steel can reported to be 0.66 inches I.D. and 0.812 inches long. This can is encapsulated in a beta shield which is 1.12 inches O.D. and 1.0 inches long. The source and source holder are depicted in Figure 2.4.

There are two salient characteristics of the KSUTMII reactor that will be discussed in this work. First the source is not inherent, but rather is a fairly bulky removable object. As such its presence, absence, removal, and insertion all affect the reactor operation. These effects are discussed in Section 5 of this work.

Second the reactor is a swimming pool type reactor with the core cooled by natural convection. Much of the heat is never extracted from the pool. Therefore the only continuous monitor on the power level is the calibrated ion chambers. The simplest and quickest technique for calibration of the ion chambers is using the calorimetric technique. This technique is discussed in Section 4 of this work.

3.0 TEMPERATURE DISTRIBUTIONS IN THE KANSAS STATE TRIGA REACTOR AS A FUNCTION OF SPACE AND TIME

Before attempting to determine the total heat output of the operating reactor, which must be accomplished for a power calibration, it is necessary to determine where in the reactor system this heat is deposited. A simple mathematical model has been designed to describe the heat transfer in the reactor pool. This model considers the reactor pool as a closed system. Because of the complicated geometry involved, it is not possible to use previously determined heat transfer correlations; therefore the model in this work is based on experimental measurements, experience, and logic.

3.1 TEMPERATURE DISTRIBUTION IN THE CORE

As a first step in the development of an analytic model of the heat transfer throughout the pool, a semi-empirical model of the heat transfer within the core is developed. The primary objective of this model is to predict the temperature distribution and heat content of the water leaving the top grid plate of the reactor core. In addition the model determines the temperature distribution in the fuel, cladding, and coolant as a function of both space and time.

The temperature distributions in the fuel and cladding are determined numerically. The temperature and velocity profiles in the coolant are determined analytically. In order to determine these distributions the following approximations are included in the model

- 1) Axial heat flow in the fuel and cladding is considered negligible.
- 2) The properties of the coolant are evaluated at the initial average pool temperature and are assumed to remain constant as the coolant is heated.

- 3) The whole system is considered to initially exist at the initial average pool temperature.
- 4) The time to reach operating power is considered negligible.
- 5) The axial power density distribution is sinusoidal.
- 6) All of the heat is deposited at the point of generation.
- 7) The power density is constant radially within each fuel element.

The model is empirical because both the contact resistance between the fuel and cladding and the radial power distribution across the core are determined by fitting the model to experimentally measured data. The calculations involved in this model use three basic operations: 1) derivation of the power density distribution in the fuel, 2) setting up the numerical analysis for determination of the fuel and cladding temperature distribution and 3) determination of the temperature and velocity profiles in the coolant.

3.1.1 DISTRIBUTION OF POWER DENSITY IN THE FUEL

Since the power density distribution is assumed to be sinusoidal in the vertical direction in the fuel element [5], the power density can be expressed as

$$Q_i(x) = Q_{\max} RQR(i)(0.6 + 0.4 \sin(\pi x/H));* \quad (\text{watts/cm}^3) \quad (3.1)$$

here, Q_{\max} is the power density at the half height of a B-ring element, H is the length of the fuel in each element, $RQR(i)$ is the relative power density in ring i , and the constants account for the flux extrapolation distance. The total heat generated in one element is

$$Q_i = \int_0^H Q_{\max} RQR(i)(0.6 + 0.4 \sin(\pi x/H)) dx \pi r_f^2$$

*Many equations throughout this work are written in standard FORTRAN style, order of arithmetic operation should be in standard FORTRAN precedence [18].

$$\text{or } Q_i = Q_{\max} RQR(i) H(0.6 + 0.8/\pi) \pi r_f^2 \quad (\text{watts}) \quad (3.2)$$

where r_f is the radius of the fuel. The total power generated in the core becomes

$$Q_T = Q_{\max} H(0.6\pi + 0.8) r_f^2 \sum_{i=B}^F RQR(i) \text{NER}(i) \quad (\text{watts}) \quad (3.3)$$

where $\text{NER}(i)$ is the number of elements in ring i . The total power generated in the core is equal to the operating power; therefore

$$Q_{\max} = \frac{Q_T}{H(0.6\pi + 0.8) r_f^2 \sum_{i=B}^F RQR(i) \text{NER}(i)} \quad (\text{watts/cm}^3) \quad (3.4)$$

The RQR 's are determined by fitting the temperature distribution predicted by the model to experimental values of the fuel center-line, half-height, steady-state temperature in each ring. A discussion of the trial and error procedure involved appears in Section 3.1.4.2.

3.1.2 FUEL AND CLADDING TEMPERATURE DISTRIBUTION

The time and space dependent solution of the temperature distribution in the fuel and cladding is complicated to solve exactly. Since the model is to be simple and fine detail of the temperature distribution is not required, a numerical solution using a fairly coarse grid network is used. The general procedure, as described in Arpaci [3], is presented in Appendix C.

The fuel is divided into cylindrical control volumes Δx high and Δr_f thick. The cladding is divided into cylindrical control volumes Δx high and r_c thick. Figure C.1 in Appendix C depicts a typical Δx section of fuel and cladding.

Using the factors defined and the nodal equations derived in Appendix C, the time dependent radial temperature distribution in a Δx section of fuel and cladding can be expressed in matrix form as

$$[T]^{n+1} = [FE][T]^n + [C] \quad (\text{deg. C}) \quad (3.5)$$

for an explicit solution; or as

$$[FI][T]^{n+1} = [T]^n + [C] \quad (\text{deg. C}) \quad (3.6)$$

for an implicit solution. In the explicit case, $[FE]$ is

$$\begin{bmatrix} 1 - K(1)/P(1) & K(1)/P(1) & \dots & \dots \\ \vdots & \vdots & \vdots & \vdots \\ K(i-1)/P(i) & \frac{1-K(i) + K(i-1)}{P(i)} & K(i)/P(i) & \dots \\ \vdots & \vdots & \vdots & \vdots \\ \dots & K(NV)/P(NL) & 1 - \frac{HG + K(NV)}{P(NL)} & HG/P(NL) \\ \vdots & \vdots & \vdots & \vdots \\ \dots & \dots & HG/P(NN) & 1 - \frac{HG + HW}{P(NN)} \end{bmatrix} \quad (3.7)$$

$[C]$ equals:

$$\begin{bmatrix} Q(1)/P(1) \\ \vdots \\ Q(i)/P(i) \\ \vdots \\ Q(NL)/P(NL) \\ HW T_o/P(NN) \end{bmatrix} \quad (\text{deg. C}) \quad (3.8)$$

Here NL is the number of internal fuel nodes, NV is the node on the fuel cladding interface, and NN is the cladding node.

For the implicit case $[FI]$ is

$$\begin{bmatrix}
 1 + K(1)/P(1) & -K(1)/P(1) & \dots & \dots \\
 -K(i-1)/P(i) & 1 + \frac{K(i) + K(i-1)}{P(i)} & -K(i)/P(i) & \dots \\
 \dots & -K(NV)/P(NL) & 1 + \frac{K(NV) + HG}{P(NL)} & -HG/P(NL) \\
 \dots & \dots & -HG/P(NN) & 1 + \frac{HG + HW}{P(NN)}
 \end{bmatrix}
 \quad (3.9)$$

Starting with all the temperatures at the ambient temperature, T_o , the temperatures at all nodes can be solved simultaneously at later times in Δt increments.

Again from the factors and nodal balances developed in Appendix C, the steady-state temperature distribution in the Δx section can be determined. The steady-state cladding temperature is

$$T_{NN} = HW/QF + T_o \quad (\text{deg. C}) \quad (3.10)$$

The fuel temperatures can be expressed in matrix form as:

$$[FSS][T] = [CSS]; \quad (\text{watts/cm}) \quad (3.11)$$

where $[FSS]$ is

$$\begin{bmatrix}
 K(1) & -K(1) & \dots \\
 -K(i-1) & K(i) + K(i-1) & -K(i) \\
 \dots & -K(NV) & HG + K(NV)
 \end{bmatrix}; \quad (\text{watts/cm deg. C})
 \quad (3.12)$$

and $[CSS]$ equals

$$\begin{bmatrix}
 Q(1) \\
 \vdots \\
 Q(i) \\
 \vdots \\
 Q(NL) + HG T_o + HG HW/QF
 \end{bmatrix} \quad (\text{watts/cm}) \quad (3.13)$$

When the fuel-cladding contact resistance, the heat transfer coefficient at the cladding-coolant interface, and the power generation distribution are known, the fuel and cladding temperatures can be determined. Equations 3.10 and 3.11 determine the steady-state temperatures. Equation 3.5 or 3.6 determines the time dependent solution.

3.1.3 THE COOLANT TEMPERATURE DISTRIBUTION

The heat is transferred out of the fuel element and into the coolant by natural convection. A derivation of the natural convection from a vertical cylinder is developed in Appendix D.

In the natural convection process all the heat is transferred from the fuel into a film of coolant concentric around the fuel element. The thickness of this film is dependent on the physical characteristics of the coolant and the outside wall temperature of the fuel element. The coolant inside the film has a temperature and velocity distribution both of which vary vertically and radially. The expressions for the temperature and velocity distributions derived in Appendix D are respectively

$$\frac{T(r,x) - T_o}{T_w(x) - T_o} = \left[\frac{r_o - r + \delta(x)}{\delta(x)} \right]^2, \quad (3.14)$$

where T_o = ambient coolant and cladding temperature,

$T_w(x)$ = fuel element wall temperature at height x ,

r_o = fuel element outside radius,

and $\delta(x)$ = film thickness at height x ;

and

$$\frac{u(r,x)}{U(x)} = \frac{r - r_o}{\delta(x)} \left[\frac{r_o - r + \delta(x)}{\delta(x)} \right]^2, \quad (3.15)$$

where

$$U(x) = \frac{g \beta \delta(x)^2 (T_w(x) - T_o)}{4\nu}, \quad (\text{cm/sec.}) \quad (3.16)$$

g = acceleration of gravity, (cm/sec^2)

β = coefficient of expansion of coolant, $(1/R^\circ)$

and ν = kinematic viscosity of coolant, (cm^2/sec) .

The film is divided into Δx sections just as is the fuel and cladding. The radial temperature and velocity profiles and the film thickness are all constant within this Δx section. From Appendix D the expression for the film thickness in the control volume at height x_i is

$$\delta(x_i)^4 = (A \delta(x_i) + C)/(r_o + 2/7 \delta(x_i)), \quad (\text{cm}^4) \quad (3.17)$$

where

$$A = B(x_i)/(T_w(x_i) - T_o)^2, \quad (\text{cm}^4) \quad (3.18)$$

$$C = 240 r_o \Delta x x_i^3 / \text{Pr Gw} \quad (\text{cm}^5)$$

$$B(x_i) = \delta(x_{i-1})^3 (T_w(x_{i-1}) - T_o)^2 (r_o + 2/7 \delta(x_{i-1})), \quad (\text{cm}^4 \text{ deg } C^2) \quad (3.18)$$

Pr = Prandtl number of coolant, and

Gw = Grashof number of coolant.

In the first control volume $B(x_1) = 0$, therefore

$$\delta(x_1)^4 = C/(r_o + 2/7 \delta(x_1)). \quad (\text{cm}^4) \quad (3.19)$$

At steady-state the expression for film thickness is the same. The general expression can be written as

$$\delta(x_i)^4 = (D/\delta(x_i) + C)/(r_o + 2/7 \delta(x_i)), \quad (\text{cm}^4) \quad (3.20)$$

where

$$D = 16 k_w^2 r_o^2 B(x_i) / Q(x_i)^2 r_f^4 . \quad (\text{cm}^6)$$

3.1.4 COMPUTER SOLUTION OF TEMPERATURES IN THE CORE

Now that the derivation of the power density distribution, compilation of the numerical analysis technique for determination of the fuel and cladding temperature distribution, and determination of the temperature and velocity profiles in the coolant have been performed, the total model can be described. In order to complete the model the temperature distribution in the fuel and cladding must be coupled to the temperature distribution in the coolant. The two are coupled by equating the heat flow out of the cladding in the control volume at x_i ,

$$q_{\text{out}}(x_i) = h_w(x_i) 2\pi r_o \Delta x (T_{\text{NN}}(x_i) - T_o) , \quad (\text{watts})$$

to the heat flow into the coolant in the control volume at x_i ,

$$q_{\text{in}}(x_i) = k_w 4\pi r_o \Delta x (T_w(x_i) - T_o) / \delta(x_i) . \quad (\text{watts})$$

It was already noted that $T_w(x_i)$ equals $T_{\text{NN}}(x_i)$. Therefore

$$h_w(x_i) = 2 k_w / \delta(x_i) . \quad (\text{watts/cm}^2 \text{ deg(C)}) \quad (3.21)$$

The final compilation of the core temperature model is two computer programs CORTSS and CORT. CORTSS determines the steady state core temperatures while CORT solves the time dependent problem.

3.1.4.1 STEADY-STATE* SOLUTION (CORTSS)

CORTSS couples the three basic operations to determine the steady-state temperatures in each control volume of the fuel, cladding, and

*Steady-state refers to the condition when the heat input and subsequent temperature rise of the coolant in passage through the core is invariant in time. The temperature of the coolant leaving the top of the core does not reach a steady-state condition.

coolant. Since the solution of film thickness in a particular control volume is dependent on the properties of the control volume immediately below it, the program starts at the lowest Δx section in a B-ring element. The program proceeds to determine the temperature in each Δx section in turn in the B-ring element. After completely determining the temperatures in the B-ring element the procedure is duplicated for the C, D, E, and F rings in turn. For each Δx section the computation involves the following sequence. Using equation 3.1, the power density ($Q(x_i)$) in that section is determined. Utilizing this information, equation 3.21 (3.20 for the first control volume) is solved iteratively to determine the film thickness, $\delta(x_i)$. Using equation 3.22, the heat transfer coefficient, $h_w(x_i)$, is determined. The cladding temperature is then determined explicitly from equation 3.10. The temperatures in the fuel are determined simultaneously using equation 3.11, and a matrix inversion routine [15]. Using the computed values of film thickness and wall temperature the program also computes the bulk water temperature in the film control volume and the heat carried out of the film control volume.

3.1.4.2 DETERMINATION OF EMPIRICAL PARAMETERS

CORTSS is utilized to determine the value of the parameters to fit the results from the model to experimental data. As previously discussed, both the radial heat generation distribution (the RQR's) and the contact resistance between the fuel and cladding (h_{gap}) must be determined empirically. The determination of these parameters requires a trial and error technique. The trial values are input into CORTSS and the resulting values for temperature are compared with experimental data. The experimental values for temperature are obtained from a thesis by J. Stauder [19]. Stauder reported

the maximum fuel temperature in each ring. The data presented in Stauder's thesis is duplicated in Figure 3.1. Using this data the maximum fuel temperatures for steady-state operation at 100 kw are linearly interpolated. These temperatures (see Table 3.1) become the criteria for fitting the model. The experimental radial temperature distribution is used as a first guess for the radial heat generation distribution. With this first approximation for the heat generation distribution and two reasonable guesses for contact resistance CORTSS is run twice. The results from these two trials appear in Table 3.1.

Table 3.1 Radial Temperature Distribution across the Core for Various Heat Generation Distributions and Contact Resistances

Parameter	Ring Fuel	Experimental Data	Input and Output CORTSS		
			Trial 1	Trial 2	Trial 3
Contact Resistance (BRU/hr ft ² deg F)		-	100	200	149
Relative heat generation	B	-	1.000	1.000	1.000
	C	-	0.975	0.975	0.968
	D	-	0.828	0.828	0.792
	E	-	0.675	0.675	0.610
	F	-	0.568	0.568	0.482
Relative maximum temperature	B	1.000	1.000	1.000	1.000
	C	0.975	0.9789	0.9801	0.9736
	D	0.828	0.8538	0.8614	0.8278
	E	0.675	0.7220	0.7363	0.6736
	F	0.568	0.6289	0.6474	0.5633
Maximum temperature (deg(C))	B	197	222.3	171.0	197.4
	C	192	217.6	167.6	192.2
	D	163	189.9	147.3	163.4
	E	133	160.5	125.9	133.0
	F	110	139.8	110.7	111.2

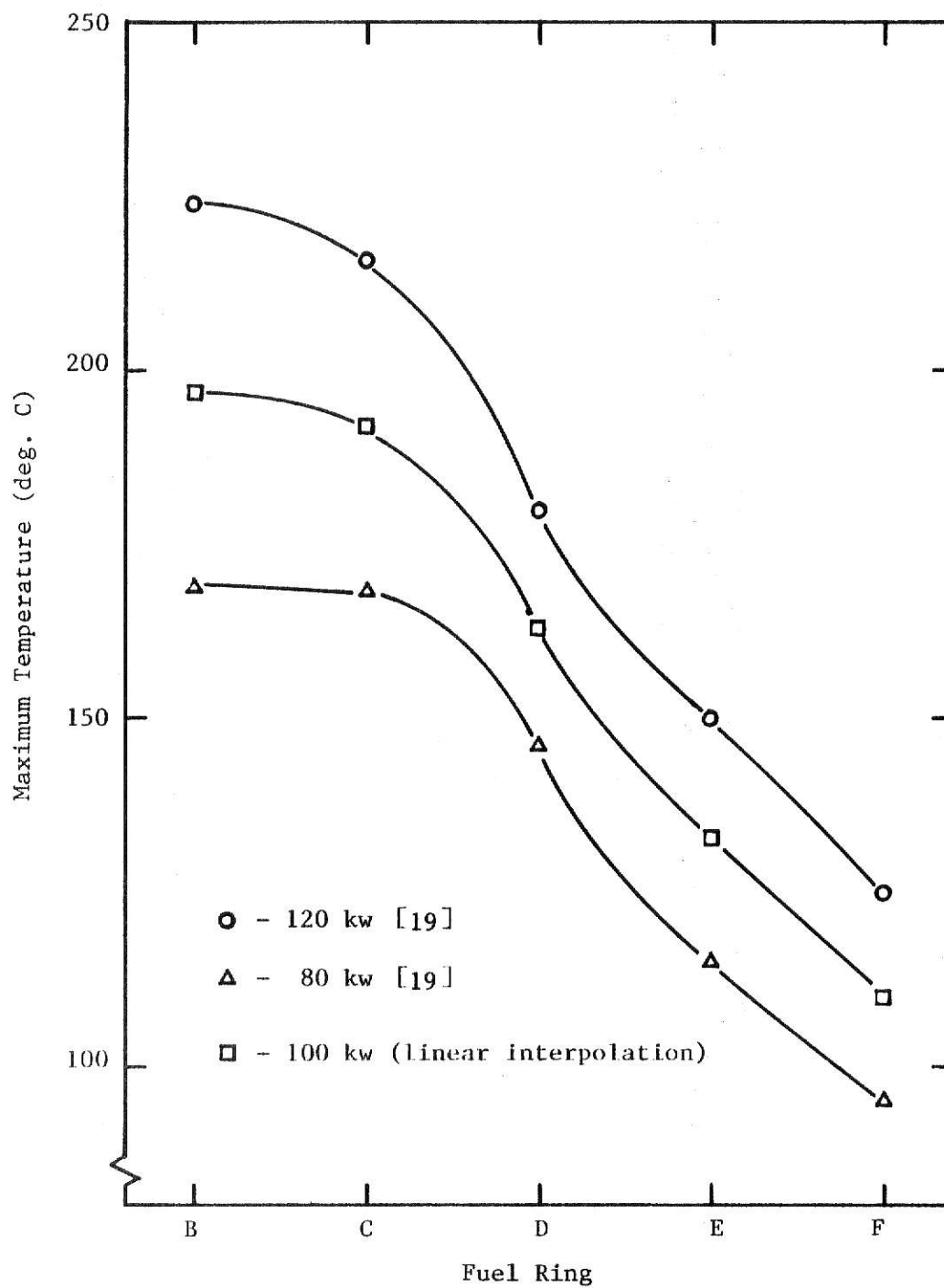


Figure 3.1 Radial Temperature Distribution across the Core

A better guess for the contact resistance is determined by interpolating between the two initial guesses. Referring to Figure 3.2 by linear interpolation the contact resistance corresponding to a maximum B-ring temperature of 197 degrees C is $149 \text{ BTU/hr ft}^2 \text{ deg F}$. In order to determine a better guess for the heat generation distribution, the values for the initial guess are plotted versus the corresponding temperature distributions resulting from CORTSS. Referring to Figure 3.2 the temperature and heat generation distributions appear to be linearly proportional. The slope of this relationship appears to dependent on the contact resistance. Using these observations a better guess for the heat generation distribution is computed. The values for the heat generation distribution corresponding to the experimental temperature distribution are interpolated from the graphs in Figure 3.2. Values are extracted for both trials and appear in Table 3.2. Since the new guess for contact resistance is equal to the average of the values used in the first two trials, the new guess for heat generation distribution is the computed average of the interpolated values for the first two trials. This new guess appears in Table 3.2.

Table 3.2 Determination of Improved Guess for Heat Generation Distribution

Fuel Ring	Experimental Temp. Distribution	Heat generation Distribution		
		Trial 1	Trial 2	Average
B	1.000	1.000	1.000	1.000
C	0.975	0.970	0.966	0.968
D	0.828	0.798	0.786	0.792
E	0.675	0.620	0.599	0.610
F	0.568	0.496	0.467	0.482

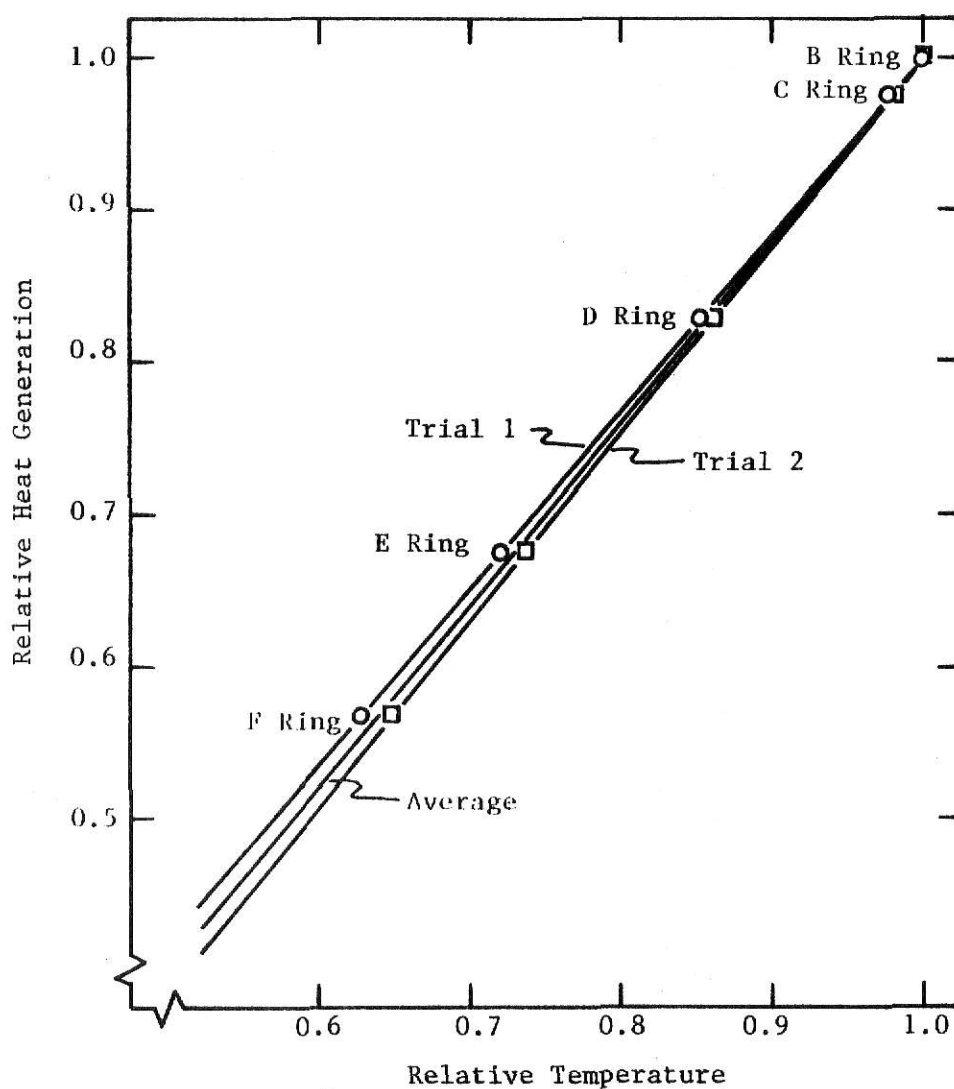
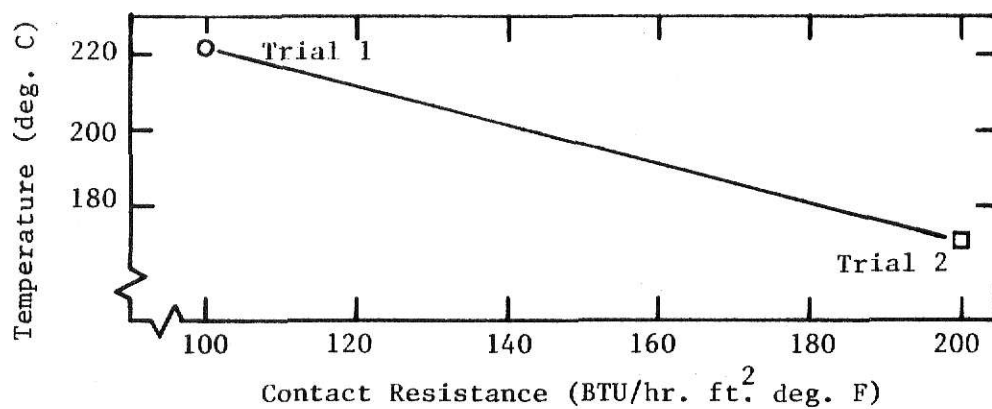


Figure 3.2 Interpolation of the Contact Resistance and Heat Generation Distribution from CORTSS Trial Data

These new guesses for contact resistance and heat generation distribution are input to CORTSS. The resulting maximum fuel temperatures appear under trial 3 in Table 3.1. All the CORTSS derived temperatures are within 0.5% of the experimental values. This is considered sufficiently precise; therefore the fuel-cladding contact resistance is set at $149 \text{ BTU/hr ft}^2 \text{ deg F}$ and the relative power densities (RQR's) are:

Fuel Ring	(i)	RQR(i)
B	1	1.000
C	2	0.968
D	3	0.792
E	4	0.610
F	5	0.482

The value for contact resistance is a physical property of the fuel-cladding interface so that unless the fuel is changed this value should remain fixed. The radial heat generation distribution (the RQR's) are dependent on the core configuration and power level. Therefore the values of RQR derived are good only for fuel loading #11 and 100 kilowatts power level. Perturbations from these values for other configurations or other power levels should, however, be small.

Using the established parameters data from CORTSS can be studied. Some of this data from CORTSS is plotted in figures 3.3, 3.4 and 3.5. Figure 3.3 is a plot of the vertical temperature profiles in a B-ring element. The center-line, fuel-cladding interface, cladding, and bulk water temperature profiles are all graphically illustrated. Note that the profiles become more upwardly skewed for locations further from the fuel center-line. Even the center-line temperature is not symmetric about the half-height of the fuel element. Instead the maximum center-line temperature appears to be 0.5 inches above the half-height. Figure 3.4 is a plot of the vertical

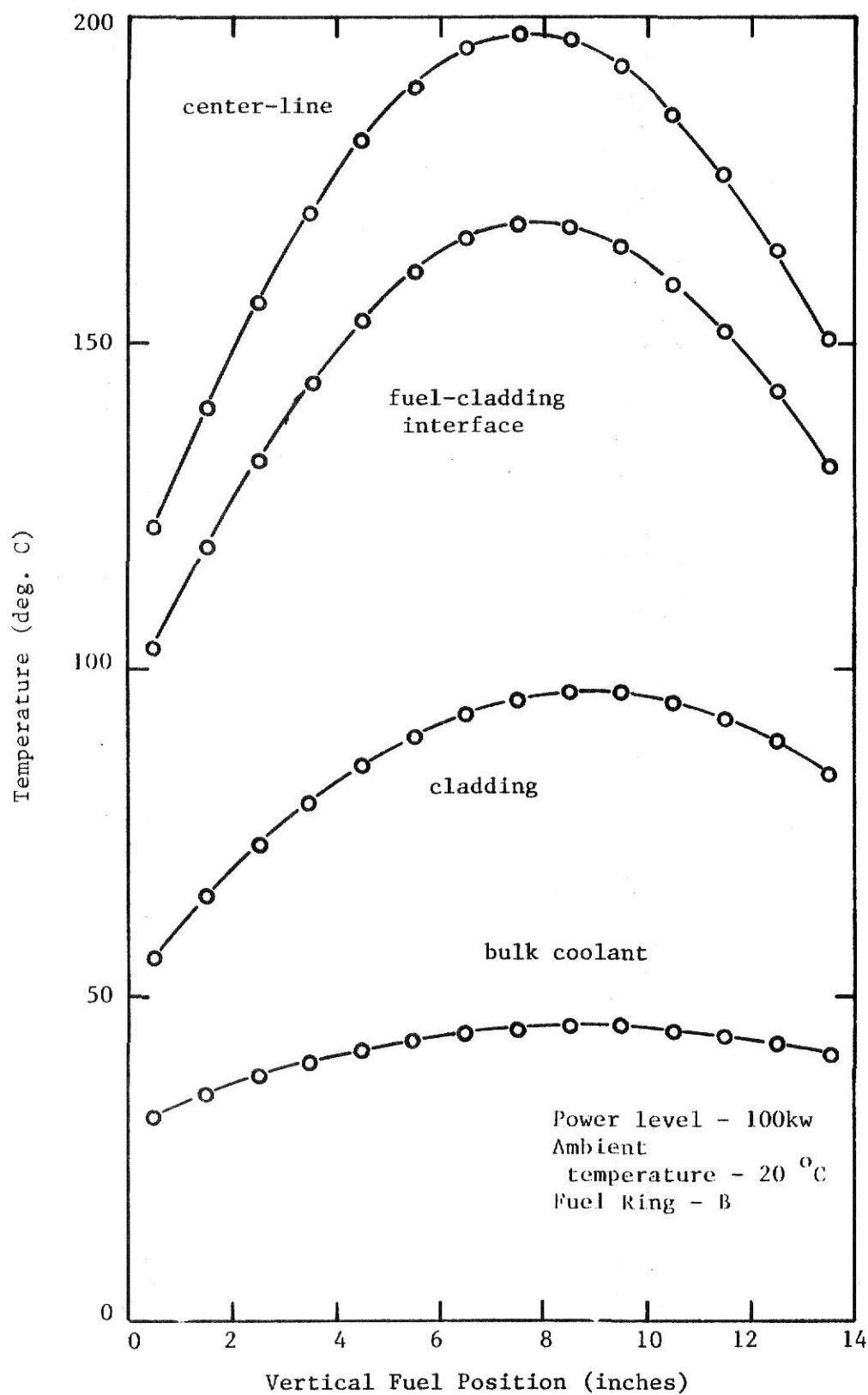


Figure 3.3 Vertical Temperature Distributions in the Core
(Results from CORTSS)

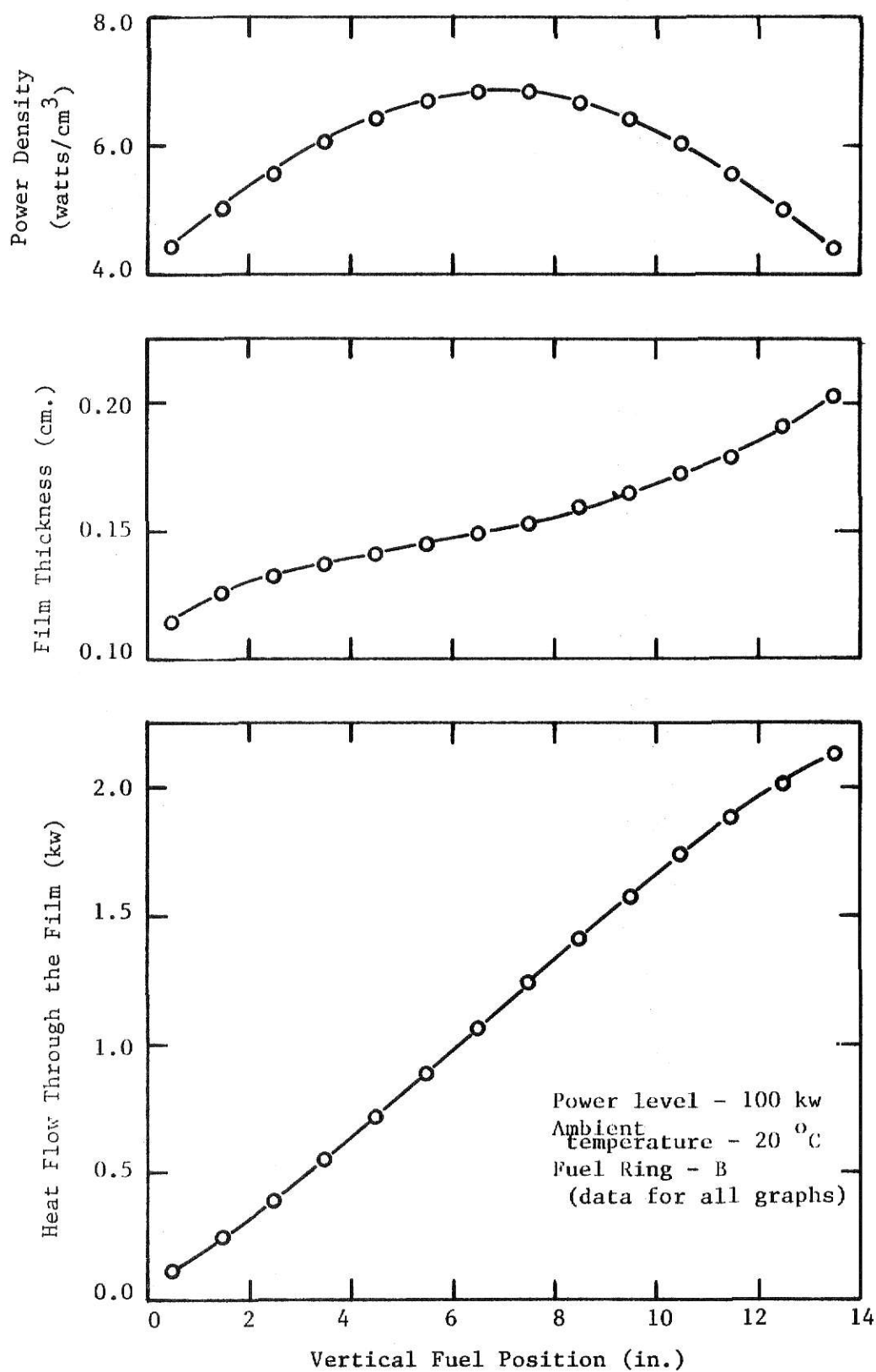


Figure 3.4 Film Thickness, Power Density and Heat Flow as a Function of Vertical Position (Results from CORTSS)

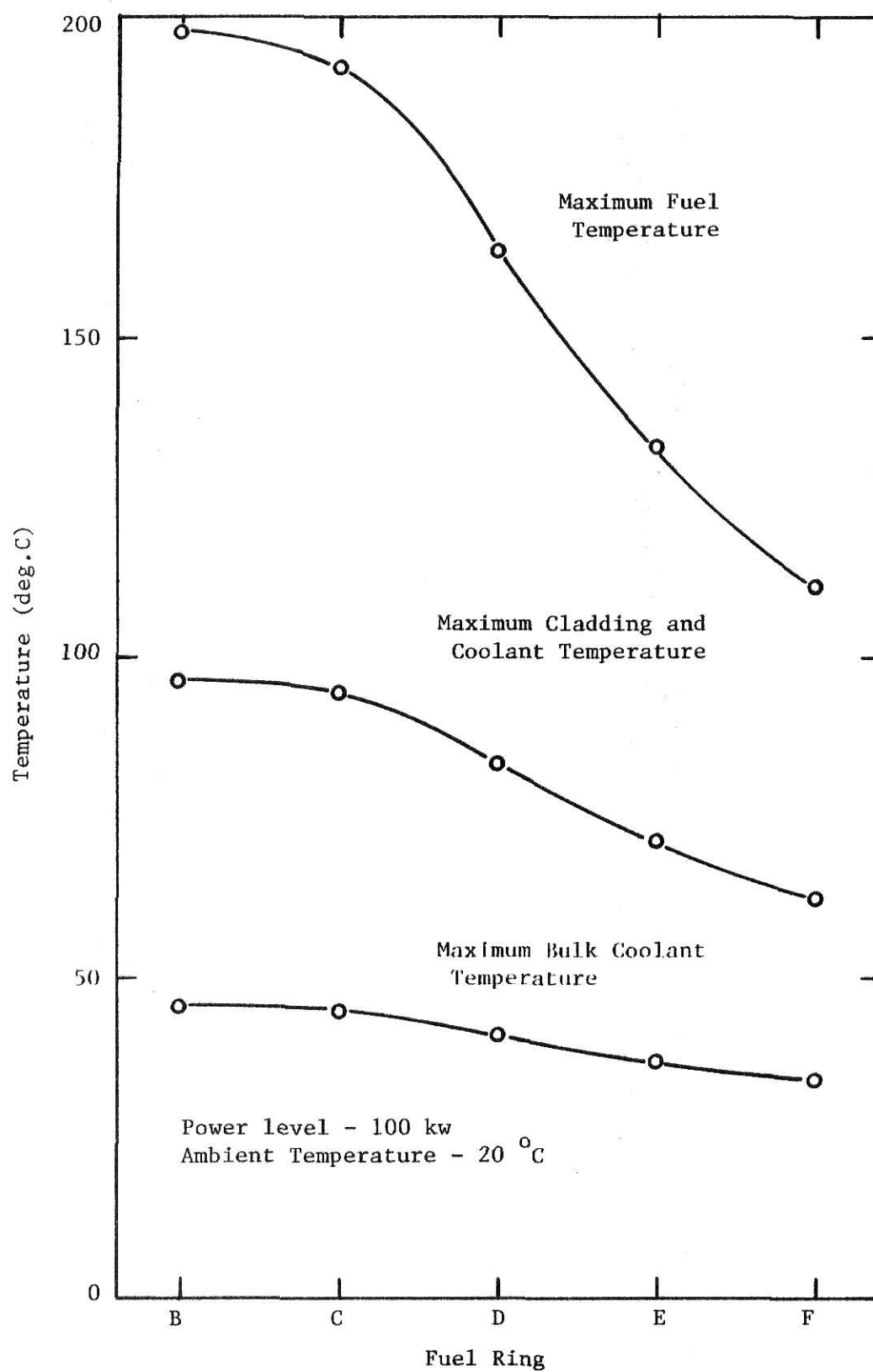


Figure 3.5 Radial Temperature Distributions in the Core
(results from CORTSS)

profiles of several other parameters. The first curve depicts the heat flow out of each control volume. The second curve shows the shape of the film boundary. The third curve shows the sinusoidal power density distribution. Figure 3.5 is a plot of the horizontal temperature profiles across the core. All the profiles are symmetric about the radial center of the core. The temperature differences are less pronounced in the coolant than in the center of the fuel element.

3.1.4.3 TIME DEPENDENT SOLUTION (CORT)

The program to determine the time dependent core temperatures, CORT, again couples the three basic operations that CORTSS utilized. CORT also uses the empirical data for contact resistance and heat generation distribution derived using CORTSS. As in CORTSS, CORT starts at the lowest Δx section in a B-ring element. After completely solving for the temperatures in a B-ring element the program solves for the temperatures in a C, D, E, and F-ring element in turn.

For each Δx section the computation involves the procedure depicted in Figure 3.6. Using equation 3.1, the power density ($Q(x_1)$) in that section is determined. For time zero all the temperatures are set to the ambient coolant temperature. Time is increased in Δt increments. Using equation 3.17 (3.19 in the lowest section), the film thickness is determined. Using equation 3.22 the heat transfer coefficient between cladding and coolant is then determined. During the first time iteration the cladding temperature and coolant temperature are equal which means the film thickness is infinite. Therefore in this case the program sets the film thickness equal to an arbitrary large number and sets the heat transfer coefficient equal to zero.

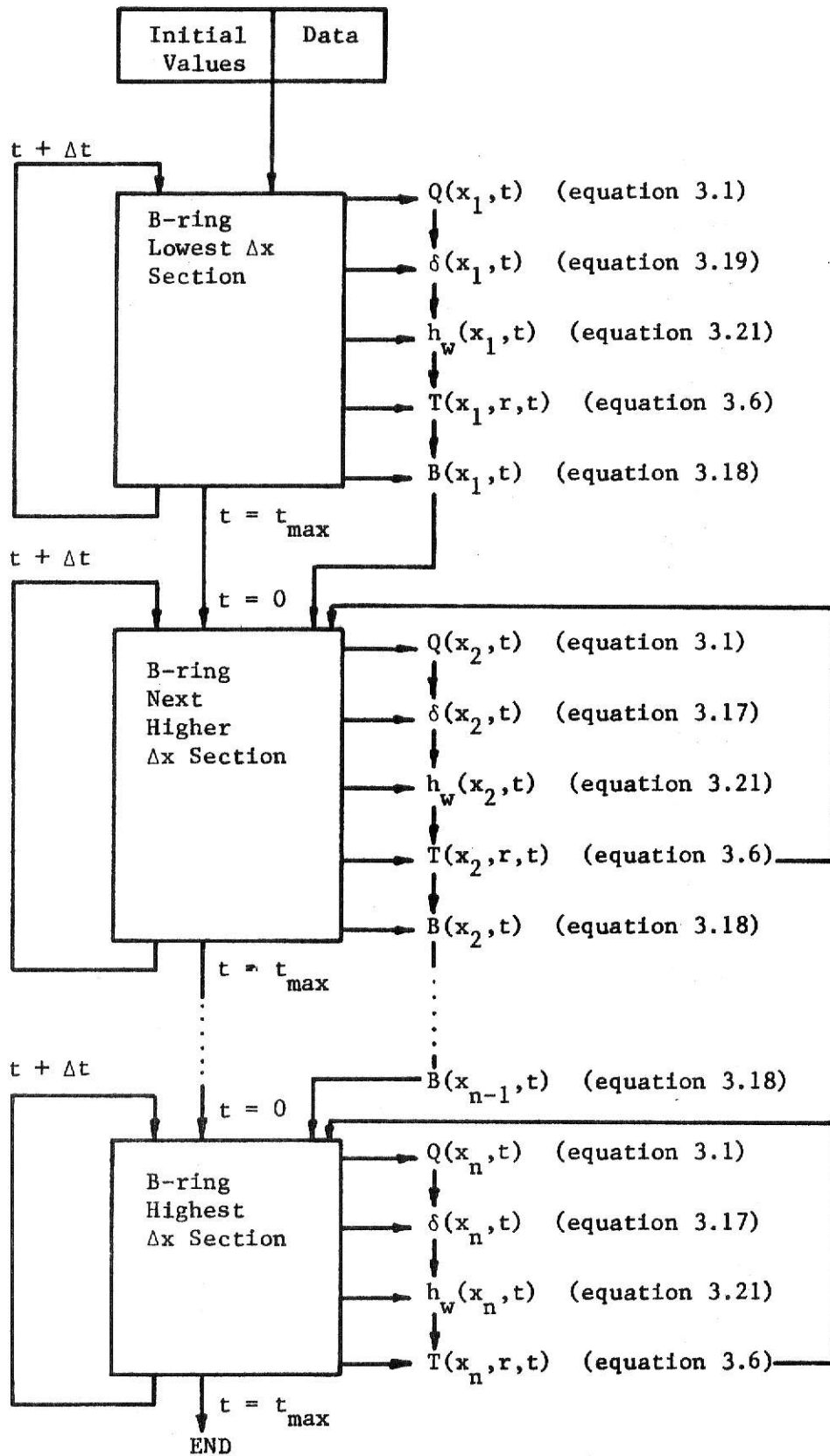


Figure 3.6 Computational Procedure for CORT

Using the present value of the heat transfer coefficient the temperatures are calculated at time t using equation 3.6. During each iteration the factor $B(x_i)$ is calculated for use in determination of temperatures in the next Δx section. After a predetermined number of time increments the program resets the time to zero and solves for temperatures in the next higher Δx section. As in CORTSS, CORT also computes the bulk coolant temperature in the film and the heat carried out of the film control volume for all times.

Some of the data from CORT is plotted in Figures 3.7, 3.8, and 3.9. Figure 3.7 depicts the change in the radial temperature profile in the fuel, cladding and coolant as a function of time. All the temperature gradients become more steep with time. The rate of change of temperature as a function of time is shown more clearly in Figure 3.8. Notice all the temperatures rise rapidly and approach the asymptotic steady-state values. The center-line fuel temperature rise is the most dramatic. The bulk coolant temperature reaches its steady-state value first. It appears safe to assume that all the core temperatures reach steady-state in 10 minutes or less.

Since the film thickness is assumed to be very large at time zero, the film thickness decreases rapidly approaching the steady-state thickness along the entire length of the fuel element as is shown in Figure 3.9. Also depicted is the heat flow out of the film. The value of this parameter indicates the total heat deposited in the coolant from all control volumes at and below a given height. Therefore the value for a fuel height of 13.5 inches indicates the heat from the entire fuel element deposited in the coolant. This value slowly approaches the steady-state value. However it appears that even after 10 minutes the steady-state value has not been reached. This is due to the accumulation of small differences throughout the core.

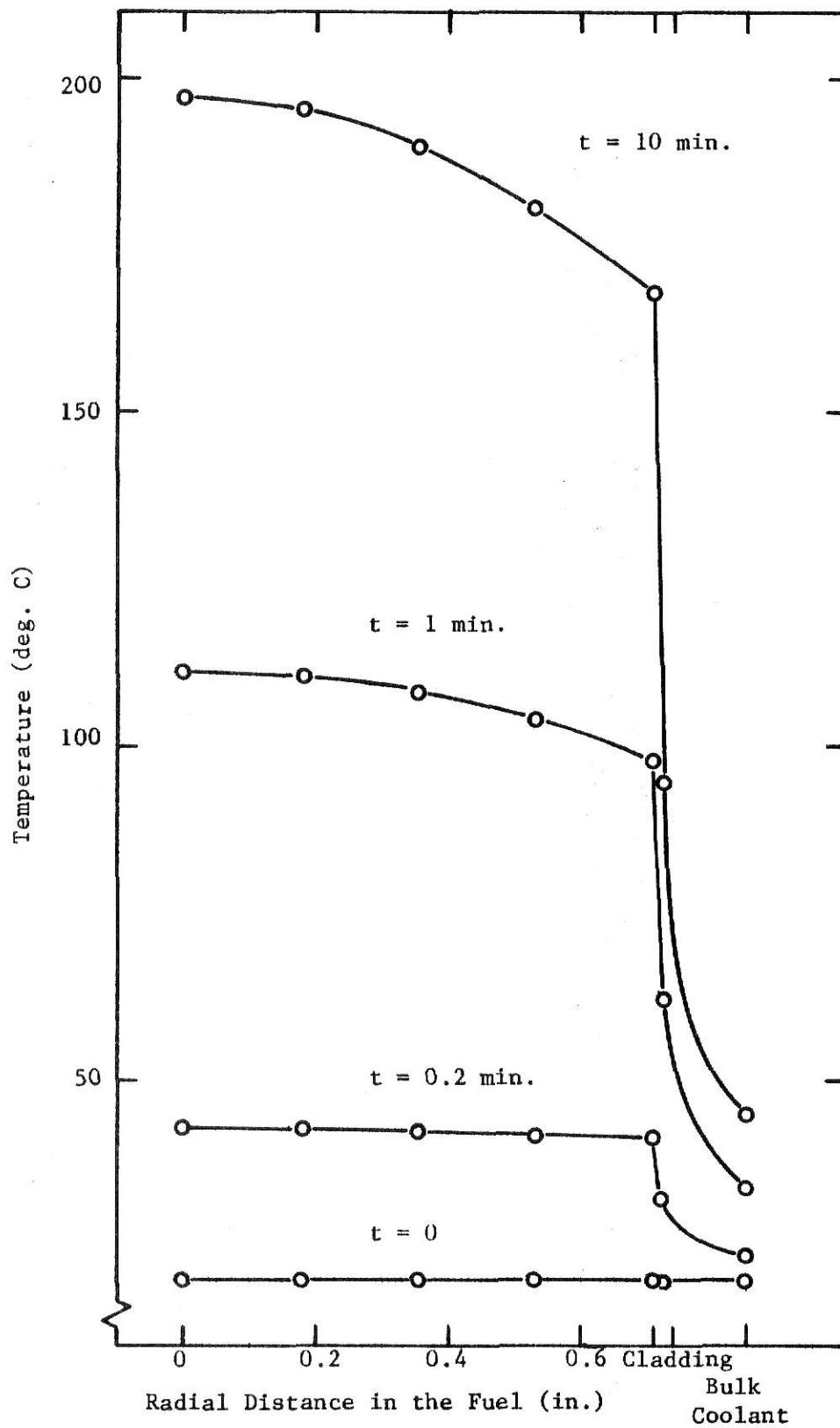


Figure 3.7 The Temperature Profile in the Fuel, Cladding and Coolant Film (Results from CORT)

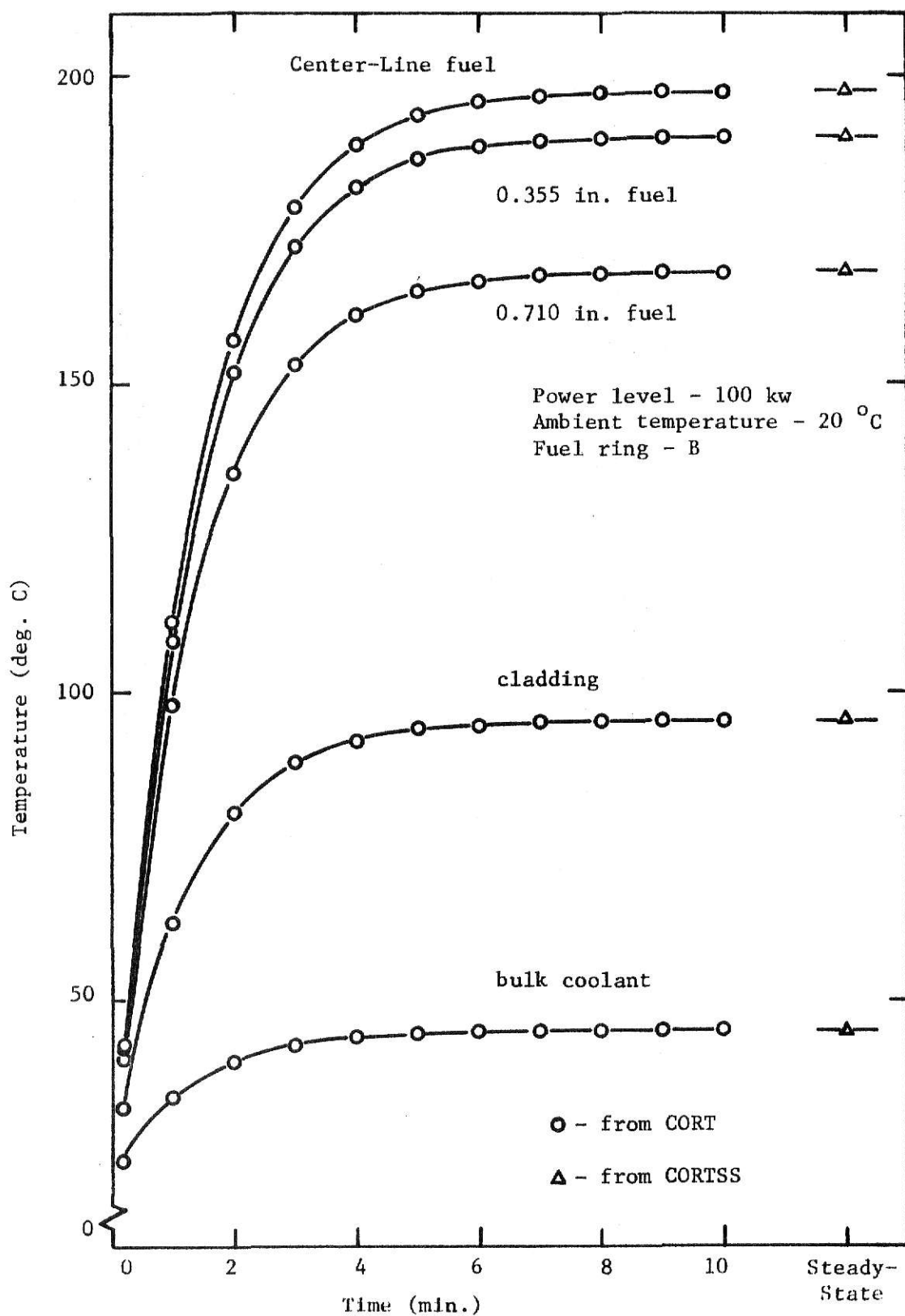


Figure 3.8 Temperatures at Various Locations in the Fuel, Cladding and Coolant Film as a Function of Time

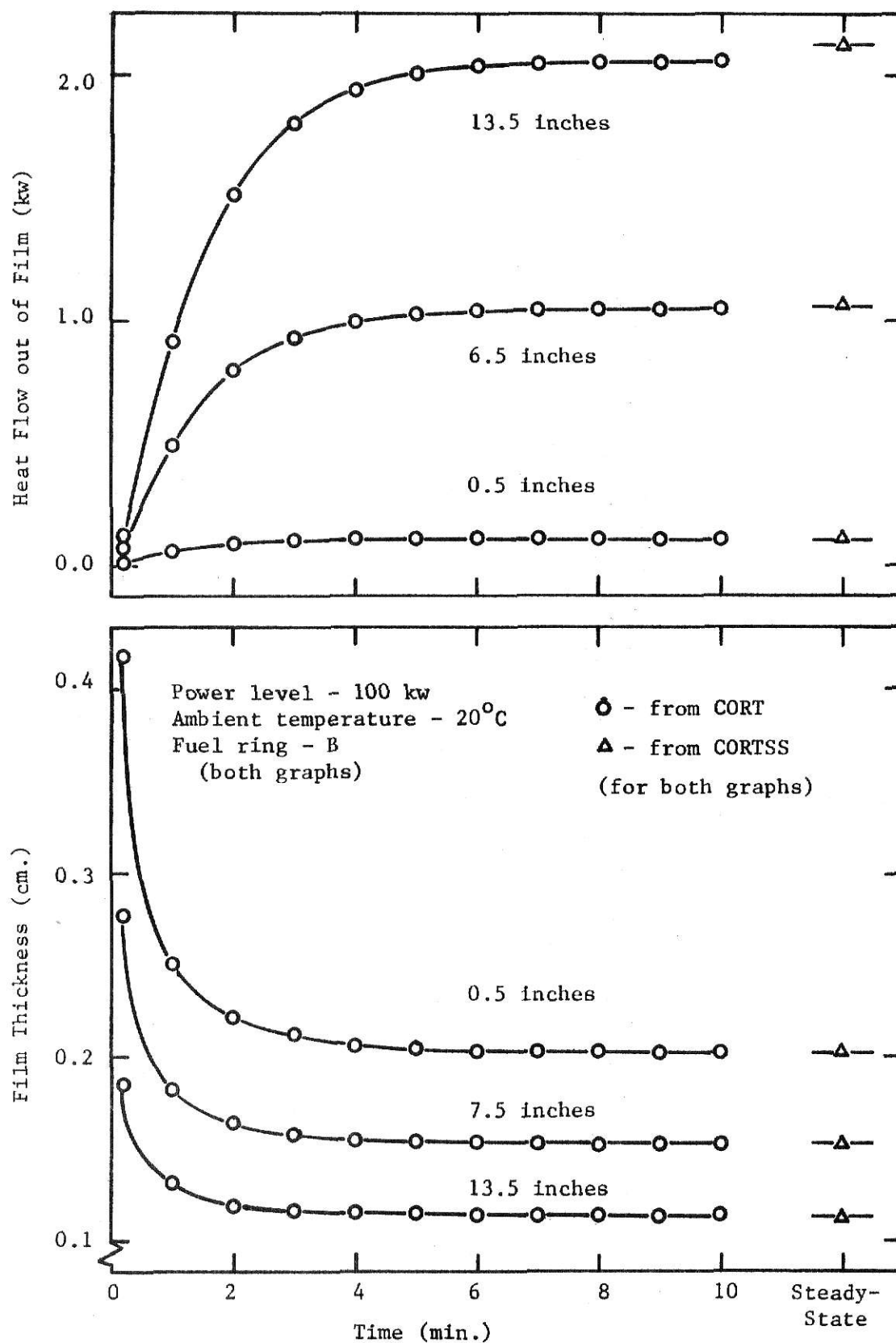


Figure 3.9 Film Thickness and Heat Flow at Various Fuel Heights as a Function of Time

In order to determine how well CORT predicts the actual time dependent temperature distribution, the values from CORT are compared to experimental data. The instrumented fuel element used in the Stauder's experiments [9] has a thermocouple on the centerline of the fuel at a height of 7.5 inches. This element is placed in a B-ring location and the temperature rise during 100 kw steady-state operation is recorded. The reactor cannot be brought to 100 kw in a step change as is assumed in CORT. In order to closely simulate this step change the following procedure is followed. The reactor is operated at steady-state zero power (1 watt) until all temperatures reach equilibrium. The reactor is then brought to 100 kw on the fastest period possible without scrambling the reactor. The power is then held steady with as little rod movement as possible. The resulting S-shaped temperature rise appears in Figure 3.10. The curve resulting from CORT is superimposed on this data.

When the CORT results are plotted with the zero time coinciding with the experimental start to 100 kw, the two results do not match closely. However when the CORT results are shifted such that the temperature from CORT coincides with the experimental fuel temperature at the time when the reactor reaches 100 kw, the values are much closer. The fact that the CORT results do so closely match the experimental results is an indication the model simulates the real situation to the necessary accuracy.

3.2 TEMPERATURE DISTRIBUTION IN THE POOL

Using data from the core temperature models as a source term, a model of the temperature distribution in the reactor pool is developed. The model is kept simple to facilitate computation. The construction of the model relies heavily on experimental data.

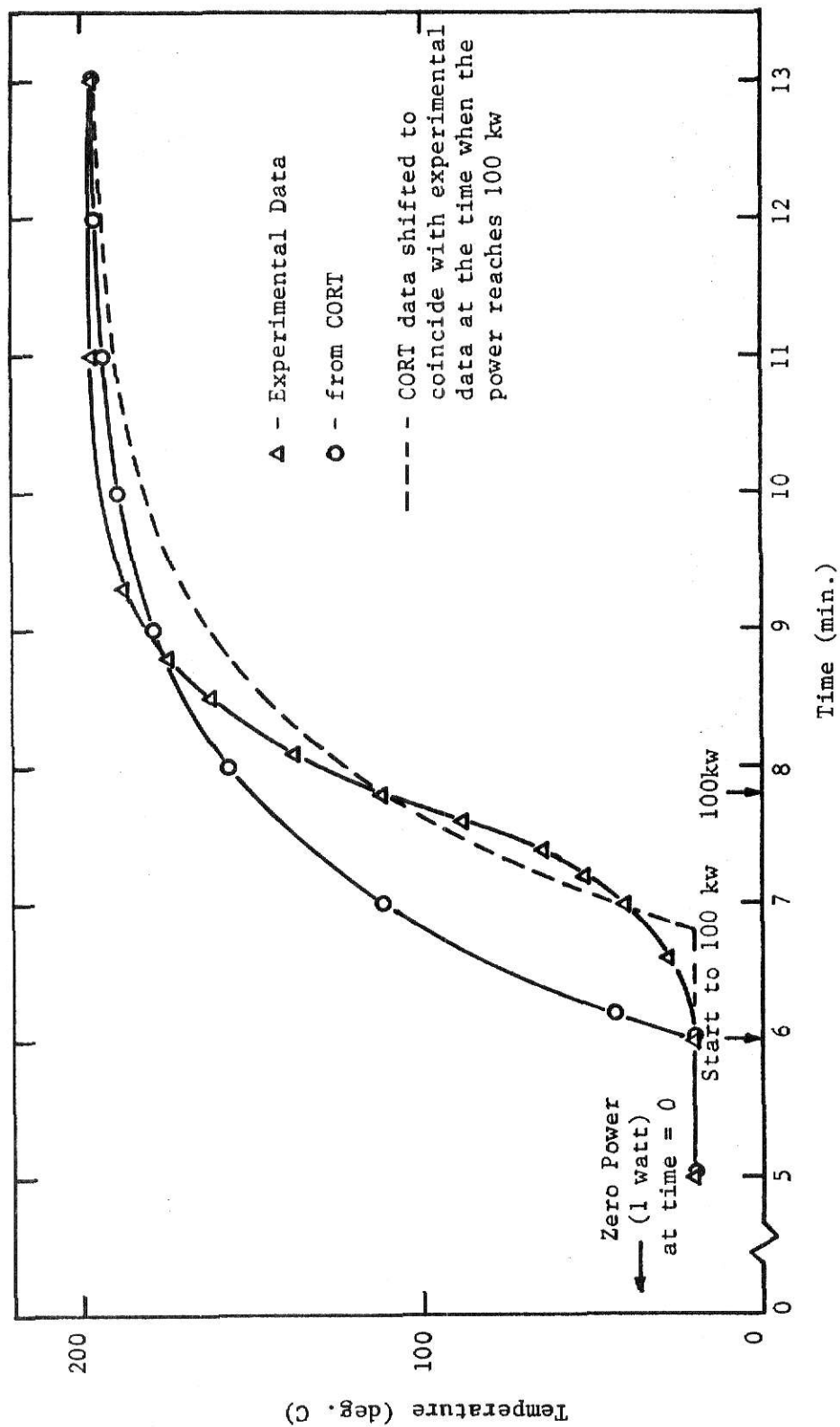


Figure 3.10 The Temperature Rise on the Center-Line of the Fuel in a B-Ring Element

3.2.1 HEAT FLOW INTO THE POOL FROM THE CORE.

In order to establish a source of heat into the pool the temperature and heat content of the coolant leaving the core must be known. From the core models the temperature distribution in the coolant film and the heat flow out of the film control volumes are known. From the description of the core in section 2, two observations can be made. First the coolant flow is greatly constricted at the top of the core. When the central thimble is inserted the heated coolant can only escape from the core through the spacers above each fuel element (see Figure 2.5). Secondly there is five inches vertically between the last fuel and the top of the upper grid plate. Because of these two factors it is safe to assume that both the temperature and velocity profiles in the film and the film boundary itself are obliterated before the coolant leaves the core. Also because of the restricted flow and large unheated volume for mixing, it is assumed the coolant becomes well mixed and leaves the core at the bulk coolant temperature. However since flow rates are substantial it is also assumed no heat is lost in this mixing and the coolant leaves the core with the same heat content as is deposited in its transit past the fuel. If the additional assumptions are made that the coolant heated by a fuel element leaves the core through the spacer at the top of that element and that the heating characteristics of all fuel elements in any one ring are identical, then the exiting coolant temperature from any one fuel ring will be the bulk coolant temperature in the upper most control volume of the film around an element from that ring. Using the results from CORT and CORTSS the temperature of the coolant leaving the core from each fuel ring is tabulated in

Table 3.3. With the assumptions made, the heat flow from any given fuel ring is equal to the heat flow out of the upper most film control volume around an element of that ring times the number of elements in that ring. Again using the results from CORT and CORTSS the heat flow out of the core is listed in Table 3.4.

3.2.2 A MODEL TO DETERMINE THE TEMPERATURE DISTRIBUTION IN THE POOL

Using the data just calculated as the source term and the data from Appendix E to gain insight into the flow patterns within the pool, a model for the temperature distribution within the reactor pool can be developed. From the experimental data in Appendix E it appears the pool temperature distribution goes through several stages of development. Initially the entire pool is assumed to be at the same ambient temperature. The first temperature change comes in a rising column of warmed water. This columnar chimney of warmer water stays well defined until it hits the surface of the water in the pool. A region of mixing and change in direction of flow is then established. The warmed water is transported down the side of the pool and past the reflector and finally flows radially into the bottom of the core. During this whole process heat is being conducted throughout the pool but on a much slower scale than the transport process. The water below the core is heated at a slower rate than the rest of the pool. Each step in this process is modeled with the final result a model of the heat flow throughout the pool as a function of time.

3.2.2.1 HEAT SOURCE

Both the temperature rise of the coolant through the core and the heat flow out of the core is approximated by the same function in time. The relationships are

Table 3.3 Bulk Water Temperature out of the Core (from CORT and CORTSS)

Time (min.)	Temperature Rise in Passage through Fuel Ring (deg C)					Average Temperature
	B (6)*	C (11)	D (17)	E (23)	F (6)	$\sum_{i=B}^F \text{NER}(i)T(i)$ 63
0	20.0	20.0	20.0	20.0	20.0	20.0
1	31.0	30.7	29.0	27.1	25.8	28.5
2	36.3	35.9	33.4	30.7	28.8	32.7
3	38.9	38.4	35.6	32.5	30.3	34.8
4	40.2	39.6	36.7	33.4	31.1	35.8
5	40.8	40.3	37.2	33.9	31.5	36.3
6	41.1	40.6	37.5	34.2	31.7	36.6
7	41.3	40.7	37.6	34.3	31.8	36.7
8	41.3	40.8	37.7	34.3	31.9	36.8
9	41.4	40.8	37.7	34.4	31.9	36.8
10	41.4	40.8	37.7	34.4	31.9	36.8
Steady- State	41.5	41.0	37.9	34.5	32.0	37.0

*Number of fuel elements in that ring for fuel loading #11 (NER(1)).

Table 3.4 Heat Flow Out of the Core (from CORT and CORTSS)

Time (min.)	Heat Flow from an Element from Fuel Ring (Heat flow from whole ring in parentheses) (kilowatts)					Whole Core (63)
	B (6)*	C (11)	D (17)	E (23)	F (6)	
0	0.000	0.000	0.000	0.000	0.000	0.000
1	0.913 (5.478)	0.882 (9.702)	0.709 (12.053)	0.534 (12.282)	0.413 (2.478)	41.993
2	1.510 (9.060)	1.459 (16.049)	1.182 (20.094)	0.898 (20.654)	0.701 (4.206)	70.063
3	1.801 (10.806)	1.742 (19.162)	1.417 (24.089)	1.083 (24.909)	0.849 (5.094)	84.060
4	1.940 (11.640)	1.877 (20.647)	1.530 (26.010)	1.173 (26.979)	0.923 (5.538)	90.814
5	2.004 (12.024)	1.940 (21.340)	1.584 (26.928)	1.217 (27.991)	0.959 (5.754)	94.037
6	2.035 (12.210)	1.969 (21.659)	1.610 (27.370)	1.238 (28.474)	0.977 (5.862)	95.575
7	2.049 (12.294)	1.983 (21.813)	1.622 (27.574)	1.248 (28.704)	0.986 (5.916)	96.301
8	2.055 (12.330)	1.989 (21.879)	1.627 (27.659)	1.253 (28.819)	0.990 (5.940)	96.627
9	2.058 (12.348)	1.992 (21.912)	1.630 (27.710)	1.255 (28.865)	0.992 (5.952)	96.787
10	2.060 (12.360)	1.994 (21.934)	1.631 (27.727)	1.256 (28.888)	0.993 (5.958)	96.867
Steady- State	2.127 (12.762)	2.059 (22.649)	1.685 (28.645)	1.298 (29.845)	1.025 (6.150)	100.060

*Number of fuel elements in that ring for fuel loading #11.

$$\dot{Q}(t)_{\text{core}} = \dot{Q}_{\text{ss}} (1 - e^{-\lambda t}) , \quad (\text{kw}) \quad (3.22)$$

and

$$\Delta T_{\text{core}} = \Delta T_{\text{ss}} (1 - e^{-\alpha t}) ; \quad (\text{deg C}) \quad (3.23)$$

where, for 100 kw operation,

$$\dot{Q}_{\text{ss}} = 100 \text{ kw} \quad \text{and} \quad \Delta T_{\text{ss}} = 17.0 \text{ deg C.}$$

From a least squares fit of the data in Table 3.3

$$\lambda = 0.67 \text{ min.}^{-1},$$

and from a least squares fit of the data in Table 3.4

$$\alpha = 0.58 \text{ min.}^{-1} .$$

The total heat input into the pool is the time integral of equation 3.22 or

$$Q(t)_{\text{core}} = \dot{Q}_{\text{ss}} (\lambda t - 1 + e^{-\lambda t}) / \lambda . \quad (\text{kwhr}) \quad (3.24)$$

3.2.2.2 FORMATION OF THE CHIMNEY

From the data in Appendix E the temperature distribution in the center of the chimney is approximated by

$$\Delta T_{\text{C}_L} = \Delta T_{\text{core}} (x^4/h^4) , \quad (\text{deg C})$$

where x is the distance from the top of the chimney and h is the height of the chimney. At any height the radial temperature distribution is approximately

$$\Delta T_{\text{col}} = \Delta T_{\text{C}_L} \cos(\pi r/2R) , \quad (\text{deg C})$$

where r is the distance from the chimney center-line and R is the maximum radius of the chimney at a given height. The rising chimney is assumed to be cylindrical with dimensions $h(t)$ and R . The temperature at any point in the chimney is

$$\Delta T_{col}(x,r,t) = \Delta T_{core}(t) (x^4/h^4(t)) \cos(\pi r/2R). \quad (\text{deg C}) \quad (3.25)$$

The total heat content of a volume element of water in the chimney is

$$dQ_{col}(x,r,t) = \rho_w c_w 2\pi r dr dx \Delta T_{col}(x,r,t) . \quad (\text{kwhr})$$

The total heat content of the rising colume is

$$Q_{col}(t) = \int_0^R \int_0^h dQ_{col}(x,r,t) , \quad (\text{kwhr})$$

or

$$Q_{col}(t) = c_w \rho_w R^2 (4/5) (1 - 2/\pi) h(t) \Delta T_{core}(t) . \quad (\text{kwhr})$$

Ignoring any heat conduction out of the column the heat content in the column at any time must equal the total heat input into the pool. Therefore

$$Q_{col}(t) = Q_{core}(t) , \quad (\text{kwhr})$$

and

$$h(t) = Q_{core}(t) / (Cl \Delta T_{core}(t)), \quad (\text{ft}) \quad (3.26)$$

$$\text{where } Cl = c_w \rho_w R^2 (4/5) (1 - 2/\pi) . \quad (\text{kwhr/deg C ft.})$$

The chimney reaches the pool surface when

$$h(t) = H , \quad (\text{ft})$$

where H is the distance from the top of the pool to the top of the core.

3.2.2.3 FLOW DOWN THE SIDES

Once the chimney is fully formed the temperature profile remains the same except the whole reference is raised. The temperature in the columnar chimney is approximated by

$$\Delta T_{col}(x,r,t) = \Delta T_{top}(t) + (\Delta T_{core}(t) - T_{top}(t)) (x^4/H^4) \cos(\pi r/2R), \quad (\text{deg C}) \quad (3.27)$$

where ΔT_{top} is the temperature rise at the top of the pool. The total heat content of the chimney is

$$Q_{col}(t) = H[C1\Delta T_{core}(t) + (C2 - C1) \Delta T_{top}(t)] \quad . \quad (kwhr)$$

where

$$C2 = c_w \rho_w \pi R^2 \quad (kwhr/deg \text{ C ft})$$

The temperature of the water outside the chimney has no radial gradient.

The temperature distribution is approximated by

$$\Delta T_{side}(x, r, t) = \Delta T_{top}(t) (1 - x^3/m^3) \quad , \quad (deg \text{ C}) \quad (3.28)$$

where x is the distance from the top of the pool and m is the distance the heated water has traversed down the side. The heat content of this falling column of water outside the chimney is

$$Q_{side}(t) = c_w \rho_w (3\pi/4) (R_o^2 - R^2) m(t) \Delta T_{top}(t) \quad , \quad (kwhr)$$

where R_o is the outer radius of the pool. Again assuming no heat is conducted out of the heated water the heat content of the pool at any time must equal the heat input into the pool. Therefore

$$Q_{col}(t) + Q_{side}(t) = Q_{core}(t) \quad , \quad (kwhr)$$

and

$$m(t) = \frac{Q_{core}(t) - [(F1)\Delta T_{core}(t) + (F2)\Delta T_{top}(t)]}{(C3) \Delta T_{top}(t)} \quad (ft)$$

where $F1 = (C1)H \quad (kwhr/deg \text{ C})$

$$F2 = H(C2 - C1) \quad (kwhr/deg \text{ C})$$

$$C3 = c_w \rho_w 3(\pi/4) (R_o^2 - R^2) \quad (kwhr/deg \text{ C ft})$$

The distance of flow down the side, $m(t)$, and the temperature at the top of the pool must be related such that when the chimney reaches the pool surface

$$m(t) = \Delta T_{top}(t) = 0 \quad .$$

Also when the flow down the side reaches the top of the reflector

$$m(t) = H, \quad \text{and} \quad \Delta T_{\text{top}}(t) = \Delta T_{\text{top}}^* .$$

Such a relation can be expressed as

$$\Delta T_{\text{top}}(t) = \Delta T_{\text{top}}^* (m(t)/H)^3 \quad (\text{deg C}) \quad (3.29)$$

then

$$m(t)^3 = \frac{Q_{\text{core}}(t) - F1 \Delta T_{\text{core}}(t)}{(\Delta T_{\text{top}}^*/H^3) [(C3)m(t) + F2]} \quad (\text{ft}) \quad (3.30)$$

3.2.2.4 FULLY ESTABLISHED FLOW

Once the flow down the sides reaches the reflector the profile remains the same except the reference is raised. The temperature distribution in the pool water outside the chimney is approximated by

$$\Delta T_{\text{side}}(x,r,t) = \Delta T_{\text{top}}^* (1 - x^3/H^3) + \Delta T_{\text{in}}(t), \quad (\text{deg C}) \quad (3.31)$$

where ΔT_{in} is the temperature rise above ambient of the water entering the core. The total heat content of the water outside the chimney is

$$Q_{\text{side}}(t) = c_w \rho_w \pi (R_o^2 - R^2) H [3/4 \Delta T_{\text{top}}^* + \Delta T_{\text{in}}(t)] . \quad (\text{kwhr})$$

the temperature of the water passing the reflector is assumed to be at the same temperature as the water entering the core. The total heat content of the water outside the reflector is

$$Q_{\text{ref}}(t) = c_w \rho_w V_{\text{ref}} \Delta T_{\text{in}}(t), \quad (\text{kwhr})$$

where V_{ref} is the volume of water passing the reflector (the thermal column, thermalizing column and beam ports greatly reduce this volume).

Assuming the heat transfer within the core is not affected by the rise in inlet temperature,

$$\Delta T_{\text{out}}(t) = \Delta T_{\text{in}}(t) + \Delta T_{\text{core}}(t) , \quad (\text{deg C}) \quad (3.32)$$

where ΔT_{out} is the temperature rise above ambient of the coolant leaving the top of the core. The temperature distribution in the chimney then becomes

$$\Delta T_{\text{col}}(x, r, t) = (\Delta T_{\text{out}}(t) - \Delta T_{\text{top}}(t)) (x^4/H^4) \cos(\pi r/2R) + \Delta T_{\text{top}}(t) . \quad (\text{deg C}) \quad (3.33)$$

The total heat content in the chimney is

$$Q_{\text{col}}(t) = [F1 \Delta T_{\text{out}}(t) + F2 \Delta T_{\text{top}}(t)] . \quad (\text{kwhr})$$

The temperature distribution below the core is approximated by

$$\Delta T_{\text{bot}}(x, r, t) = \Delta T_{\text{in}}(t) (x/\Delta x)^2 . \quad (\text{deg C}) \quad (3.34)$$

where x is the distance from the bottom of the pool and Δx is the distance from the bottom of the pool to the bottom of the core. The total heat content of the water below the core is

$$Q_{\text{bot}}(t) = c_w \rho_w \pi R_o^2 (\Delta x/3) \Delta T_{\text{in}} . \quad (\text{kwhr})$$

Assuming no heat escapes from the water in the pool the total heat content of the water in the pool must equal the heat input into the pool, or

$$Q_{\text{col}}(t) + Q_{\text{side}}(t) + Q_{\text{ref}}(t) + Q_{\text{bot}}(t) = Q_{\text{core}}(t) . \quad (\text{kwhr})$$

Then

$$\Delta T_{\text{in}}(t) (F1 + F4 + F5 + F6) + F1 \Delta T_{\text{core}}(t) + F2 \Delta T_{\text{top}}(t) + F3 \Delta T_{\text{top}}^* = Q_{\text{core}}(t) ; \quad (\text{kwhr})$$

$$\text{where } F3 = H C3 , \quad (\text{kwhr/deg C})$$

$$F4 = 4/3 C3 , \quad (\text{kwhr/deg C})$$

$$F5 = c_w \rho_w V_{\text{ref}} , \quad (\text{kwhr/deg C})$$

$$F6 = c_w \rho_w \pi R_o^2 \Delta x/3 . \quad (\text{kwhr/deg C})$$

From equation 3.33

$$\Delta T_{top}(t) = \Delta T_{in}(t) + \Delta T_{top}^* , \quad (\text{deg C}) \quad (3.35)$$

therefore

$$\Delta T_{in}(t) = \frac{Q_{core}(t) - F1 \Delta T_{core}(t) - (F2 + F3) \Delta T_{top}^*}{F1 + F2 + F4 + F5 + F6} \quad (\text{deg C}) \quad (3.36)$$

3.2.2.5 NUMERICAL SOLUTION TO POOL TEMPERATURE DISTRIBUTION (POOLT)

A computer program, POOLT, is used to facilitate computation of the temperature distribution in the pool as a function of time. Figure 3.11 depicts the procedure followed. Time is incremented in Δt steps. For each time $Q_{core}(t)$ and $\Delta T_{core}(t)$ are computed using equations 3.24 and 3.22 respectively. The height of the rising column is computed using equation 3.26. Temperatures in the rising column are computed using equation 3.25. When the height of the rising column is computed to be greater than the distance from the top of the pool to the top of the core, the program switches to the flow down the side case. In this case the distance the flow has traversed down the side is solved iteratively using equation 3.30. The temperature at the top of the pool is determined from equation 3.29. During the flow down the side temperatures outside the chimney are calculated using equation 3.28 and temperatures inside the chimney are calculated using equation 3.27.

Once the flow down the side reaches the top of the reflector the flow is considered fully established. The temperature at the core inlet is calculated using equation 3.36. The temperature of the water leaving the core is determined from equation 3.32 and the temperature at the top of the pool is determined from equation 3.35. After the flow is fully established the temperatures inside the chimney are calculated using equation 3.33, the

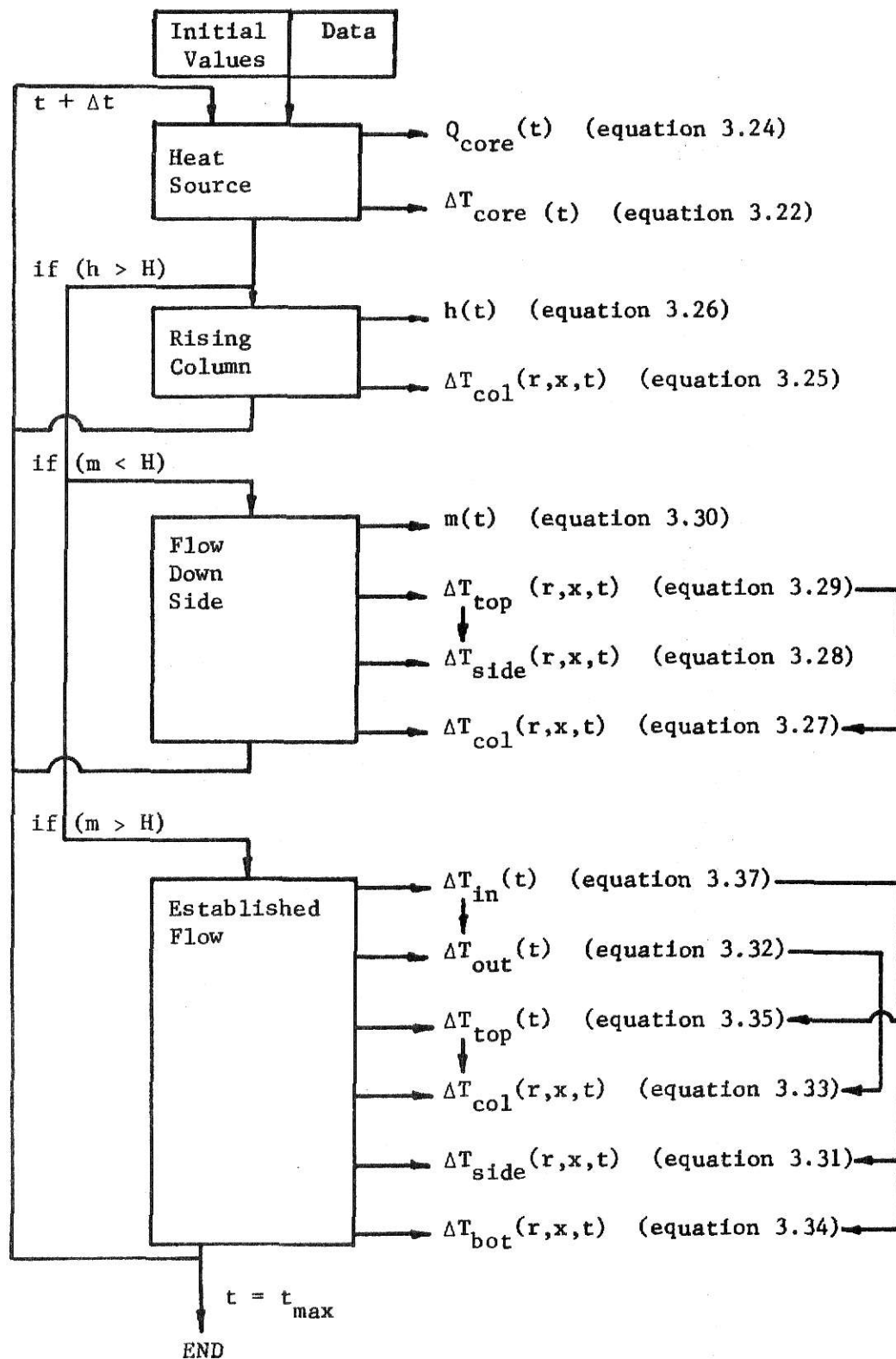


Figure 3.11 Computational Procedure for POOLT

temperatures outside the chimney are calculated using equation 3.31, and the temperatures below the core are calculated using equation 3.34. The temperature outside the reflector is assumed to be equal to the temperature of the water entering the core.

3.3 RESULTS AND CONCLUSIONS

Some of the results from POOLT are plotted in Figure 3.12 and 3.13. Also plotted in Figure 3.12 and 3.13 are some experimental results from Appendix E. From the analysis depicted in Figure 3.10, the time the reactor reaches 100 kw corresponds to one minute after model time zero. The data from Appendix E is plotted using this observation. The model predicts that after 15 minutes (14 minutes after the reactor reaches 100 kw) all the temperatures in the pool except in the region below the core are rising at the same rate. The region below the core has a temperature gradient $1/4$ that in the rest of the pool. The asymptotic temperature gradient predicted by the model is 5.36 deg C/hr or 0.0894 deg C/min. This corresponds to a total heat capacity of 18.65 kwhr/deg C. The experimental data closely follows the results from the model. As time increases the experimental values drop below those predicted by the model. This drop is due to heat losses external to the pool.

The fact that the model predicts a constant heating rate throughout the pool leads to a technique for calibrating the operating power of the reactor. The constant temperature gradient is measured and the operating power is determined by multiplying this gradient times the total heat capacity. Such a technique is called calorimetric calibration and a study of this technique is the subject of Section 4 of this paper.

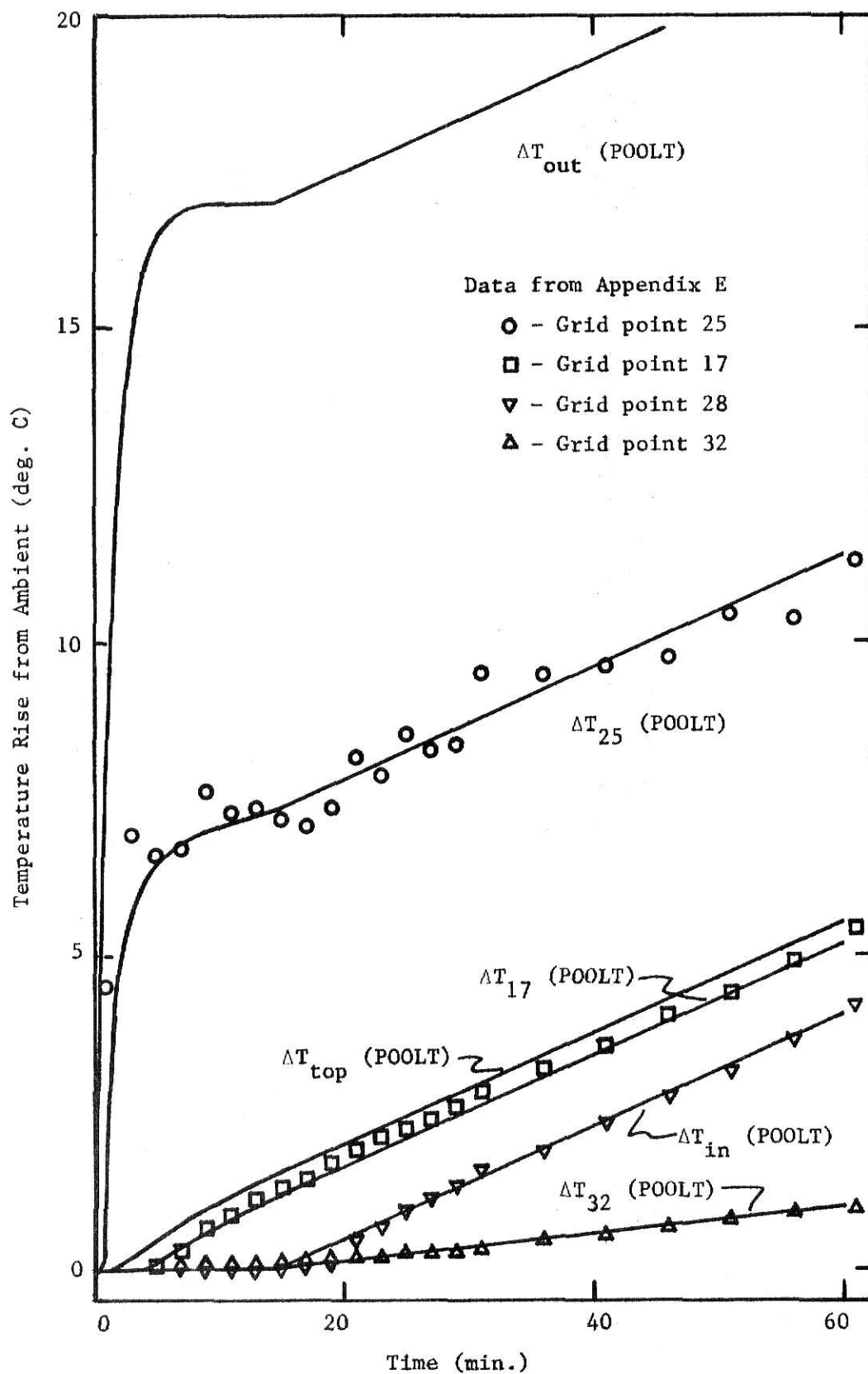


Figure 3.12 Results of POOLT Compared to Experimental Data (for Short Times)

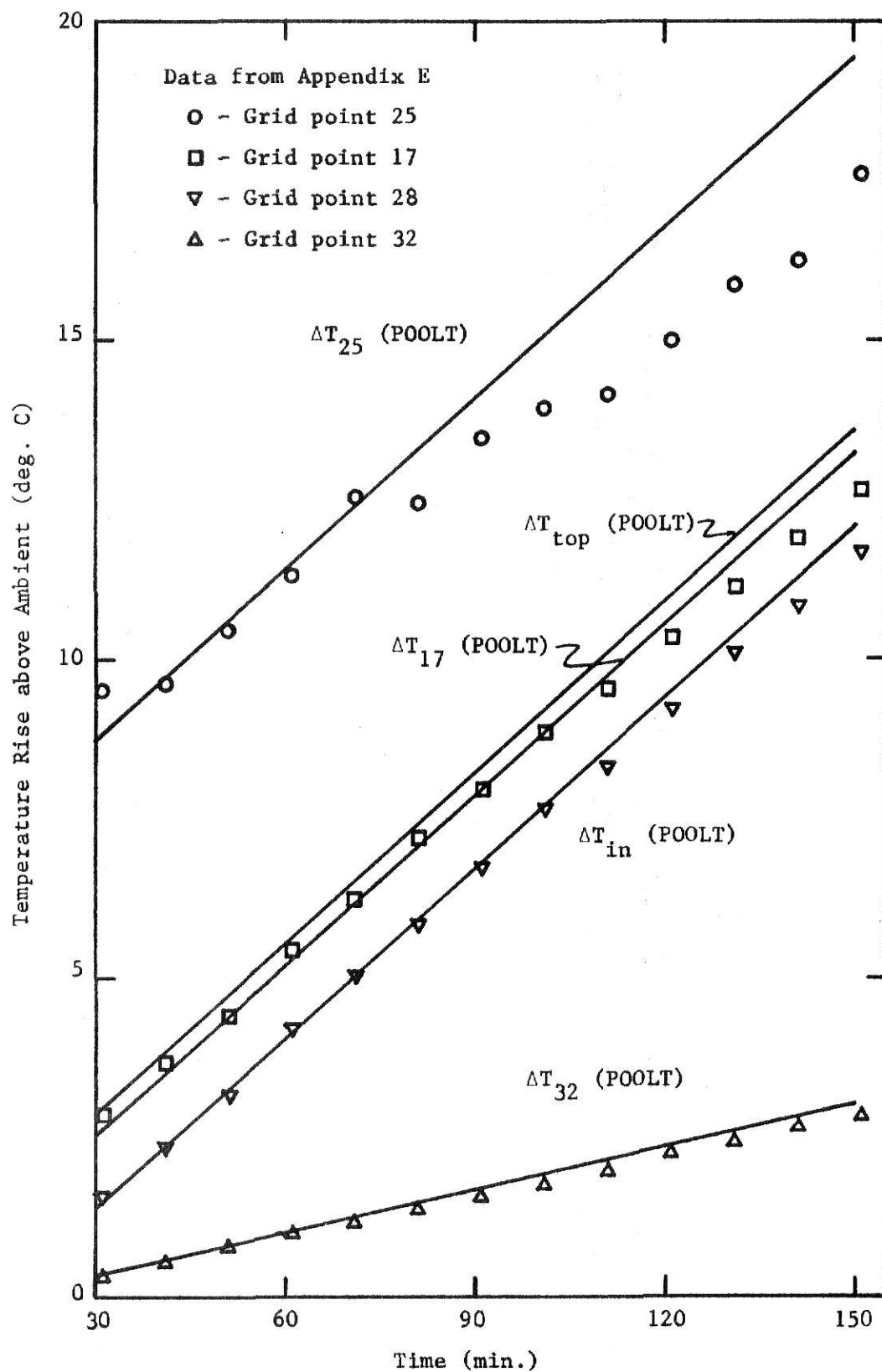


Figure 3.13 Results of POOLT Compared to Experimental Data (for Long Times)

The total heat capacity predicted by POOLT is based on the assumption of no heat losses external to the coolant. Obviously there are heat losses; to the air above the pool even with the pool covers closed, to the concrete shield surrounding the pool, and to the non-water components in the reactor pool. The magnitude of these heat losses greatly affects the validity of the value of total heat capacity predicted by POOLT. The heat losses are small enough that the prediction of constant heating in the pool is not affected. No measurements are made to determine heat losses from the coolant. Also a reliable experimental value for the total heat capacity of the KSUTMII reactor is not available. A theoretical value of 20 kwhr/deg C is reported [7] and a value of 18.85 kwhr/deg C is computed in Section 4 of this work. An experimental value for total heat capacity of the Torrey Pines TRIGA reactor is reported [7] as 19.01 kwhr/deg C. Using either theoretical development or experimental results to determine heat losses, POOLT could be extended to predict the temperatures in the pool with heat losses external to the coolant. It might also be of interest to determine if the models developed in this section can be extended to operating powers other than 100 kw.

4.0 CALORIMETRIC POWER CALIBRATION

4.1 MONITORING THE POWER LEVEL

The Kansas State TRIGA Mark II Nuclear Reactor is designed to be inherently safe. In addition the AEC licensing is designed to insure this safety. Almost all of the safety mechanisms involved with the operation of the reactor are dependent on remote console instrumentation. This instrumentation is intended to reflect the conditions in the reactor vessel. It is important that the mechanism for transmission of data from the reactor vessel to the console be both accurate and precise.

One of the more important parameters monitored at the console is the power level. Changes in power level are indicative of changes in neutron flux and fission density. For a given core configuration a particular power level should correspond to particular fission densities in the core and flux levels throughout the reactor [5]. In a small experimental reactor like the TRIGA, where no attempt is made to utilize the thermal energy, the power level indication is strictly a neutron level monitor.

In the TRIGA Mark II the signals received at the console for all power level monitors originate in ionization chambers. These ionization chambers are positioned around the outside of the reflector. They are not permanently fixed therefore they can be positioned at any depth in the pool. The signal from one compensated ionization chamber is fed into a "log n" circuit and then into a logarithmic power scale on the console. The signal from another compensated ionization chamber is amplified and fed into a linear power scale on the console. A third signal is from an uncompensated ionization chamber. This signal is amplified and is fed into a percent power meter on the console (where 100% corresponds to license maximum steady-state

power level). The power generated in the core is proportional to the neutron flux at the ionization chambers and thus proportional to the signal generated in the ionization chamber. To obtain a read out in terms of power level from the signal generated in the ionization chambers the system must be calibrated. The power monitors on the console have been calibrated during the installation of the reactor and should be recalibrated periodically.

In order to accomplish calibration of the power monitors the actual power level must be determined. There are several techniques for determination of power level.

One technique involves determination of the absolute flux and the flux distribution throughout the core. From this information, the fission rate and in turn the heat produced by fission can be determined. Integrating over all fission sources would give the total thermal power produced by the reactor. Not all the heat produced in fission is recoverable; some is carried into the biological shield by high energy gamma rays. Between 91% and 97% [9] of the heat is eventually deposited in the coolant or reactor components in the pool. Therefore another technique for power determination is the measurement of heat deposition in the reactor vessel.

4.2. CALORIMETRIC POWER CALIBRATION

The measurement of heat deposition in the reactor is analogous to a simple calorimetry experiment. The energy released in fission manifests itself as heat. This heat eventually causes a temperature rise throughout the reactor vessel. When the coolant is not externally cooled the reactor vessel behaves like a large calorimetry can.

A true calorimetry experiment [21] consists of a homogeneous liquid in an insulated container heated uniformly by a constant heat source. If the

liquid is well mixed, the temperature at all points within the container should be the same. Measuring the temperature as a function of time results in a constant temperature gradient. The total heat capacity of the liquid (the heat capacity times the volume) is computed by dividing this gradient by the power of the heat source. Such an experiment is usually performed using small calorimetry vessels that are well insulated and have a low heat capacity. The vessels are filled with a homogeneous liquid with a high heat capacity. The liquid volume is small. The liquid is stirred continuously to maintain a uniform temperature. The heat source (usually an electric heater) is maintained at a constant power by controlling the current and voltage. Usually an accurate mercury thermometer placed near the center of the liquid is used to measure the temperature. Using equipment of this kind very accurate and precise results are obtained with a minimum of effort.

Compare the reactor system with each of the requirements for an ideal calorimeter. The heater, in this case the fission density, can be held constant. In this case the heater power is not known but is rather the unknown to be determined. Comparing further, the analogy does not appear so clear. First the "liquid" contained in the reactor vessel is not homogeneous. In fact it is not even all liquid. The reactor vessel contains mostly water but also contains graphite, aluminum, uranium-moderator mixture, boron, air, and small amounts of other materials, all located throughout the reactor vessel. One technique for overcoming this seemingly immense discrepancy is treating the reactor vessel as if it contained an unknown liquid. An equivalent total heat capacity, which takes into account geometry, physical properties, and volumes of the constituent elements in the reactor vessel, can be determined. Instead of determining an unknown power level, a known power level (using electric

heaters) can be introduced into the reactor vessel. Using the calorimetry procedure the equivalent total heat capacity of the contents of the reactor vessel is determined. This equivalent total heat capacity can be approximated theoretically (see Table 4.1). If obtained correctly the empirical total heat capacity is an important parameter which is necessary for accurate power calibration by the calorimetric technique. Once determined the empirical total heat capacity should not change if the composition and geometry of the reactor vessel is not altered drastically.

Another seeming discrepancy between the reactor vessel calorimetry and true calorimetry is the non-uniform heating in the reactor vessel. This nonuniform temperature throughout the vessel is because of both the large size of the pool and the localized heat source. About 99% [9] of the heat deposited in the reactor vessel is originally deposited in the fuel-moderator mixture. The remainder of the reactor vessel constituents, including most of the water, is heated by the flow of heated water from the core. The non-uniform heating does not pose a real problem. The absolute temperature of the reactor vessel contents is not required, but rather the change in temperature with time. If this temperature gradient is constant throughout the reactor vessel, it is as if the whole vessel is at a uniform temperature. The model developed in Section 3 predicts a constant temperature gradient throughout the pool except in the region below the core.

Still another discrepancy lies in the description of the calorimetry vessel. In the ideal case the vessel consisted of a low heat capacity container encased in insulating material. The reactor vessel is a can constructed of low heat capacity metal, which is encased in concrete. Since concrete is a moderate insulator, the temperature gradient at the outer

Table 4.1 Calculation of Equivalent Total Heat Capacity of Reactor Vessel

Material	Primary Location	Total Volume (ft ³)
Graphite	Reflector (axial and radial), Thermal Column, Thermalizing Column	38.6
Air	Beam ports, Thermalizing Column, Ion Chambers, Specimen rack	7.6
Aluminum	Reflector support, Water-proof coverings	2.0
Fuel-moderator	Fuel elements	0.8
Water	Remainder of the vessel	615.0

Material	Specific Heat (BTU/lb deg F) [9]	Specific Heat weighted) Volume (equivalent water volume) (ft ³)
Graphite	0.165	6.36
Air	0.23	1.75
Fuel-moderator	0.05	0.04
Aluminum	0.215	0.43
Water {	Below Core	0.25*
	Remainder	1.00
Total equivalent Water	1.00	573.68 = 3.58×10^4 lb.

Total Heat Capacity = 18.85 kwhr/deg C ; h = 0.0531 deg C/kwhr

*See Section 3.3.

radius of the vessel never becomes very large; therefore the heat loss through the concrete walls is small. Very little heat is transferred out of the top of the reactor vessel when the pool covers are closed. This is because of the dead air layer formed between the pool surface and the pool covers. Another factor that minimizes the effect of heat losses through the vessel walls is the use of an empirical total heat capacity. If the experiment run to determine the power level is run under conditions (power and duration) similar to those used to determine the total heat capacity, any heat loss through the walls of the vessel should be compensated by the empirical total heat capacity. Even if conditions are not similar, the heat loss after reasonable times should be negligible.

There appears to be a just analogy between the reactor system and the ideal calorimetry experiment. A method of measuring the temperature gradient is next to be developed.

4.3 MEASUREMENT OF THE TEMPERATURE GRADIENT

The major task of this section is to establish a sophisticated and precise system for monitoring the temperature gradient. Once such a system is available, assuming the total heat capacity has also been established, very accurate and precise power calibration can be performed.

4.3.1 TECHNIQUES FOR MEASUREMENT

The original calibration of the Kansas State TRIGA Mark II Reactor has been performed by Gulf Atomix Corporation. The techniques they used involves removing a sample of water from the pool surface and measuring the temperature with a mercury thermometer [7]. These measurements are made every 15 minutes during steady-state operation. This technique has been used for subsequent power calibrations until the time of this work. Even

though the results are satisfactory, this water bucket and thermometer technique seems rather unsophisticated. Therefore a simpler and possibly more precise technique to obtain the temperature gradient is established.

Originally a scheme is devised using thermocouples positioned at various locations in the reactor pool [7]. Thermocouples must be calibrated and their readings are critically dependent on the reference junction temperature. Any temperature variance in the reference junction greatly alters the signal output. Another problem inherent with thermocouples is the weak signal output (in the mv range). In order to obtain an appreciable signal an amplifier is needed. The final reading is then dependent on the stability of the cold junction temperature and the stability of the amplifier.

There are three readily available electrical temperature sensing devices. They are thermocouples, resistance temperature detectors, and thermistors. A comparison of some of the more important characteristics of the devices appears in Table 4.2. Because of its unique feature of great sensitivity over a short span it appears the thermistor is the best device for calorimetry work. Also the high impedance aids in remote monitoring of the temperature without the need for compensating for long leads.

4.3.2 MEASUREMENT OF THE TEMPERATURE GRADIENT USING THERMISTORS

The thermistor is a very temperature sensitive resistor of semi-conductor material. As a resistive branch of an electronic circuit, the thermistor's response to temperature changes causes high bridge imbalance which in turn causes a flow of current. Equipment is available which has inherent a power supply, a bridge network, and a visual display of the current indicating meter calibrated in Centigrade degrees.

Table 4.2 Comparison of Electrical Temperature-Sensing Devices [16]

Parameter	Device		
	RTD	Thermocouple	Thermistor
Accuracy* (repeatability)	0.05 to 0.1 deg F	2 to 15 deg F	0.2 to 2 deg F
Stability*	Less than 0.10% drift in 5 years	1 to 2 deg drift in one year	0.2 to 5 deg drift in one year
Sensitivity*	0.2 to 10 ohms/deg C	10 to 50 micro- volts/deg C	100 to 1000 ohms/deg C
Interchangeability	$\pm 0.5\%$	$\pm 0.75\%$	$\pm 0.5\%$ (3% without selection)
Temperature range	-200 to 1600 deg F	-300 to 3100 deg F	-150 to 550 deg F
Signal Output	1 to 6 v	0 to 60 mv	1 to 3 v
Power (with 100- ohm load)	4×10^{-2} watt	1.6×10^{-7} watt	8.1×10^{-1} watt
Minimum Size	9/32" dia, x 1/4" long	0.015" dia. [†]	0.014" dia.
Unique Features	Greatest accuracy over wide spans; very stable	Greatest economy; highest range	Greatest sensitivity (most accurate for short spans); high impedance minimizes lead effects.

*This data varies with range and point on scale.

[†]Chromel-Alumel wire is available in sizes down to 0.0007" diameter.

4.3.2.1 DESCRIPTION OF THE EQUIPMENT

The actual equipment used in this work is purchased from Atkins Technical, Incorporated, Gainesville, Florida. The equipment consists of the following:

1. Six thermistor probes with 30 feet of attached cable (one brass and five stainless steel "water sounding" probes with Atkins series #3 sensors). The technical parameters appear in Table 4.3.
2. One battery powered temperature indicator with multiple inputs (Atkins model 3L01J (-0.5° to 50.5° C)). More information is given in Table 4.5.
3. One battery powered automatic switchbox (Atkins model A64 adapted to 24 volts DC). More information is given in Table 4.4.
4. One scale expanding recorder adapter (Atkins model A92). More information is found in Table 4.6.

The equipment can be utilized in several ways. The temperature indicator can be used alone with one or more probes. The switchbox can be used to rotate probe readings automatically. The recorder adapter can be used to adjust the temperature indicator output to a recorder's range. The setup used in this work is shown in Figure 4.1.

4.3.2.2 EXPERIMENTAL PROCEDURE

In order to conduct the temperature gradient experiment properly the following procedure should be followed:

1. Several hours prior to running the experiment cool the pool water to approximately 20° C. This insures that the coolant temperature will not exceed license limits during the experiment.

Table 4.3 Characteristics of the Thermistor Sensor and Probe.

#3 Series Thermistor Characteristics [2]			
Temperature (deg C)	Resistance (ohms)	Interchangeability Tolerance (deg. C)	Not more than 1° C error will be caused by extension cables* as long as: (ft)
-50	334,750	± 0.5	More Than 50,000
0	16,430	± 0.2	More Than 50,000
50	1,798.25	± 0.2	5,300
100	336.25	± 0.2	820
150	89.64	± 0.8	170

*Two 18 AWG copper conductors.

"Water Sounding" Probe (Atkins P67-3) [2]
Characteristics

Material - Brass, Stainless Steel

Size - 1/8" dia tip, Weight and cage 1 1/4" dia x 4" H.

Response Time Constant - 4 sec.
(exponential response to
step temperature change)

Cable Length and Connector - 50' vinyl cable market to show immersion
depth, locking connector

Table 4.4 Characteristics of the Automatic Switchbox

Characteristic	Value for Atkins Model #A64 [2]
Number of probes	3, 7, 12, or 20 in sequence
Dwell Time	10 Sec., 1 min., or 5 min. on each point
Power Supply	adapted to 24 v DC

Table 4.5 Characteristics of the Temperature Indicator

Characteristic	Value for Atkins Model #3L01J(-0.5° to 50.5° C) [2]
Accuracy	$\pm 0.1^{\circ}$ C, Instrument checked at five points on each range before shipment, and a calibration card is provided to achieve $- .01^{\circ}$ C accuracy.
Readability	1.02 cm/deg C, 0.102 cm/minor division
Reproducibility	Better than Readability
Speed of Response	Faster than thermal response of probe
Recorder Output	0 to 50 mv into recorders with at least 100,000 ohms input impedance
Scale Linearity	Better than 99%
Electrical Isolation	Circuit fully floating, all probe connections made by screw down rings
Power Supply	Mercury batteries (Mallory RM12R or equivalent), capacity for six weeks continuous operation
Meter movement	Taut band suspension, shock resistant
Temperature Compensation	All circuits compensated to 0.1° C for operation over 0 to 40 deg C ambient temperature
Ranges	five, manual selection
Probe Inputs	Ten, manual selection for reading

Table 4.6 Characteristics of the Recording Adapter

Characteristic	Value for Atkins Model #A92 [2]
Input	0 to 50 mv output of temperature indicator
Output	Variable, set to desired scale expansion
Sensitivity	0.01°C/recorder division or less
Temperature Simulation	Sets temperature indicator at desired temperature for setting up output on recorder

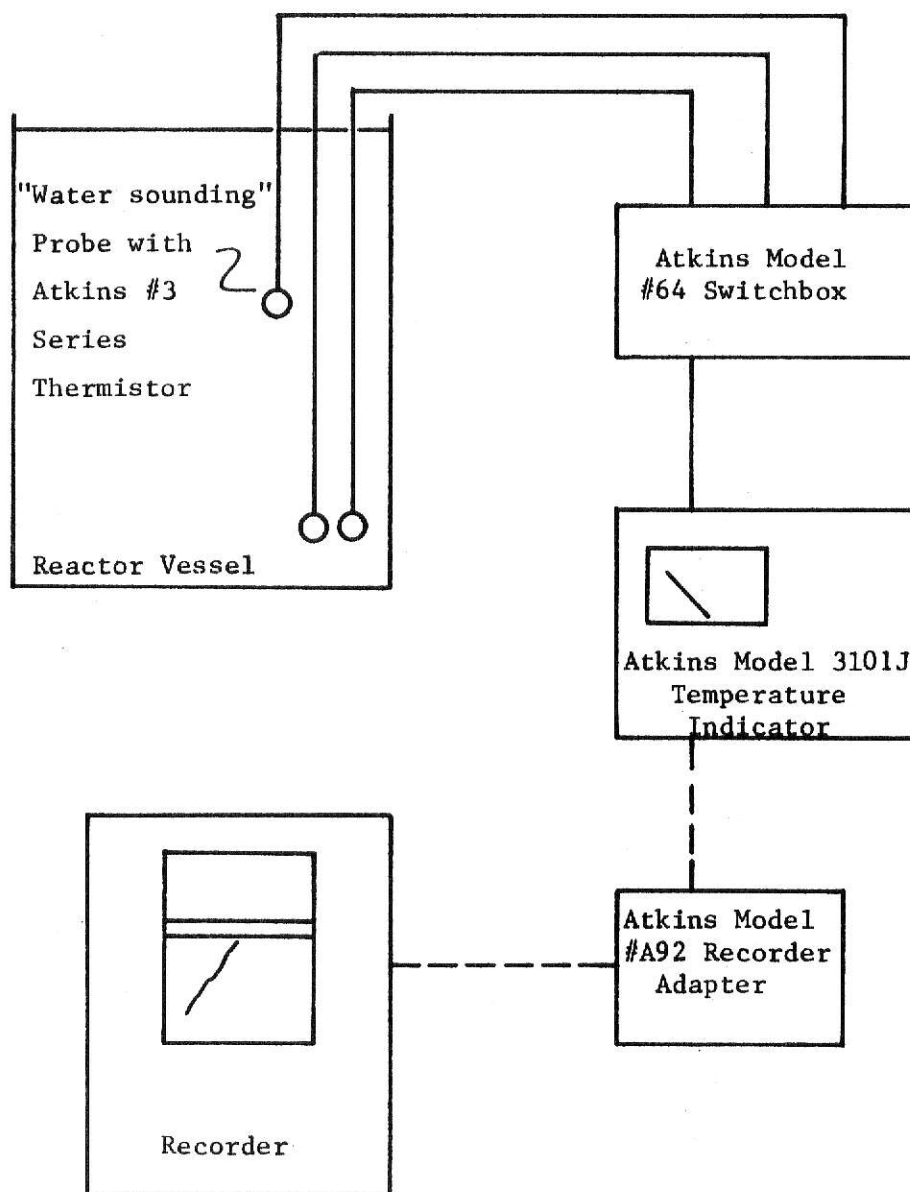


Figure 4.1 Experimental Set-Up for the Temperature Gradient Measurement

2. Allow the water in the pool stand with the cooling off, the underwater lights extinguished, and the reactor shut down until any large temperature gradients are gone.
3. Place the thermistor probe or probes in the desired locations.
4. Connect the probes to the connectors on the temperature indicator and check for proper operation by monitoring the ambient temperature. (If automatic switching of the probes is desired the automatic switchbox should be placed in series between the probes and temperature indicator, Figure 4.1)
5. If a continuous permanent record is desired connect the recorder adapter to the temperature indicator recorder output. Connect the recorder to the recorder adapter. Adjust the output of the recorder adapter using the temperature simulator until the desired temperature scale appears on the recorder.
6. Bring the reactor to steady-state operation at zero power (1 watt).
7. On a rapid period (30 seconds was used in this work) bring the reactor to the desired indicated power level. Hold the power steady at the indicated power level with as little rod movement as possible.
8. Simultaneously with the start to power, continuously monitor all probes.
9. Take temperature readings at convenient equal time intervals.
(In this work readings are taken approximately every 1.5 minutes).
10. Take data for about three hours or until succumbing to exhaustion.
11. Scram the reactor. Disconnect and stow away all equipment.

The printed record from the recorder or the data taken at equal time intervals is analyzed to determine the temperature gradient.

4.3.2.3 ANALYSIS OF RESULTS

If only a recorder trace is made the temperature gradient can be determined by graphically measuring the slope on the recorder trace. Both the time and temperature scale factors must be accurately determined. For a more precise analysis temperatures should be extracted from the record at equal time intervals and analyzed as below.

If the temperature readings are taken visually from the temperature indicator or extracted from the recorder trace, the data is analyzed by least squares analysis as described in Appendix B. Such an analysis is accomplished with the 42 different temperature gradients measured in the experiment described in Appendix E. These gradients are measured at different points throughout the pool. Two measurements of the temperature gradient in the air above the pool are made. Typical results from these measurements appear in Figure 4.2. Figure 4.2 shows the most extreme cases but all the temperature profiles have some differences. The location of the probe such that it accurately and precisely determines the asymptotic temperature gradient is determined from the analysis of data from the experiment described in Appendix E.

4.3.3 PROBE LOCATION

The criteria for determining the best probe location are the following:

1. Linearity over a long time period (asymptotic slope).
2. Accuracy of the asymptotic slope.
3. Variance of the slope (precision).

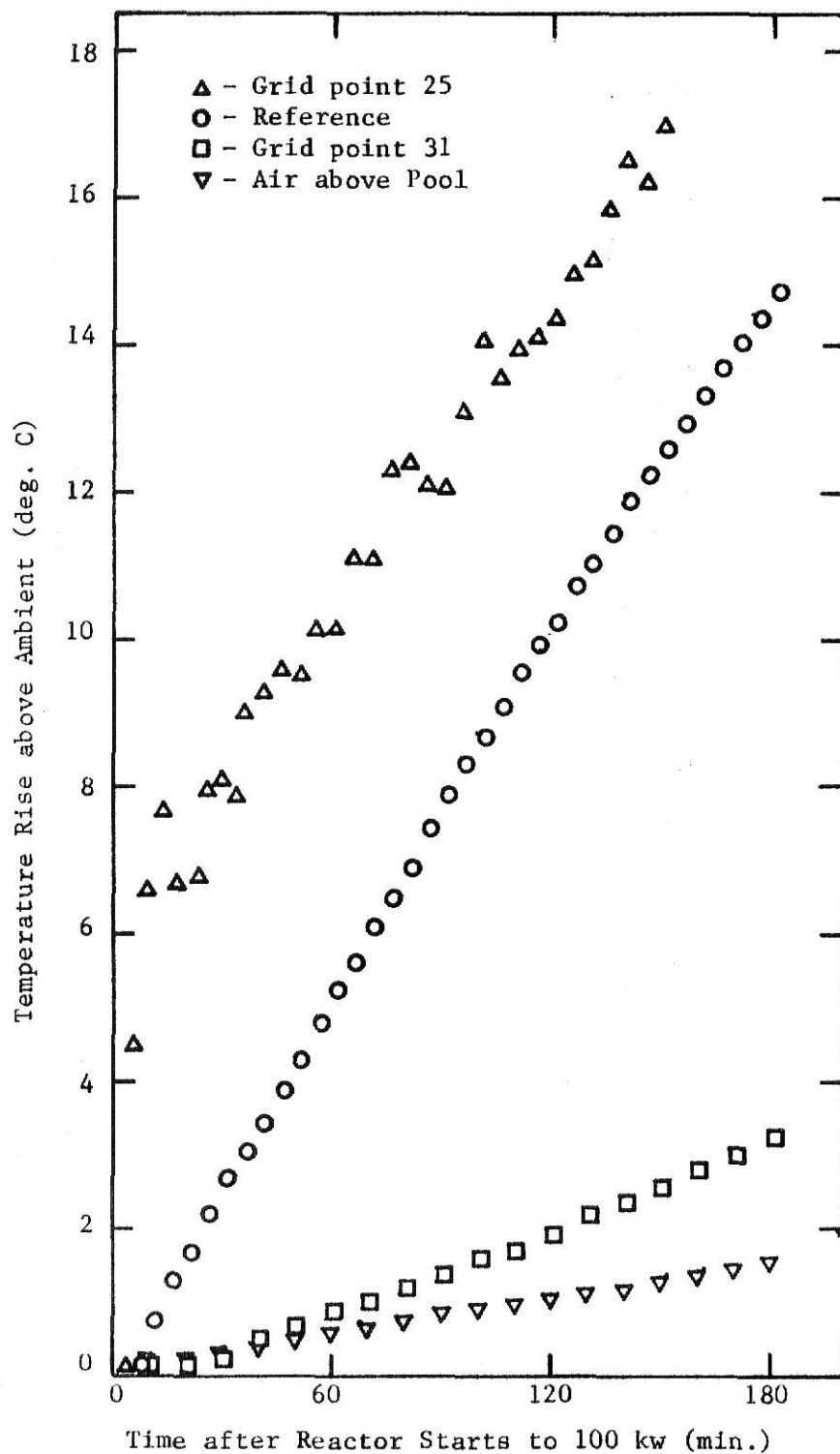


Figure 4.2 Temperature Rise at Various Locations During 100 kw Steady-State Operation

The asymptotic slope is determined by the homogeneity test described in Appendix B. The data from one grid location is divided into ten minute subsets starting from the time the reactor reaches a power of 100 kw. The slope at the i th time is determined by least squares fit of the data from the $i-1$ and i subsets. Therefore each slope except the first is computed using 20 minutes of data. The first slope (at the time the reactor reaches 100 kw) is computed using data from the time the reactor starts to 100 kw till the time it reaches 100 kw (about 6 minutes, Table E.1) plus the first 10 minute subset. These divisions are made such that each slope is computed using at least 10 data points. A computer program, SLOPE, is used to facilitate computation. Typical output from SLOPE appears in Table 4.7, and is plotted in Figure 4.3. The data for all grid locations is plotted and certain grid locations can be eliminated from further analysis from visual inspection of this data. The plot of the SLOPE data for grid location 31, Figure 4.3, is typical of all the grid locations at 1 foot from the pool bottom. The slope may reach an asymptotic slope that this slope is not indicative of constant heating throughout the pool. This further substantiates the analysis in Appendix E that this region below the core is not heated like the rest of the pool. Therefore grid points 30, 31, 32, and 33 were eliminated from further analysis.

The SLOPE data for the remaining grid points is analyzed further. First the obviously deviate slopes are eliminated (e.g., the slope for time 5.75 for grid point 22 in Figure 4.3). Starting with the first apparently "good" slope, that slope and every other slope after it are analyzed together for homogeneity (every other slope is employed so that the data is used only once).

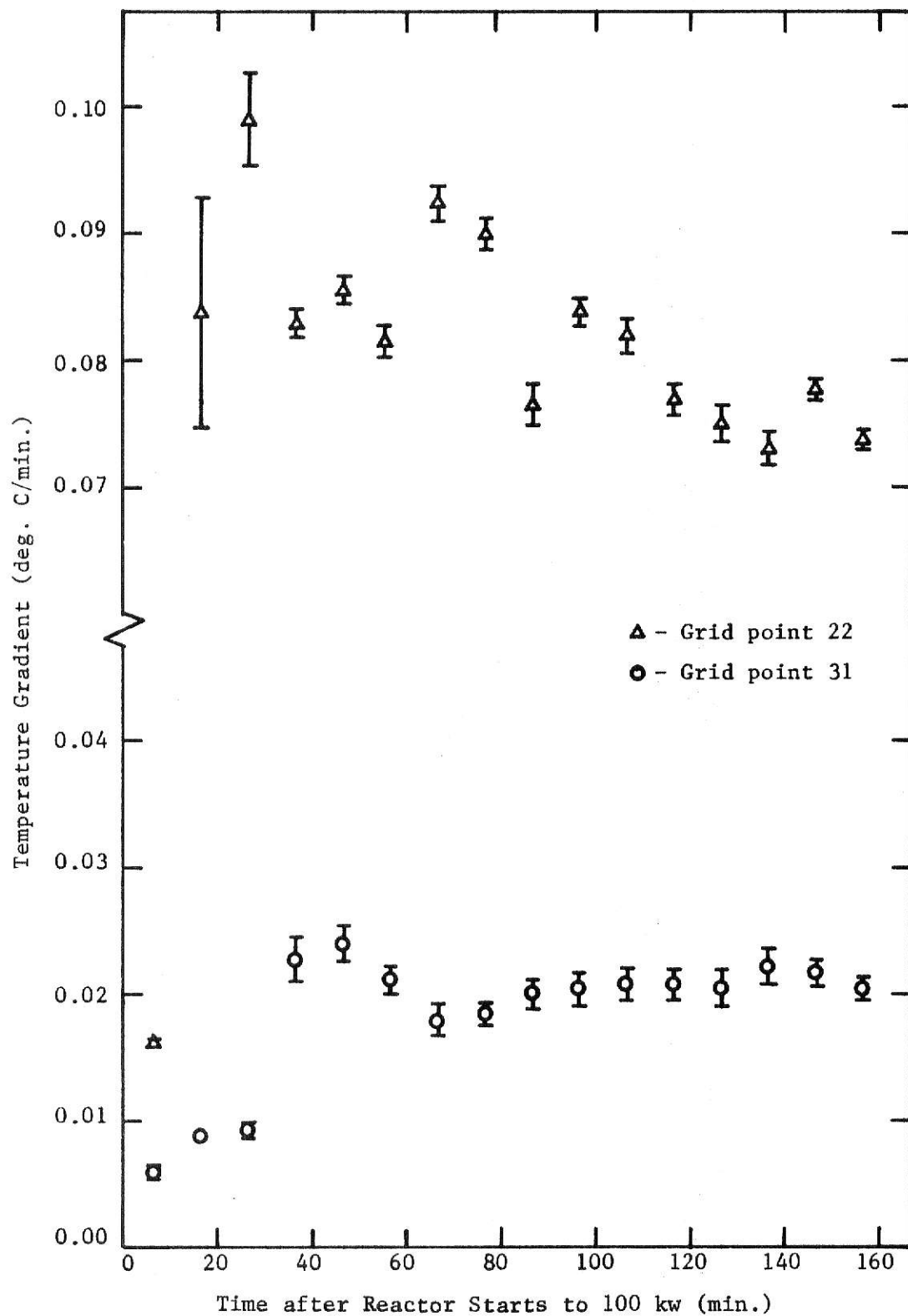


Figure 4.3 The temperature Gradient During 100 kw Steady-State Operation (from SLOPE)

Table 4.7 Typical Results from SLOPE.

Grid point 22				
Time from Start to 100 kW (min.)	No. of Data Points in Subset	Slope (deg. C/min.)	Std. Dev. of Slope (deg. C/min.)	Conditional Std. Dev. (deg. C)
5.75	10	0.001638	0.0003276	0.004404
15.75	13	0.08377	0.009158	0.1829
25.75	14	0.09889	0.003592	0.08022
35.75	14	0.08279	0.001092	0.02438
45.75	13	0.08565	0.001122	0.02240
55.75	13	0.08165	0.001324	0.02644
65.75	14	0.09244	0.001481	0.03307
75.75	14	0.08994	0.001292	0.02886
85.75	13	0.07645	0.001557	0.03109
95.75	13	0.08365	0.001149	0.02293
105.75	14	0.08186	0.001454	0.03247
115.75	14	0.07663	0.001246	0.02781
125.75	14	0.07508	0.001451	0.03239
135.75	13	0.07301	0.001373	0.02741
145.75	13	0.07784	0.0008975	0.01792
155.75	14	0.07383	0.0008345	0.01863

If the slopes are found to be non-homogeneous the last slope is eliminated and the remaining slopes are tested. If this set of data is non-homogeneous the last slope is returned to the set and the first slope is eliminated. If both reduced data sets are non-homogeneous the set with the smallest statistical F test value is retained and the last and first slope in this data set are alternately eliminated and the resulting smaller sets are tested for homogeneity. The number of slopes in the set is selectively reduced until the homogeneity test is passed or less than three slopes remain (i.e. less than 60 minutes of data). In the case where the homogeneity test is never passed the minimum F value is found. The data set remaining after the homogeneity test is passed or the data that results in the minimum F value defines the asymptotic slope. The average weighted slope and its standard deviation are computed for this asymptotic slope. A computer program, STRAT?, is used to facilitate the computations. The results from STRAT? appear in Table 4.8.

On the basis of non-linearity grid points 3 and 4 are eliminated from further analysis. This non-linearity is expected in the region just below the water line because of the mixing occurring there and heat losses through the pool surface.

The majority of the standard deviations of the average asymptotic slope are in the range 0.009-0.0017 deg C/min. The grid points with standard deviations outside this range are 8, 9, 10, 14, 15, 19, 20, 24, and 25. All these points are in the chimney that forms above the core. There are two possible causes for imprecision in measurements taken in the chimney. First the warm water leaving the core does take some time to become well mixed; thus real temperature discontinuities may exist. Secondly because of the rapid moving water in the chimney the probes may move. Any movement will

Table 4.8 Results from STRAT?

Grid Point	Slope (deg C/min.)	Std. Dev. of Slope (deg C/min.)	Asymptote		Total (min.)
			Start (min.	End from start to 100 kw)	
1	0.09106	0.001669	5.80	85.80	95.8
2	0.08664	0.001251	5.80	105.80	115.8
3	---	---	--	---	<60
(min. F)	0.09028	0.001687	5.80	85.80	95.8
4	---	---	--	---	<60
(min. F)	0.09340	0.001650	15.80	95.80	100
5	0.08407	0.001428	35.80	135.80	120
6	0.8894	0.001645	5.03	65.03	75.03
7	0.08755	0.001484	5.03	85.03	95.03
8	0.08355	0.001805	55.03	115.03	80
9	0.08544	0.001808	35.03	135.03	120
10	0.09571	0.003469	15.03	95.03	100
11	0.08366	0.001215	95.85	135.85	60
12	0.09205	0.001296	5.85	125.85	135.85
13	0.08674	0.001583	45.85	125.85	100
14	0.08968	0.002386	15.85	155.85	160
15	0.09204	0.002925	25.85	145.85	140
16	0.08618	0.000914	37.0	77.0	60
17	0.08630	0.001247	37.0	77.0	60
18	0.08600	0.001345	47.0	107.0	80
19	0.08540	0.002516	7.0	147.0	157
20	0.08681	0.005527	57.00	137.0	100

Table 4.8 (continued)

Grid Point	Slope (deg C/min.)	Std. Dev. of Slope (deg C/min.)	Asymptote		Total (min.)
			Start (min.	End from start to 100 kw)	
21	0.08296	0.001521	15.75	115.75	120
22	0.08308	0.001482	15.75	115.75	120
23	0.08332	0.001481	15.75	115.75	120
24	0.08631	0.002661	25.75	85.75	80
25	0.07790	0.008368	15.75	155.75	160
26	0.08292	0.001549	26.00	106.00	100
27	0.08444	0.001084	26.00	146.00	140
28	0.08528	0.001238	26.00	126.00	120
29	0.08542	0.001218	26.00	126.00	120

cause discontinuities in the temperature indication. Whatever the cause these grid locations are eliminated from further analysis on the basis of imprecision.

The final criteria for location of the probe is accuracy of the asymptotic slope. To obtain an index of accuracy the reference data from the experiment in Appendix E is analyzed. The first two hours of reference data for each run is analyzed using STRAT?. The results appear in Table 4.9. The resultant slopes are considered to be the "true" slope for each run. The asymptotic slopes for the remaining grid points are compared with the "true slope" during the same run using the statistical "t test." The results from this analysis appear in Table 4.10. Grid points 1, 11, 13, 26, and 27 are significantly deviate from the "true" slope, therefore these points are eliminated on the basis of inaccuracy.

The grid points remaining are all "good" probe locations. The region defined by these grid points appears in Figure 4.4. This "best" region for probe location eliminates any regions where temperature gradients would not satisfy one or more of the criteria of linearity, precision, and accuracy. Generally the probe should be located 6 to 18 inches from the outside pool wall and 5 to 15 feet from the pool bottom. This 10 square foot cross section defines the "best" location.

4.4 CONCLUSIONS

When determining the power by calorimetric techniques the procedure for conducting a temperature gradient experiment described in Section 4.3.2.2 should be followed. In addition:

1. Place the termistor probe within the "best" region (Section 4.3.3).
2. After about an hour of linear temperature rise graphically determine the asymptotic slope.

Table 4.9 Analysis of Reference Data

Run No.	Slope (deg. C/min.)	Std. Dev. of Slope (deg. C/min.)	F Value	F (0.05)
1	0.09009	0.001364	0.9992	2.29
2	0.08696	0.001179	1.996	2.29
3	0.08535	0.001343	0.8811	2.29
4	0.08626	0.001181	2.825	2.29
5	0.09157	0.001237	4.208	2.29
6	0.08860	0.001045	5.738	2.29
7	0.08664	0.001078	2.698	2.29

Table 4.10 Comparison of Asymptotic Slopes and "True" Slopes

Grid Point	Asymptotic Slope (deg C/min.)	"True" Slope (deg C/min.)	Std. Dev. Asymp. Slope (%)	t Value
1	0.09106	0.08664	1.83	2.648
2	0.08664	0.08664	1.44	0.000
5	0.08407	0.08664	1.70	-1.800
6	0.08894	0.08860	1.85	0.207
7	0.08755	0.08860	1.70	-0.708
11	0.08366	0.09157	1.45	-6.510
12	0.09205	0.09157	1.41	0.370
13	0.08674	0.09157	1.82	-3.051
16	0.08618	0.08626	1.06	-0.088
17	0.08630	0.08626	1.44	0.032
18	0.08600	0.08626	1.56	-0.193
21	0.08296	0.08535	1.83	-1.571
22	0.08308	0.08535	1.78	-1.532
23	0.08332	0.08535	1.78	-1.371
26	0.08292	0.08696	1.87	-2.608
27	0.08444	0.08696	1.28	-2.325
28	0.08528	0.08696	1.45	-1.357
29	0.08542	0.08696	1.43	-1.264
$t(0.05) = \pm 2.000$				

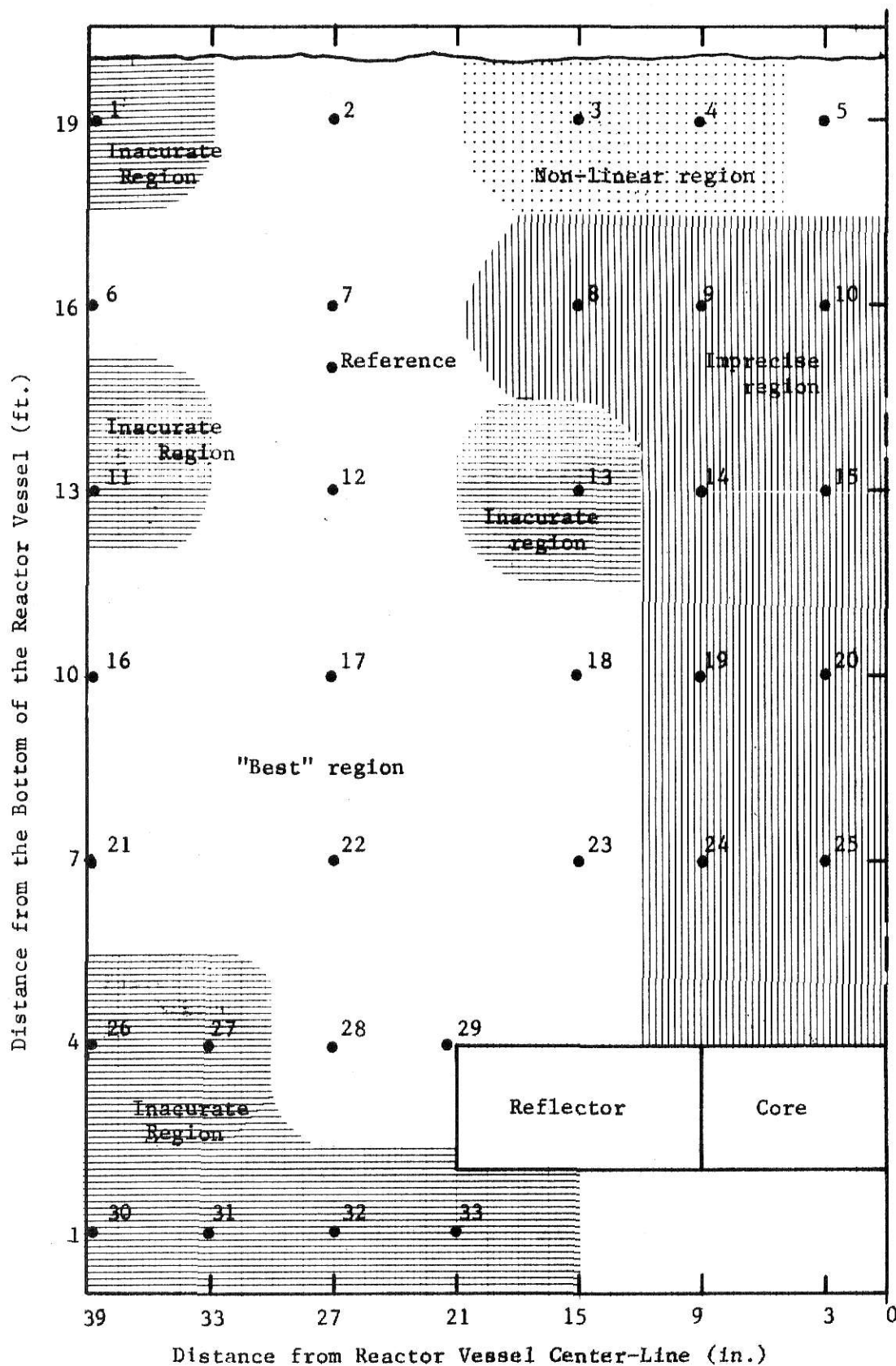


Figure 4.4 Cross section of the Reactor Vessel Showing the "Best" Region for Probe Location

3. Using the total heat capacity factor determine the actual power.

(Actual power (kw) = temperature gradient (deg. C/hr.) x total heat capacity (kw hr./deg C)).

4. Manually adjust the ion chambers one at a time until all three power meters indicate the actual power.

If further analysis of the data is desired the temperature data can be analyzed using least squares analysis. A computer program POWCAL is designed to facilitate this analysis (see Appendix F). For example if the data for grid point 17 in the experiment in Appendix E is taken as a power calibration experiment the asymptotic slope is graphically determined as in Figure 4.5. The ion chambers are adjusted to indicate 103.3 kilowatts. The data analyzed by POWCAL yields the results shown in Figure 4.6.

There are several areas where further study would be desirable. First all the analysis in this work is done at 100 kw. Since the power calibration is a one point calibration it could always be done at a nominal 100 kw. However this restriction may not be necessary. This study can be extended to other power levels and the limits, if any, of the application of calibration using calorimetry could be determined. Another area of study involves the sophistication of the read out system. With the strong electrical output of the temperature indicator as input, an analog system could be designed to continuously monitor the temperature gradient. To further sophisticate the system the temperature gradient signal could be adjusted to appear at the console as a visual readout in terms of power level. Finally in order to determine the accuracy and precision of the power level resulting from the calorimetric calibration experiment the total heat capacity factor used to convert temperature gradient to power level must be accurately determined and a precision index assigned.

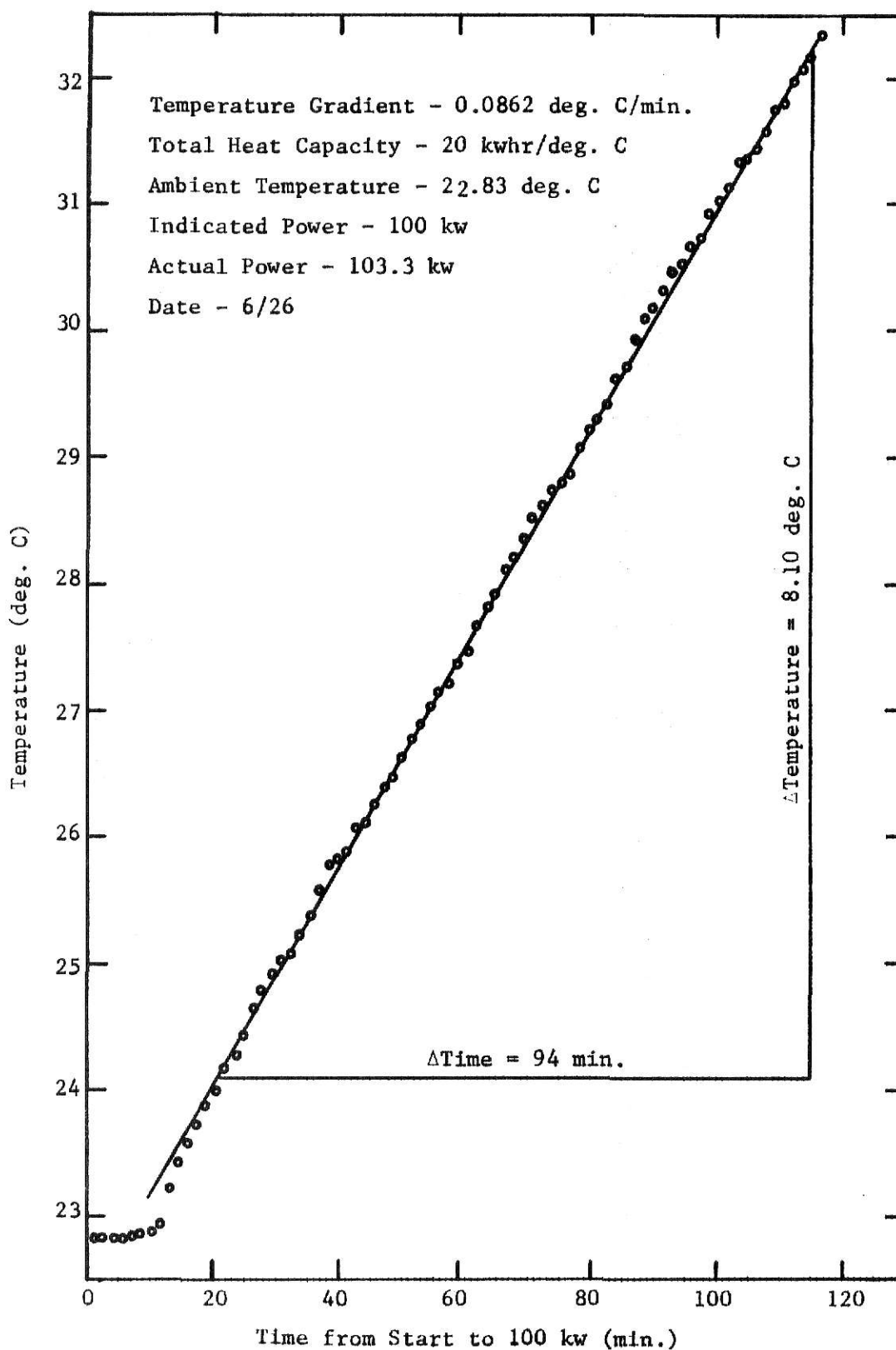


Figure 4.5 Graphical Determination of the Power Level from Calorimetry Data

LEAST SQUARE FIT TO POWER CALIBRATION DATA

DATE 6-26 PROBE NO. - 2

TEMPERATURE GRADIENT INFORMATION

NUMBER OF DATA POINTS ON ASYMPTOTE	-	64	
ASYMPTOTIC SLOPE	-	8.647E-02	DEG. C/MIN.
CONDITIONAL STD. DEV.	-	5.128E-02	DEG. C
STD. DEV. OF SLOPE	-	2.350E-04	DEG.C/MIN.

TOTAL HEAT CAPACITY INFORMATION

TOTAL HEAT CAPACITY	-	2.000E 01	KWHR/DEG. C
STD. DEV. OF HEAT CAPACITY	-	0.000E-01	KWHR/DEG. C

POWER INFORMATION

ACTUAL POWER	-	1.038E 02	KW
STD. DEV. OF POWER	-	2.820E-01	KW

Figure 4.6 Determination of the Power Level from Calorimetry Data using POWCAL

Figure 4.6 (continued)

LEAST SQUARE FIT TO POWER CALIBRATION DATA

DATE 6-26 PROBE NO. - 2

DATA

POINT NO.	TIME	TEMPERATURE RISE
1	1.24	0.00
2	2.72	0.00
3	4.19	0.00
4	5.67	0.01
5	7.15	0.01
6	8.62	0.02
7	10.10	0.04
8	11.58	0.11
9	13.05	0.39
10	14.53	0.60
11	16.01	0.74
12	17.48	0.90
13	18.96	1.05
14	20.44	1.17

START ASYMPTOTIC DATA

15	21.91	1.35
16	23.39	1.44
17	24.87	1.61
18	26.34	1.82
19	27.82	1.95
20	29.30	2.09
21	30.77	2.20
22	32.25	2.25
23	33.73	2.39
24	35.20	2.55
25	36.68	2.74
26	38.15	2.94
27	39.63	2.99
28	41.11	3.05
29	42.58	3.23
30	44.06	3.29
31	45.54	3.43
32	47.01	3.56
33	48.49	3.65
34	49.97	3.80
35	51.44	3.95
36	52.92	4.06
37	54.40	4.19
38	55.87	4.33
39	57.35	4.40
40	58.83	4.55
41	60.30	4.64
42	61.78	4.85
43	63.26	4.99
44	64.73	5.10
45	66.21	5.29
46	67.69	5.39
47	69.16	5.54

Figure 4.6 (continued)

48	70.64	5.70
49	72.12	5.80
50	73.59	5.92
51	75.07	5.97
52	76.55	6.04
53	78.02	6.24
54	79.50	6.39
55	80.98	6.47
56	82.45	6.60
57	83.93	6.80
58	85.41	6.89
59	86.88	7.11
60	88.36	7.27
61	89.84	7.36
62	91.31	7.49
63	92.79	7.64
64	94.27	7.70
65	95.74	7.84
66	97.22	7.91
67	98.70	8.11
68	100.17	8.19
69	101.65	8.31
70	103.13	8.51
71	104.60	8.53
72	106.08	8.61
73	107.56	8.75
74	109.03	8.92
75	110.51	8.97
76	111.98	9.15
77	113.46	9.24
78	114.94	9.34

END ASYMPTOTIC DATA

79	116.41	9.51
80	117.89	9.59
81	119.37	9.79
82	120.84	9.89
83	122.32	10.00
84	123.80	10.12
85	125.27	10.17
86	126.75	10.31
87	128.23	10.47
88	129.70	10.53
89	131.18	10.70
90	132.66	10.75
91	134.13	10.88
92	135.61	11.08
93	137.09	11.16
94	138.56	11.20
95	140.04	11.37
96	141.52	11.52
97	142.99	11.69
98	144.47	11.70
99	145.95	11.85
100	147.42	11.94
101	148.90	12.05
102	150.38	12.20
103	151.35	12.30
104	153.33	12.43

5.0 REACTIVITY OF REACTOR SOURCES

5.1 ANALOG SIMULATION OF THE REACTOR

The development of a model to predict the reactivity of reactor sources involves the point reactor kinetics equations. The final formulation of the point reactor kinetics equations [20] appear below:

$$\frac{dn}{dt} = \frac{\rho - \beta}{\ell} n + \sum_{i=1}^m \lambda_i \bar{C}_i + S_o, \quad (5.1)$$

and

$$\frac{d\bar{C}_i}{dt} = \frac{\beta_i}{\ell} n - \lambda_i \bar{C}_i \quad i = 1, 2, \dots, m; \quad (5.2)$$

where ρ = reactivity = $(k_{\text{eff}} - 1)/k_{\text{eff}}$,
 β = total delayed neutron fraction,
 ℓ = neutron generation time,
 n = neutron density,
 \bar{C}_i = i th precursor density,
 λ_i = i th precursor decay constant,
 β_i = i th precursor delayed neutron fraction,
 S_o = source strength,

and m = number of delayed neutron groups.

This system of $m+1$ linear equations in $m+1$ unknowns must be solved using the characteristics of the TRIGA reactor. A simple and graphic exact solution to these equations can be found using analog computer techniques. To facilitate analog simulation and to isolate source effects, the kinetic equations are written in the following form:

$$\frac{dn}{dt} = \frac{\rho_R}{\ell} n - \sum_{i=1}^m \frac{d\bar{C}_i}{dt} + S_o + \frac{\rho_S}{\ell} n , \quad (5.3)$$

$$\text{and} \quad \frac{d\bar{C}_i}{dt} = \frac{\beta_i n}{\ell} - \lambda_i \bar{C}_i \quad i = 1, 2, \dots, m ; \quad (5.4)$$

where ρ_R = reactivity of the rods,

and ρ_S = reactivity of the source.

The actual network used to solve these equations is shown in Figure 5.1, in standard analog notation [10].

Instead of employing an integrator and a set of potentiometers to simulate the kinetics of each precursor group, a network of passive elements is utilized. This network, with built in passive elements, is available from the manufacturer of the analog system [8]. The values of these passive elements are determined from the delayed neutron parameters for U-235. No provisions are provided for adjusting these parameters in order to reflect values more accurate than those used by the manufacturer other than replacing the electrical components. It is felt, however, that the values used by the manufacturer are close enough to the values reported in ANL-5800 [1] to preclude changing the electrical components. A more complete description of the circuit theory involved and the parameters used in the simulator appears in Appendix A.

The TRIGA Mark II reactor at Kansas State University, as is described in Section 2.0 of this paper, utilizes an external source which can easily be removed from the core. Reactivity losses because of temperature and Xenon buildup become noticeable at high powers [1,19]. Therefore only in the low power region does only the source affect steady-state operation.

Thus with the source removed, steady-state operation is indicative of a critical configuration at low power levels.

It is important to emphasize that critical configuration denotes not only fuel loading but also control rod position. The three control rods are independent in movement but not in worth. Because of flux perturbations in conjunction with rod movement and resulting shadowing effects on the other rods, there is no guarantee of criticality at combinations of rod positions indicating the same reactivity withdrawal. Hence, it is important that all data be taken close to rod positions used to determine the rod calibration curve.

Zero-power criticality is represented by zero reactivity feedback in the simulator. Therefore referring to Figure 5.1, when simulating zero-power criticality the SOURCE switch is in the OUT position (open) and the RODS switch is in the ZERO position (open). The INITIAL CONDITION potentiometer in unit 2.475 (see Appendix A) is used to set the initial voltage corresponding to the steady-state power level. The maximum voltage output of the analog unit is 10 volts and the noise level limits the minimum voltage to about 0.01 volts. As is described in Appendix A the proportionality factor for neutron density (i.e. power level) is set at 10 volts/watt. Therefore the effective range of study is confined between 1 watt and 0.001 watt. Within this range the total variety of source effects can be simulated. Briefly what has been determined so far is that with the SOURCE and RODS switches open the analog unit is capable of simulating the reactor in a zero-power criticality configuration operating at any given power level between 0.001 watt and 1 watt.

The simulation of reactivity insertions is accomplished with the combination of potentiometer #1 and the RODS switch. To simulate a step insertion of reactivity potentiometer #1 is set at the desired reactivity. The analog unit is then placed in the "OPERATE mode." The indicated power should then be constant at the steady state level preset by the INITIAL CONDITION potentiometer. The step insertion is simulated by placing the RODS switch in the UP position for a positive reactivity insertion and in DN position for negative reactivity insertion. Inverter 5 is added to the basic set up shown in Appendix A in order to simulate negative reactivity insertions. A test of the total reactor simulator appears in Figure 5.2. The manufacturer provided a set of test curves for step insertions of $-0.0005 \delta k/k$ and $-0.0025 \delta k/k$. Using the same scaling factors, the experimental test curves and the manufacturer's curves compare favorably. This result supplies positive evidence that the system functions properly.

It is not necessary to make reactivity insertions step-wise; in fact the reactivity insertions in the reactor are not step-wise. Realistic continuous insertions are easily simulated. For a continuous insertion potentiometer #1 is set to zero. Then as in the step insertion case the analog unit is placed in the "OPERATE mode." Depending on the desired kinetic effect, the RODS switch is placed in the UP or DN position and potentiometer #1 is manipulated until the desired effect is achieved. Using this technique the steady-state power level is adjusted in the reactor simulator. As long as the SOURCE switch is open steady-state operation is only achieved when potentiometer #1 is set at zero or the RODS switch is in the ZERO position.

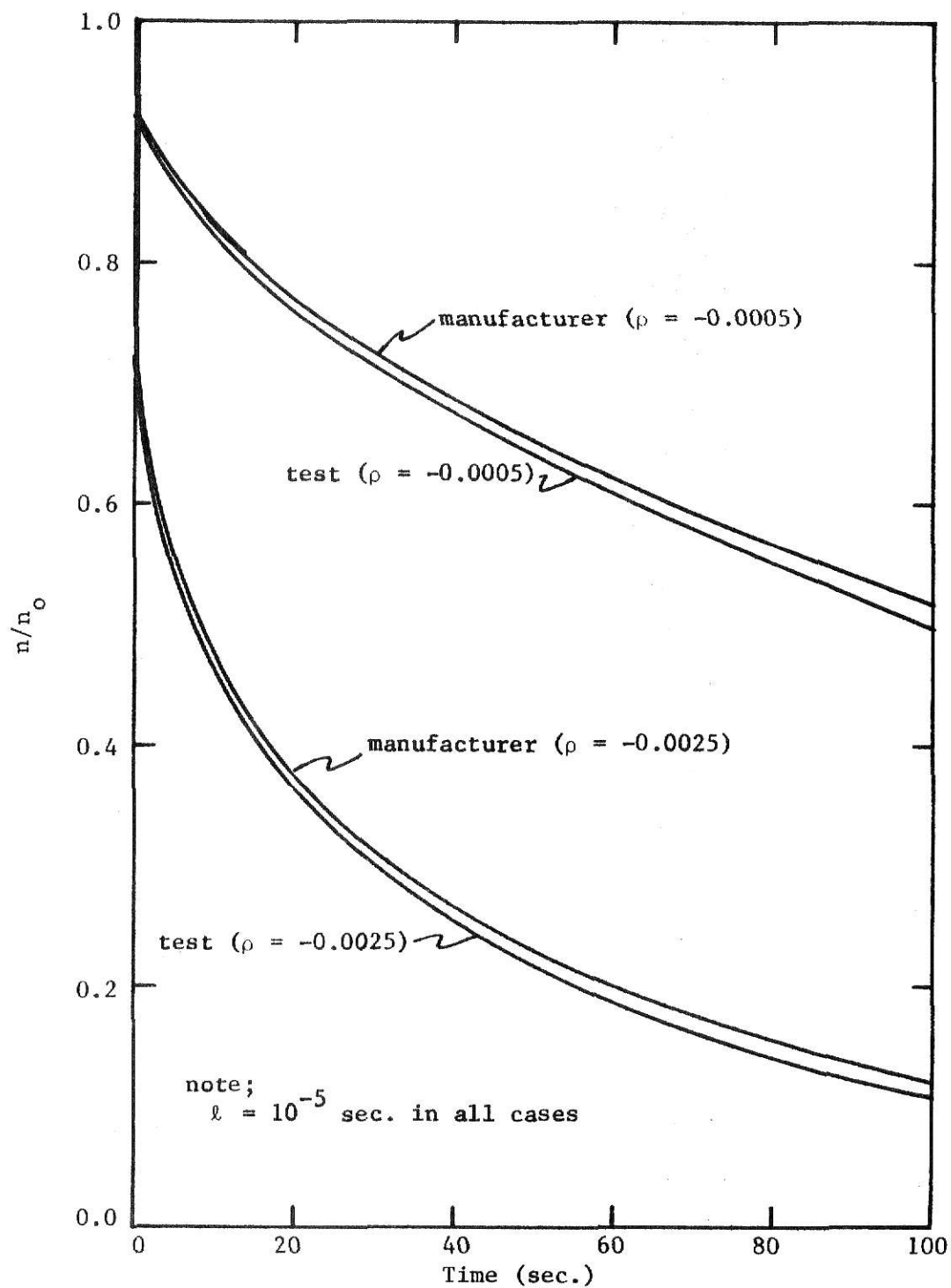


Figure 5.2 Comparison of Test Curves and Manufacturer's Data

In summary, both step and continuous reactivity insertions are accomplished by setting the desired polarity of reactivity with the RODS switch and by adjusting the amplitude of the reactivity insertion with potentiometer #1. The relationship between potentiometer setting and the magnitude of reactivity is described in Appendix A and a brief summary is in Table 5.1.

Finally the simulation of external source removal and insertion is accomplished utilizing the SOURCE switch. When the analog unit is in the "OPERATE mode," independent of the kinetics already being simulated, placing the SOURCE switch in the IN position simulates step insertion of the source. Conversely placing the SOURCE switch in the OUT position simulates step removal of the external source. The source affects the reactor in two ways. First, the source and source holder assembly act as a poison and have a negative reactivity effect (a feedback effect similar to the rods). The magnitude of this effect is denoted as the source worth. Second, the neutron output of the source acts as a constant input (no feedback effect). The magnitude of this effect is denoted as source strength. Potentiometer #2 is used to adjust the source worth. Potentiometer #3 is used to adjust the source strength. The derivation of the relationships between these potentiometer settings and the effects of the source they represent is described in Appendix A. Using the data from Appendix A, Tables 5.2 and 5.3 are constructed for the analog system shown in Figure 5.1.

Note that the effect of potentiometer #2 is decreased 10-fold by reducing the voltage by a factor of 0.1 in summing junction 3. Also the effect of potentiometer #3 is decreased 100-fold by reducing the voltage by a factor of 0.1 in summing junction 3 and 0.1 in the inverter (amplifier 6). In order to make the source worth negative the basic set up of Figure A.1, Appendix A,

Table 5.1 The Relationship between Potentiometer Setting and Reactivity for Potentiometer #1 (Rod Simulator)

Potentiometer Setting	$(\delta k/k)$	Reactivity (ρ_R) (\$)
1.0	0.0050	0.767
0.5	0.0025	0.383
0.1	0.0005	0.077

Table 5.2 The Relationship between Potentiometer Setting and Source Worth for Potentiometer #2

Potentiometer Setting	$(\delta k/k)$	Source Worth (ρ_S) (\$)
1.0	-0.00050	-0.0767
0.5	-0.00025	-0.0383
0.1	-0.00005	-0.0077

Table 5.3 The Relationship between Potentiometer Setting and Source Strength for Potentiometer #3

Potentiometer Setting	Source Strength (S_0) (watts/sec.)*
1.0	0.50
0.5	0.25
0.1	0.05

*The unit watts/sec. is explained on page 126, Appendix A.

is altered. The changes can be seen in Figure 5.1. The simulation of source removal and insertion is accomplished simply by selecting the OUT and IN positions of the SOURCE switch respectively assuming potentiometers #2 and #3 are set properly.

5.2 EXPERIMENTAL DETERMINATION OF SOURCE PARAMETERS

In order to simulate the actual TRIGA Mark II Reactor at Kansas State University the source parameters, source worth and source strength, must be determined. These parameters are used to set potentiometers #2 and #3.

5.2.1 STEADY-STATE DETERMINATION OF SOURCE WORTH

Since the source worth effect is power dependent (linearly proportional to power) and the source strength effect is not dependent on power, the two effects can be separated. At higher power levels the source strength effect is negligible. At higher power, withdrawal or insertion of the source is equivalent to withdrawal or insertion of reactivity equal to the worth of the source. Using this information an experiment is constructed to determine the source worth. The normal technique employed at Kansas State University to directly measure the worth of reactivity insertions is the positive period method. This entails introducing the reactivity as nearly step-wise as possible and measuring the resultant asymptotic period. Unfortunately, at power levels high enough to insure negligible source neutron contribution the temperature coefficient of reactivity becomes significant [19]. Therefore an indirect technique is employed to determine the source worth. The technique is indirect because it relies on the control rod calibration curves for the reactor. The experiment involves achieving steady-state operation at

100 watts with the source in and recording the rod positions. The source is then removed and steady-state operation is achieved at exactly the same power level and again the rod positions are recorded. This procedure is repeated ten times. The experiment is repeated at 1 and 10 kilowatts. In order to minimize the difficulty in reproducing rod positions only the reg rod is moved during the experiments. The differences in reg rod positions between source-in and source-out are converted to reactivity using the control rod calibration curves. This reactivity value represents the worth of the source. The average value of the source worth is computed at each power level. The standard deviations of these observed values are determined using the root mean square deviations. All the raw data and computed values appear in Table 5.4.

From the analysis of variance in Table 5.5, it appears that the values of the source worth at the three power levels are not significantly different. This indicates all three sets of data are taken with the power level high enough to mask source strength effects. Since this is the case the estimate for source worth is recomputed using the pooled data. This compilation is presented in Table 5.6.

5.2.2 STEADY-STATE DETERMINATION OF SOURCE STRENGTH.

The source strength effect is most dominant at very low power levels. Therefore an experiment is performed at 0.01 watt to determine the source strength effect. The experiment is similar to the experiment performed to determine source worth, in that source-in and source-out steady-state operation is achieved. Steady-state operation is achieved with the source out and the corresponding shim and reg rod positions are recorded. The

Table 5.4 Source Worth Data from Steady-State Experiments

Source Worth Data (100 watts)				
Steady-State* Rod Positions				
Shim Position	Reg Position (Worth [†])		$\Delta\rho$ (\$)	Deviation from the mean (\$)
	Source In	Source Out		
525	401.5 (79.3)	387.0 (84.5)	-0.052	-0.0056
525	397.1 (81.0)	385.4 (85.0)	-0.040	+0.0064
525	398.5 (80.5)	385.3 (85.0)	-0.045	+0.0014
525	398.0 (80.6)	385.0 (85.2)	-0.046	+0.0004
525	403.5 (78.6)	390.8 (83.2)	-0.046	+0.0004
525	402.0 (79.2)	388.9 (83.9)	-0.047	-0.0006
525	401.2 (79.5)	388.5 (84.0)	-0.045	+0.0014
525	402.5 (79.0)	390.2 (83.3)	-0.043	-0.0034
525	404.5 (78.3)	390.4 (83.3)	-0.050	-0.0036
525	402.1 (79.0)	388.5 (84.0)	-0.050	-0.0036
$\overline{\Delta\rho} = 4.64 \pm 0.11\text{¢}$			$\$ = 0.0036$	
Source Worth Data (1 kw)				
525	408.0 (77.0)	396.0 (81.4)	-0.044	+0.0045
525	408.4 (76.8)	396.5 (81.2)	-0.044	+0.0045
525	408.1 (76.9)	395.0 (81.7)	-0.048	+0.0005
525	408.8 (76.6)	395.1 (81.6)	-0.050	-0.0015
525	409.8 (76.3)	395.3 (81.5)	-0.052	-0.0035
525	407.6 (77.1)	393.3 (82.3)	-0.052	-0.0035
525	407.9 (77.0)	396.0 (81.4)	-0.044	+0.0045
525	407.0 (77.4)	393.5 (82.2)	-0.048	+0.0005
525	407.0 (77.4)	392.5 (82.5)	-0.051	-0.0025
525	406.1 (77.6)	392.0 (82.8)	-0.052	-0.0035
$\overline{\Delta\rho} = 4.85 \pm 0.11\text{¢}$			$\$ = 0.0034$	

Table 5.4 (continued)

Source Worth Data (10 kw)				
540	401.8 (79.2)	390.0 (83.5)	-0.043	+0.0047
540	402.2 (79.0)	389.2 (83.7)	-0.047	+0.0007
540	402.3 (79.0)	388.5 (84.0)	-0.050	-0.0023
540	401.9 (79.2)	390.0 (83.5)	-0.043	+0.0047
540	404.0 (78.5)	390.8 (83.2)	-0.047	+0.0007
540	402.5 (79.0)	389.1 (83.8)	-0.048	-0.0003
540	402.9 (78.8)	390.8 (83.2)	-0.044	+0.0037
540	403.9 (78.5)	390.9 (83.2)	-0.047	+0.0007
540	404.5 (78.2)	390.0 (83.5)	-0.053	-0.0053
540	405.1 (78.0)	390.0 (83.5)	-0.055	-0.0073
$\overline{\Delta\rho} = 4.77 \pm 0.13\%$				$\delta = 0.0040$

*No detectable pen movement for 2 minutes.

[†]From reg rod calibration curve (see Figure 5.3).

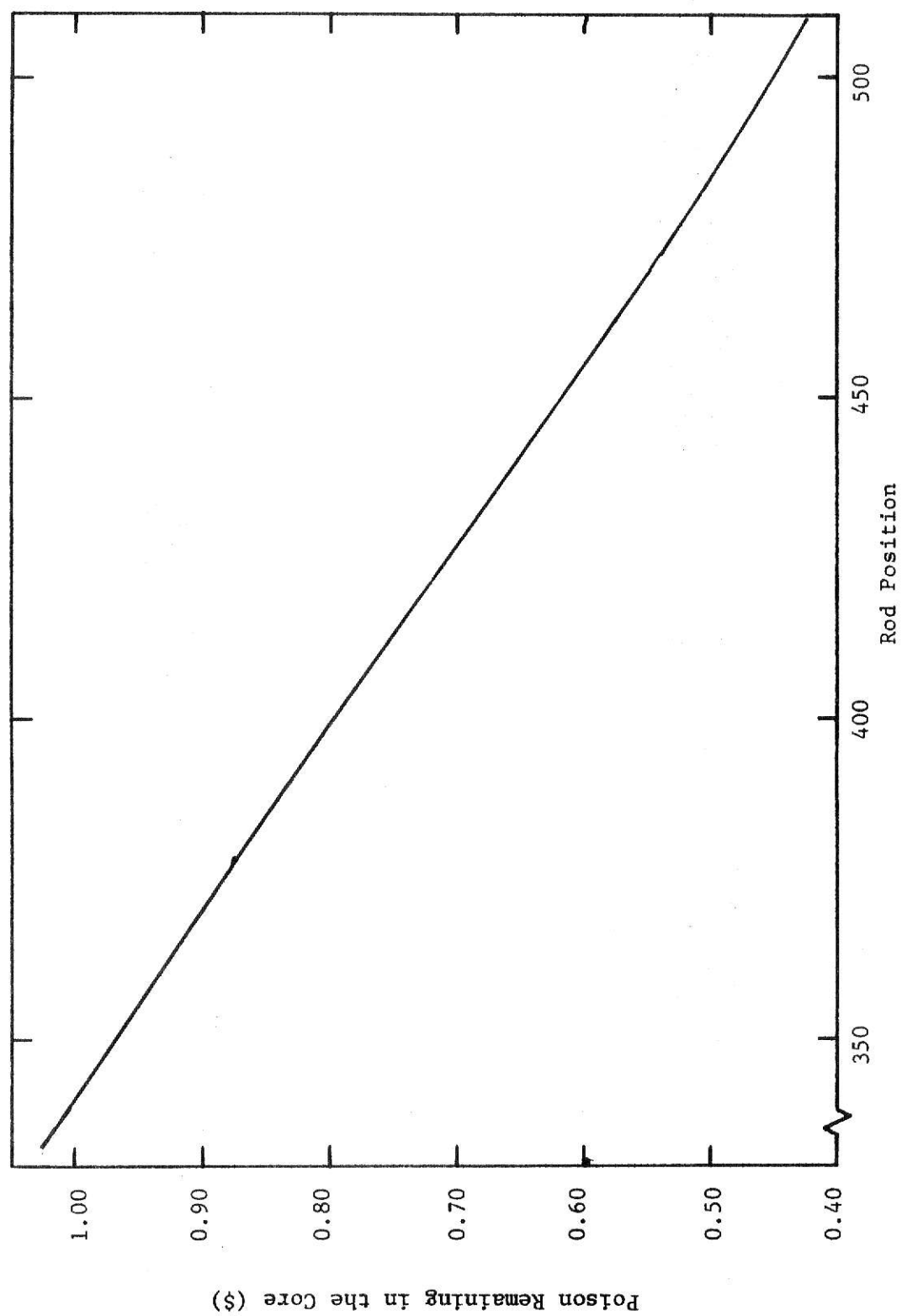


Figure 5.3 Expanded Reg Rod Calibration Curve

Table 5.5 Analysis of Variance for Source Worth Data

	n	Σx	$(\Sigma x)^2$	$(\Sigma x)^2/n$
100 watts	10	-46.4	2152.96	215.296
1 KW	10	-48.5	2352.25	235.225
10 KW	10	-47.7	2275.29	227.529
Pooled	30	-142.6	20334.76	677.825
$\Sigma x^2 = 681.72$				

Summary Table

Source of Variation	Sum of Squares	Degrees of Freedom	Mean Square	F Ratio
Between sets of data	0.225	2	0.112	0.828
Within each set of data	3.670	27	0.136	
Total	3.895	29		

The critical F value that cuts off the upper 25% of the distribution with 2 and 27 degrees of freedom is 1.46

Conclusion: The hypothesis that there is no significant difference between the means of the data sets cannot be rejected at a reasonable significance level.

Table 5.6 Combined Source Worth Data from Steady-State Experiments

Measured Value (¢)	Frequency	Deviation from the mean (¢)
-4.0	1	0.75
-4.3	3	0.45
-4.4	4	0.35
-4.5	2	0.25
-4.6	2	0.15
-4.7	4	0.05
-4.8	3	-0.05
-5.0	4	-0.25
-5.1	1	-0.35
-5.2	4	-0.45
-5.3	1	-0.55
-5.5	1	-0.75
Average Source Worth = $-4.75 \pm 0.07\text{¢}$		$\bar{s} = 0.37$

source is inserted and only the reg rod is adjusted until steady-state operation is again achieved. The reg and shim positions corresponding to this steady-state operation are recorded. This procedure is repeated ten times moving only the reg rod each time. Using the expanded reg rod calibration curve (Figure 5.3) the worth of the reg rod at each position is determined. The differential worth between source-in and source-out steady-state operation is calculated for all ten measurements. An average differential worth is determined and error limits are calculated using the root mean square deviations from the average. The data and results appear in Table 5.7.

This result indicates the reactor is actually $38.1 \pm 1.8\%$ subcritical with the source in and the reactor power steady at 0.01 watt. During steady-state source in operation the reactor kinetics equations simplify to

$$dn/dt = 0 = \rho n_0 / \ell + S_0 \quad . \quad (5.5)$$

Therefore

$$S_0 = -\rho n_0 / \ell \quad ,$$

where

$$\rho = \rho_R + \rho_S \quad . \quad (5.6)$$

The value just determined is ρ_R . Using this value and the previously determined value of ρ_S , the source strength can be determined. The steady-state power level is also used in this determination. Unfortunately neither the accuracy nor the precision of the power level is known. Therefore no precision index can be assigned to the resultant value of source strength.

The relationship between console power indication and actual power level is discussed in section 4 of this paper. However a discrepancy is evident when the source strength data is examined more closely. The first six data are taken during the same period with an indicated power of 0.01

Table 5.7 Source Strength Data from Steady-State Experiment at 0.01 Watt

Steady-State* Rod Positions				
Shim Position	Reg Position (Worth [†])		Δp (\$)	Deviation from the mean (\$)
	Source In	Source Out		
495	352.0 (96.5)	453.5 (61.0)	-0.355	-0.0261
495	347.0 (98.1)	453.0 (61.1)	-0.370	-0.0111
495	347.0 (98.1)	452.5 (61.3)	-0.368	-0.0131
495	344.1 (99.1)	452.5 (61.3)	-0.378	-0.0031
495	344.2 (99.0)	451.5 (61.6)	-0.374	-0.0071
495	343.1 (99.5)	451.7 (61.5)	-0.380	-0.0011
490	357.0 (94.8)	473.5 (54.0)	-0.408 [‡]	0.0269
490	358.0 (94.5)	473.8 (53.9)	-0.406 [‡]	0.0249
490	359.9 (93.9)	473.3 (54.0)	-0.399 [‡]	0.0179
490	366.0 (91.8)	472.1 (54.5)	-0.373 [‡]	-0.0081
$\overline{\Delta p} = -38.11 \pm 0.55\text{c}$				$\$ = 0.0175$

*No detectable pen movement for 2 minutes.

[†]From the expanded reg rod calibration curve (Figure 5.3).

[‡]Data taken at a later time.

Table 5.8 Zero Power Source Insertion Data

run #	shim position	reg position (worth*(¢))		poison removal (¢)	initial power (watts)
		@ zero power critical	after insertion		
1	513.5	405.5 (78.0)	414.0 (75.0)	3.0	0.00375
2	513.5	406.0 (77.8)	420.5 (72.5)	5.3	0.00375
3	513.5	405.0 (78.2)	422.0 (72.0)	6.2	0.00338
4	513.5	405.5 (78.0)	421.0 (72.4)	5.6	0.00288
5	---	400.0 (80.0)	413.6 (75.0)	5.0	0.1018
6	---	400.0 (80.0)	413.6 (75.0)	5.0	0.01044

watt. The last four data (marked with a symbol, "#," in Table 5.7) are taken during a different period with the indicated power again 0.01 watt. If the power is the same during these two periods the means of the two data sets should not be significantly different. However from the results in Table 5.9 the means are significantly different. This indicates the actual power is different during the two periods.

In order to determine the source strength the actual power level and the precision of this value must be evaluated. This requirement would be eliminated if the source strength could be determined by a technique that is not dependent on the knowledge of the actual power level.

5.2.3 SOURCE INSERTION EXPERIMENTS

The technique just discussed involves introducing the source into the reactor while the reactor is operating in a steady-state condition at a low power level (i.e. zero power critical). The kinetics equations describing source insertion at zero power criticality are

$$\frac{dn}{dt} = \rho_s n / \ell - \sum_{i=1}^m \frac{d\bar{C}_i}{dt} + S_o \quad , \quad (5.7)$$

$$\text{and} \quad \frac{d\bar{C}_i}{dt} = \beta_i n / \ell - \lambda_i \bar{C}_i \quad i = 1, 2, \dots, m \quad . \quad (5.8)$$

When $t = 0$; $n = n_o$ (i.e., steady-state power level), and $\bar{C}_{i_o} = \frac{n_o \beta_i}{\ell \lambda_i}$,

Using Laplace transforms the kinetics equations can be linearized to

$$sN(s) - n_o = \frac{\rho_s N(s)}{\ell} - \sum_{i=1}^m (s\bar{C}_i(s) - \bar{C}_{i_o}) + \frac{S_o}{s} \quad , \quad (5.9)$$

Table 5.9 Analysis of Variance for Source Strength Data

	Group 1	Group 2
n	6	4
Σx	-222.5	-158.6
$(\Sigma x)^2/n$	8251.04	6288.49
Σx^2	8255.09	6296.30
\bar{x}	-37.08	-39.65
s_x^2	0.81	1.61
$s_{\bar{x}}^2$	0.33	0.81

Difference of means 2.57

Std. Dev. 0.79

t value 3.27

The critical t value that cuts off the upper 5% of the distribution with 8 degrees of freedom is 2.306

Conclusion: The hypothesis that there is no significant difference between the means of these data sets can be rejected at a significance level of 0.05.

and

$$C_i(s) = \frac{\beta_i N(s)}{\ell(s+\lambda_i)} + \frac{\bar{C}_{i0}}{(s+\lambda_i)} \quad i = 1, 2, \dots, m \quad (5.10)$$

Therefore

$$N(s) = \frac{n_o(\ell + \sum_{i=1}^m \beta_i/(s+\lambda_i))}{s\left[\ell + \sum_{i=1}^m \beta_i/(s+\lambda_i) - \frac{\rho_S}{s}\right]} + \frac{S_o \ell}{s^2\left[\ell + \sum_{i=1}^m \beta_i/(s+\lambda_i) - \frac{\rho_S}{s}\right]} \quad (5.11)$$

For large times, s is small compared to λ_i ; therefore after sufficient time

$$N(s) = \frac{n_o}{s-\rho_S/A} + \frac{S_o \ell}{A} \frac{1}{s(s-\rho_S/A)} \quad (5.12)$$

where

$$A = \ell + \sum_{i=1}^m \beta_i/\lambda_i \quad .$$

Therefore

$$n(t) = (n_o + S_o \ell/\rho_S) \exp(\rho_S t/A) - S_o \ell/\rho_S \quad , \quad (5.13)$$

and

$$\frac{dn(t)}{dt} = (n_o \rho_S/A + S_o \ell/A) \exp(\rho_S t/A) \quad . \quad (5.14)$$

If the source worth could be nulled out ($\rho_S = 0$) the rate of change of power with respect to time becomes linear. The slope of this linear relationship between power and time is equal to $S_o \ell/A$. Knowing this slope, S_o could easily be determined. This value would be independent of actual initial power level. However the reactor controls are not accurate nor responsive enough to exactly null out the source worth. It is not necessary to completely null out the source worth in order to determine the source strength. Equation (5.14) can be linearized as below:

$$\ln\left\{\frac{dn(t)}{dt}\right\} = (\rho_S/A) t + \ln(n_o \rho_S/A + S_o \ell/A) \quad . \quad (5.15)$$

In this case the slope of $\ln\left(\frac{dn(t)}{dt}\right)$ versus time determines ρ_S . Using this value of ρ_S the intercept determines S_0 .

It is still desirable to have the source worth and power influence as small as possible. Therefore an experiment is designed to minimize source worth effect but still utilize the technique of source insertion into a zero power critical reactor. The experiment involves reaching a steady-state condition in the reactor at a low power level without the source present. After steady-state operation is assured, the source is inserted as nearly step-wise as possible. Simultaneously the reg rod is withdrawn. The amount of poison removed by withdrawing the reg rod should be approximately equal to the source worth. The data from six such experiments appear in the Table 5.8.

The equation describing this experiment is as developed before;

$$\ln\left(\frac{dn(t)}{dt}\right) = (\rho/A)t + \ln(n_0\rho/A + S_0\lambda/A) \quad , \quad (5.16)$$

where

$$\rho = \rho_R + \rho_S \quad .$$

This equation is only applicable for large values of time. The data from the six experiments described in Table 5.8 is plotted in Figures 5.4 and 5.5. It is obvious that the slope of power versus time decreases as a function of time in runs 1 and 2, whereas the slope increases in runs 3, 4, 5 and 6. The case of source worth completely nulled out lies somewhere between run 2 and run 4.

The first step in the determination of source strength and source worth from the data is to determine the slope of the function at each data point. Since only a discrete number of data points are available, the slope at each point is found by numerical differentiation [17]. It is assumed the function can be fitted to a

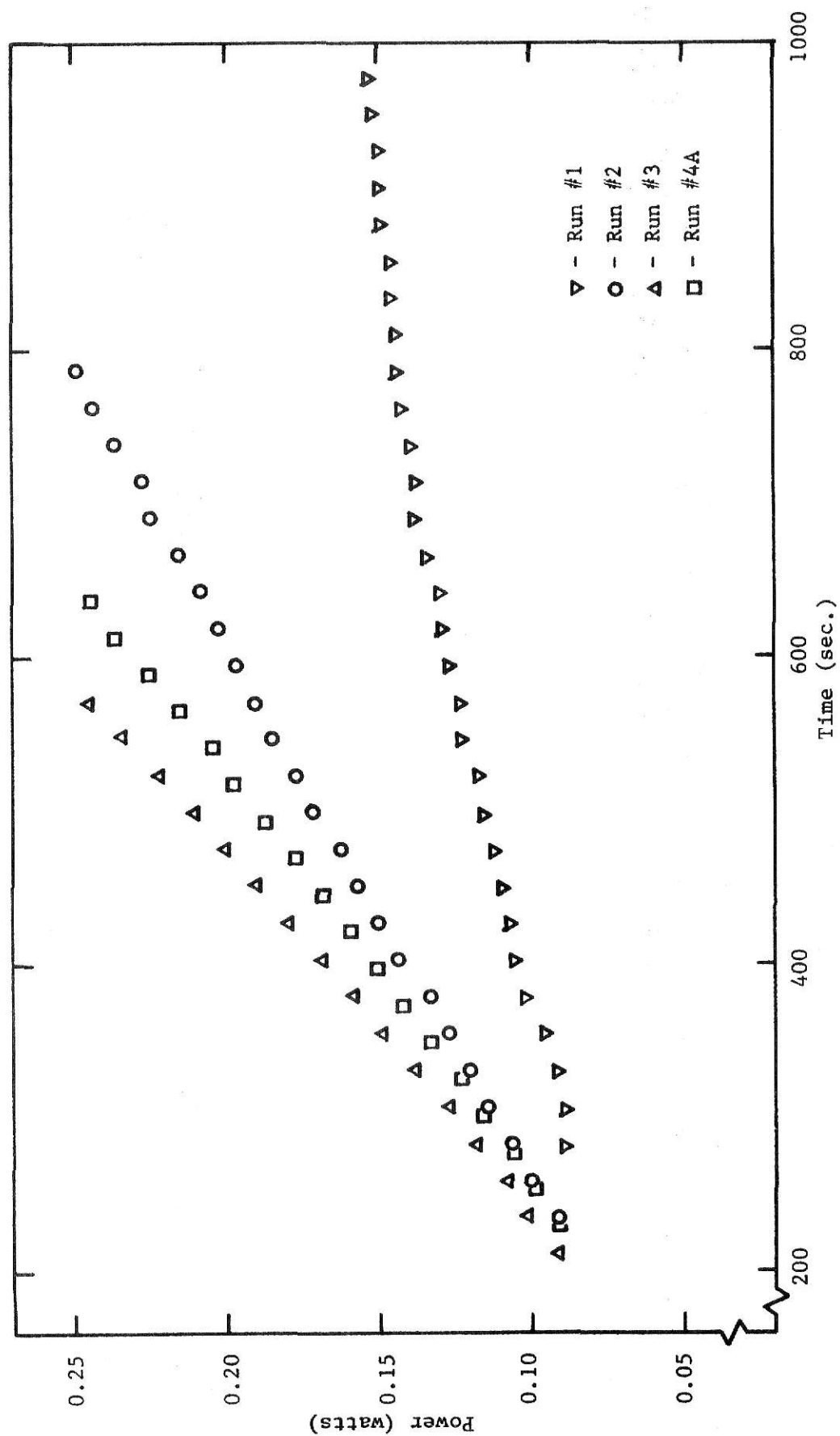


Figure 5.4 Zero Power Source Insertion Data

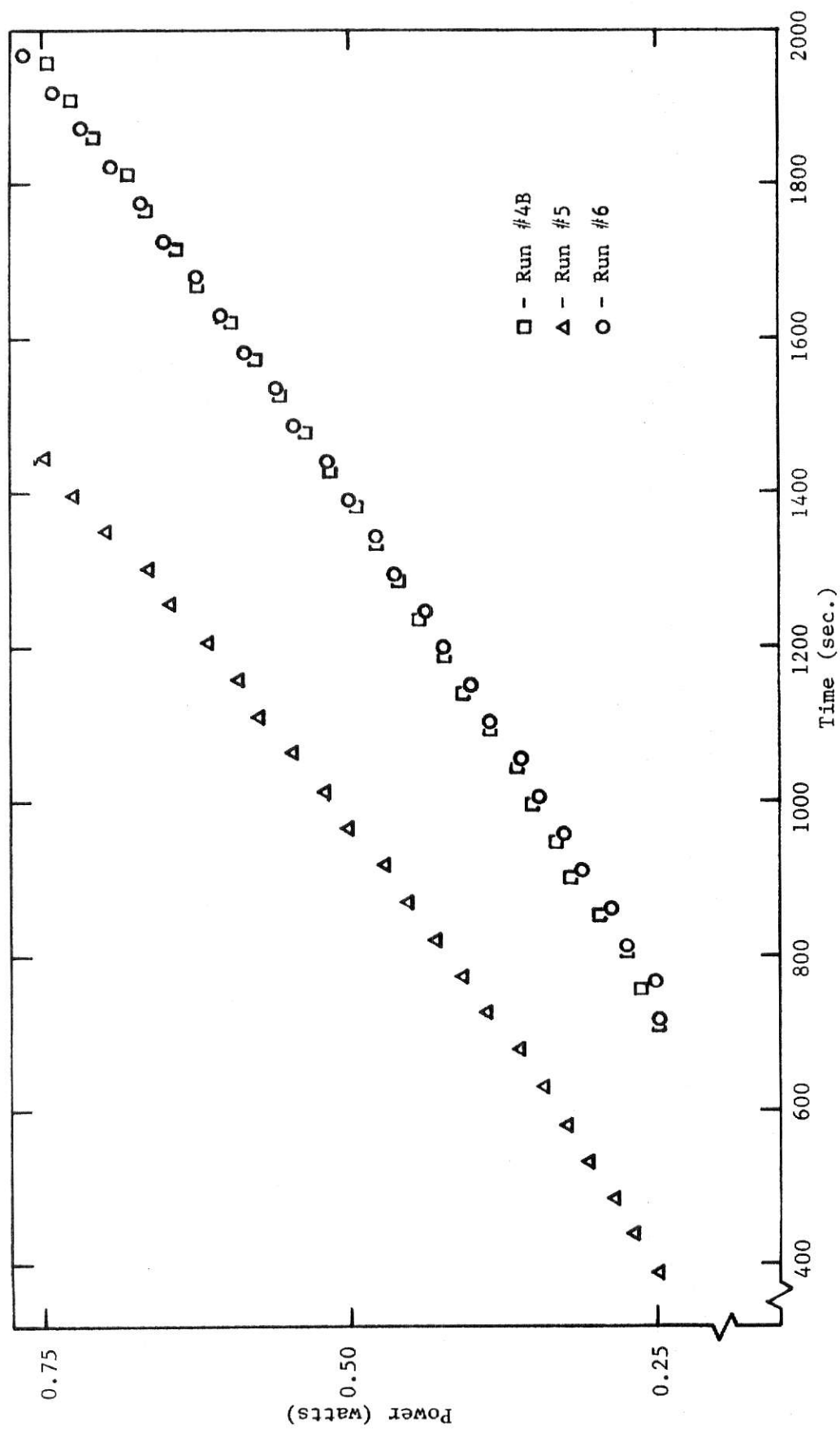


Figure 5.5 Zero Power Source Insertion Data

polynomial of fourth or lower degree. The slope at the i th data point can be expressed as

$$\left(\frac{dn}{dt}\right)_{t=t_i} = 1/12h(n_{i-2} - n_{i+2} - 8(n_{i-1} - n_{i+1})) \quad , \quad (5.17)$$

where h = time interval between data.

The natural logarithm of these computed slopes are fitted to a straight line using the method of least squares as developed in Appendix B. The slope of the resultant fit is equal to ρ/A . The intercept is equal to $\ln(n_0 \rho/A + S_0 l/A)$. The data from all six runs is analyzed using a computer code to facilitate computation. The results appear in the Table 5.10 and are plotted in Figures 5.6, 5.7, and 5.8.

The results from this set of experiments can be compared with the results from the set of experiments discussed previously. In Table 5.11 the resulting values of source worth from the source insertion experiment (test 2) are compared with the resulting values of source worth from the steady-state experiment (test 1). The t test is used to determine if the mean values of source worth from each experiment are significantly different. When all the source insertion data is considered, the mean value of source worth is significantly different from the mean value of source worth from the steady-state experiments. There are several possible explanations for this significant discrepancy.

The value of reactivity removal by rod movement (ρ_R) is only measured once during each source insertion experiment. Table 5.10 shows a standard deviation of 0.37 for each of these values. However this standard deviation is estimated using the data from the steady-state experiments. The true variance is not known. Therefore the standard deviations for source worth shown in Table 5.10 are only an estimate. The actual values may be

Table 5.10 Results of Least Square Fit of Source Insertion Data

Run #	Slope	Intercept	Source Strength (S_o) (watts/sec)
1	-0.000263 ± 0.000079	-7.85 ± 0.53	0.340 ± 0.176
2	-0.0000164 ± 0.0000252	-8.09 ± 0.13	0.261 ± 0.035
3	0.0000807 ± 0.0000285	-8.07 ± 0.11	0.262 ± 0.030
4A	0.0000543 ± 0.0000225	-8.11 ± 0.10	0.254 ± 0.026
4B	0.0000250 ± 0.0000069	-8.15 ± 0.11	0.244 ± 0.023
5	0.0000412 ± 0.0000103	-8.04 ± 0.10	0.239 ± 0.027
6	0.0000238 ± 0.0000047	-8.09 ± 0.07	0.258 ± 0.017

Table 5.10 (continued)

Run #	$\rho(\epsilon)$	$\rho_R(\epsilon)$	$\rho_S(\epsilon)$
1	-3.44 ± 1.03	3.0 ± 0.37	-6.44 ± 1.09
2	-0.21 ± 0.33	5.3 ± 0.37	-5.51 ± 0.50
3	1.05 ± 0.37	6.2 ± 0.37	-5.15 ± 0.52
4A	0.71 ± 0.29	5.6 ± 0.37	-4.89 ± 0.47
4B	0.33 ± 0.09	5.6 ± 0.37	-5.27 ± 0.38
5	0.54 ± 0.13	5.0 ± 0.37	-4.46 ± 0.39
6	0.31 ± 0.06	5.0 ± 0.37	-4.69 ± 0.37

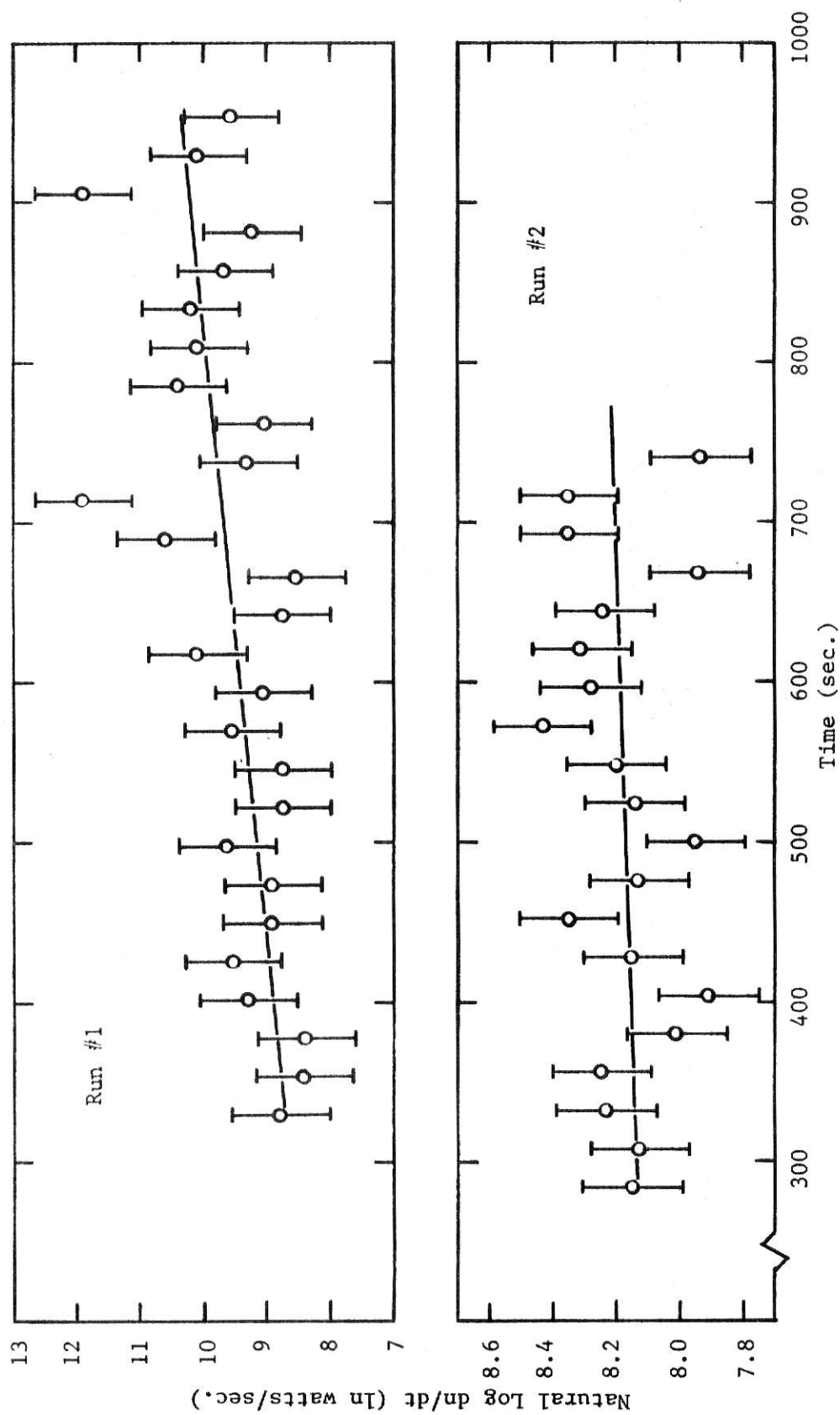


Figure 5.6 Least Squares Fit of Zero Power Source Insertion Data

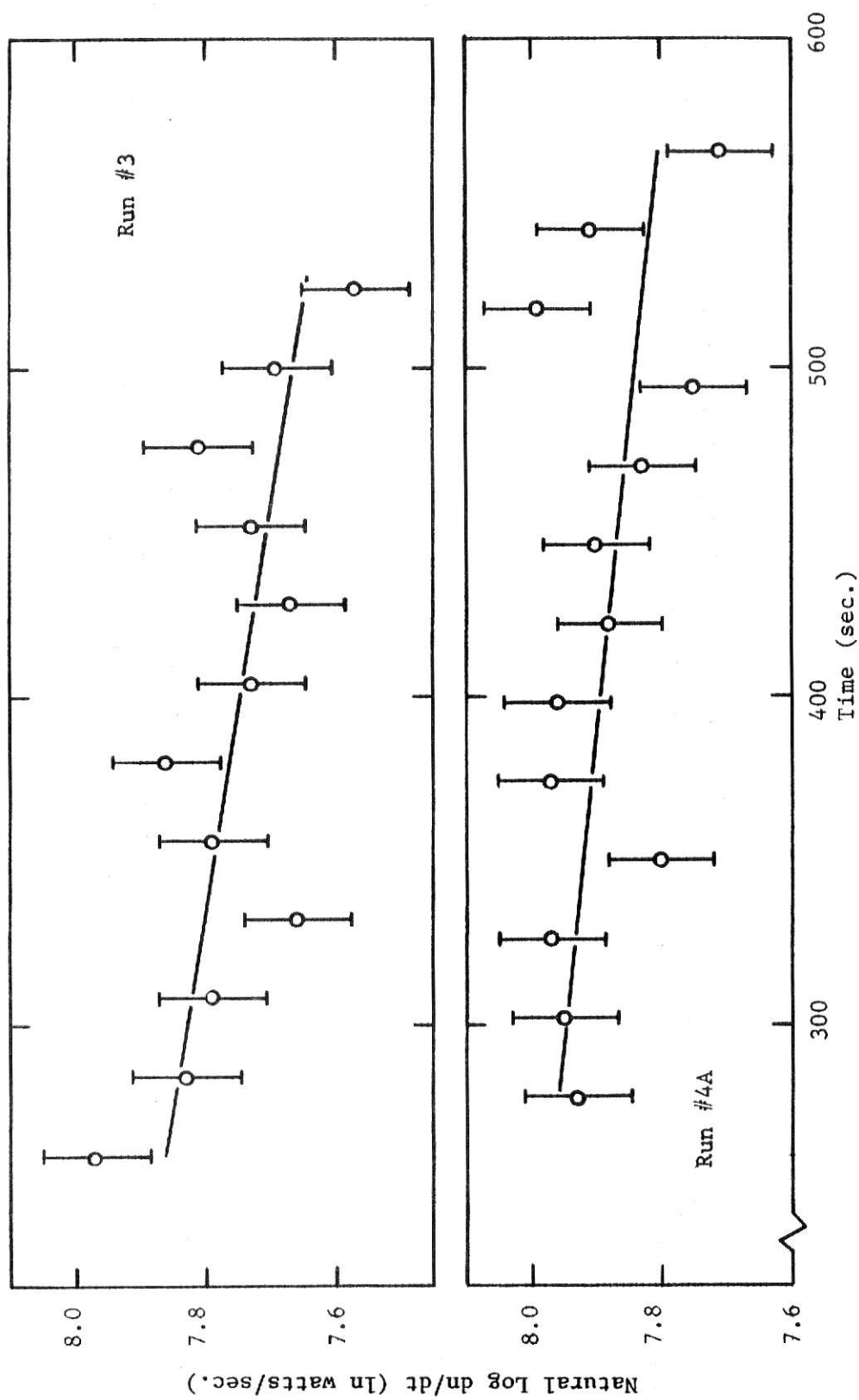


Figure 5.7 Least Squares Fit of Zero Power Source Insertion Data

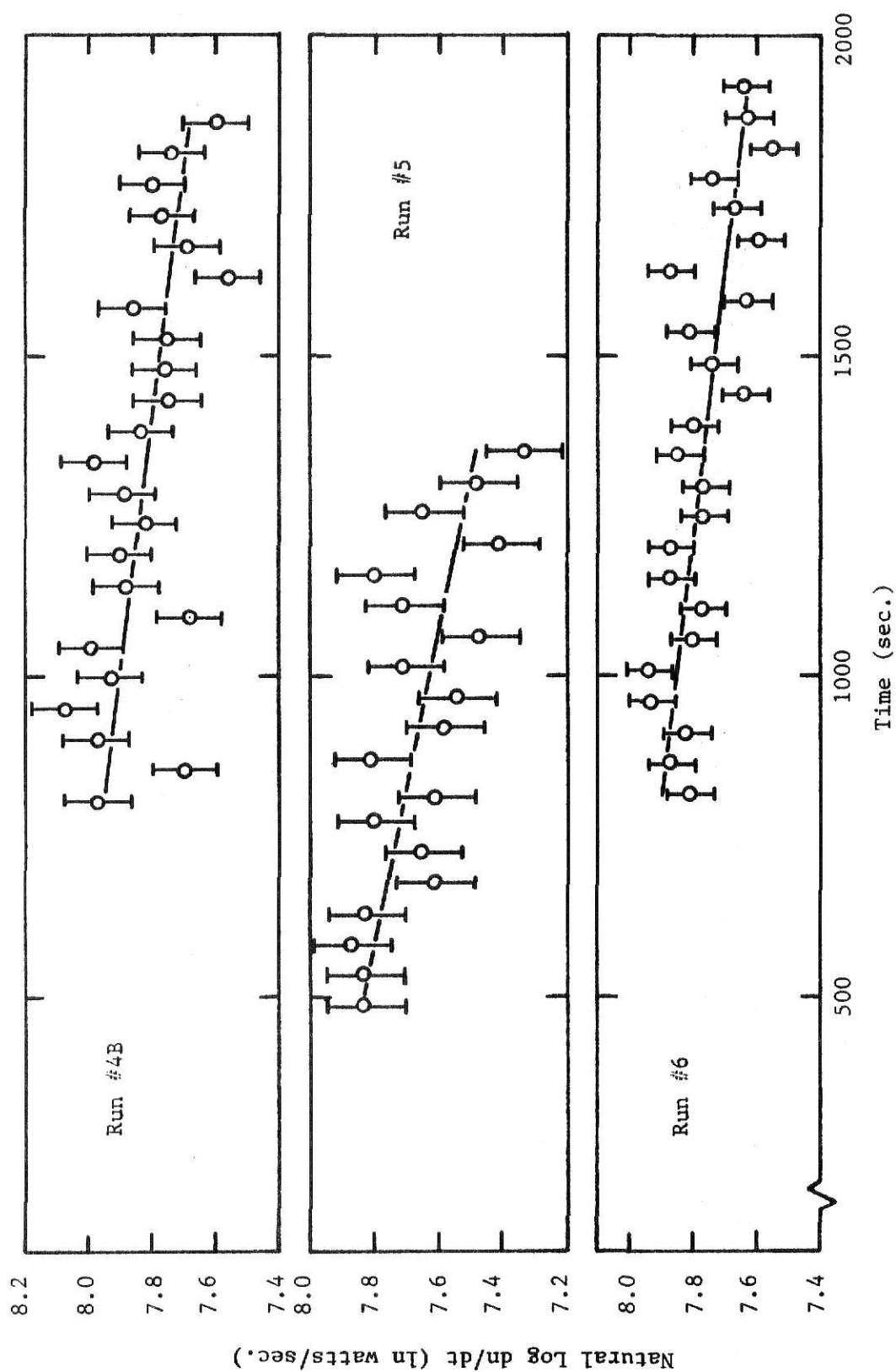


Figure 5.8 Least Squares Fit of Zero Power Source Insertion Data

Table 5.11 Analysis of Variance for Source Worth Computations

	Test 1	Test 2	Test 2A	Test 2B	
n	30	7	3	3	
Σx	-142.6	-36.41	-15.55	-14.42	
$(\Sigma x)^2/n$	677.825	189.38	80.601	69.312	
Σx^2	681.72	191.93	80.795	69.660	
	Sum of Squares	Degrees of Freedom	Mean Square	Std. Dev.	
Test 1	3.895	29	0.134	0.37	
Test 2	2.55	6	0.425	0.65	
Test 2A	0.196	2	0.098	0.31	
Test 2B	0.348	2	0.174	0.42	
	\bar{x}	Std. Dev.	Difference	Std. Dev.	t value
Test 1	4.75	0.067	---	---	---
Test 2	5.20	0.25	0.45	0.180	2.49
Test 2A	5.18	0.181	0.43	0.218	1.97
Test 2B	4.81	0.241	0.06	0.274	0.22

Test $H_0: \mu_1 = \mu_2$ against $H_1: \mu_1 \neq \mu_2$

Reject H_0 at 95% confidence level if: $-t_{95} \geq t \geq t_{95}$

$t_{95} \approx 2.04$ for all cases

Conclusions: With 95% confidence: $\bar{x}(\text{Test 1}) \neq \bar{x}(\text{Test 2})$

$\bar{x}(\text{Test 1}) = \bar{x}(\text{Test 2A})$

$\bar{x}(\text{Test 1}) = \bar{x}(\text{Test 2B})$

significantly different. The standard deviations of ρ shown in Table 5.10 are calculated from the source insertion data. These values are indicative of the precision with which ρ is determined. As can be seen the variances can be grouped into three sets; run 1, runs 2, 3 and 4A, and runs 4B, 5, and 6. In runs 4B, 5, and 6 all data are recorded for times longer than 5 minutes after source insertion. The time interval between data is twice as long as that used in the other runs. In runs 2, 3, and 4A the variance of ρ is 2 to 3 times as large as the variance in runs 4B, 5, and 6. In run 1, besides the timing differences, ρ is significantly larger than in the other runs. In this case the variance is 3 times as large as the variance in runs 2, 3, and 4A. Because of these significant differences the results from the source insertion experiments are compared to the results from the steady-state experiments using a different technique. First the value of source worth from run 1 is discarded because of its lack of precision. Secondly, runs 2, 3, and 4A are grouped together and called test 2A. Runs 4B, 5 and 6 are grouped together and called test 2B. From the results of the t tests shown in Table 5.11 the mean value of source worth for both tests 2A and 2B is not significantly different from the mean value of source worth from the steady-state experiments. However, the value for the difference in means between test 2A and test 1 is far out in the tail of the t distribution. Whereas the difference between the means of test 2B and test 1 is almost in the center of the t distribution.

From this analysis it appears the most accurate and precise value of source worth is that gleaned from the steady-state experiments. Therefore the source worth is taken as $-4.75 \pm 0.37\%$. Potentiometer #2 is set to 0.620 to correspond to this value. When analyzing the source strength results one must remember the objective of the source insertion experiment is to eliminate

any dependence on power. If the source worth could have been nulled out completely, the effect of power would have been eliminated. Since this is impractical the power effect shows up in the term $n_0 \rho / \lambda$ in Eq. (5-19). The relative contribution of this factor to the total value for source strength appears in Table 5.12.

In only runs 1 and 5 is the relative contribution greater than 1%. Therefore the mean value of source strength is calculated using the data from the remaining 5 runs. From this data the average value of source strength is 0.256 ± 0.003 watts/sec. The source strength is taken as 0.256 ± 0.007 watts/sec. Potentiometer #3 is set to 0.512 to correspond to this value.

5.3 DETERMINATION OF SOURCE EFFECTS USING ANALOG SIMULATION.

Using the calculated values of source worth and source strength the analog model closely simulates the reactor. The model can be used to study the kinetic behavior of the reactor without requiring reactor operation. In order to illustrate the type of studies that can be accomplished, a study is made of source effects.

5.3.1 STEADY-STATE OPERATION IN THE PRESENCE OF THE SOURCE.

Using the reactor simulator a study is made of the reactivity necessary to maintain steady-state operation on the presence of the source. Only the setting on potentiometer #1 is varied, thus simulating rod movement. Steady operation is achieved at several power levels and the corresponding setting on potentiometer #1 is recorded. The results appear in a Table 5.13 and are plotted in Figure 5.9. As can be seen the source influence is power dependent. As is previously assumed the source worth effect is predominant at

Table 5.12 Power Dependent Contribution to Source Strength

Run No.	n_o (watts)	ρ (ϕ)	$n_o \rho / l$ (watts/sec.)	S_o (watts/sec.)	Relative Contribution (%)
1	0.00375	-3.44	-0.0084	0.340	-2.5
2	0.00375	-0.21	-0.00051	0.261	-0.2
3	0.00338	1.05	0.0023	0.262	0.9
4A	0.00288	0.71	0.0013	0.254	0.5
4B	0.00288	0.33	0.00062	0.244	0.25
5	0.1018	0.54	0.0358	0.239	15.0
6	0.01044	0.31	0.0021	0.258	0.8

Table 5.13 Reactivity Required to Achieve Steady-State Operation in the Presence of the Source

Power (watts)	Analog Settings		ρ_R (ϕ)
	Rod Switch	Potentiometer #1	
0.01	DN	0.450	-34.5
0.02	DN	0.194	-14.9
0.05	DN	0.0405	-3.1
0.10	UP	0.011	0.8
0.20	UP	0.0365	2.8
0.50	UP	0.052	4.0
1.00	UP	0.057	4.4

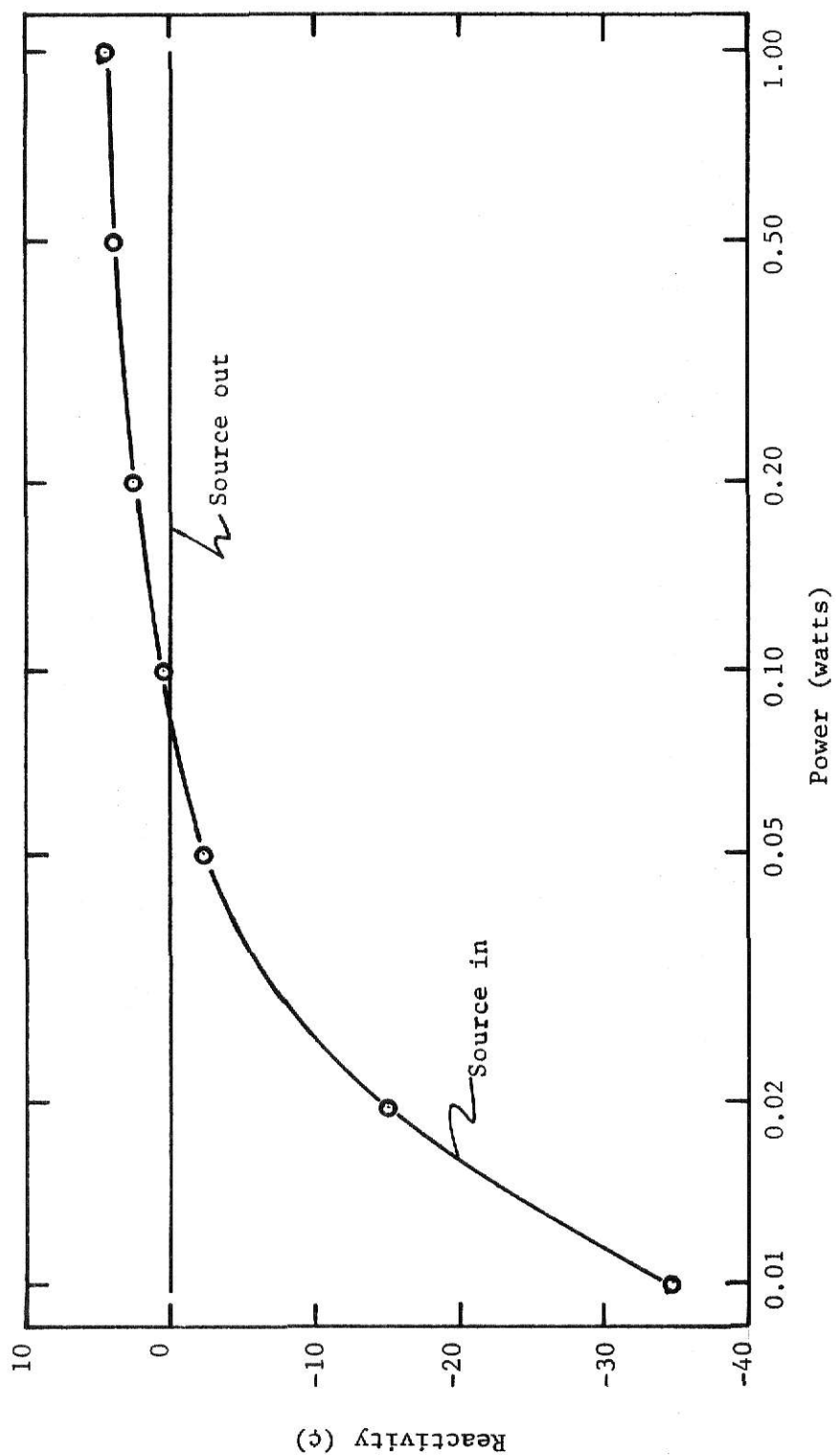


Figure 5.9 Reactivity Required to Maintain Steady-State Operation (Data from Analog Simulator)

high powers whereas the source strength influence is predominant at lower powers. The transition point (i.e. $\rho_R = 0$) is at 0.083 watts. At this point the source worth and source strength effects are equal. No reactivity insertion or removal is necessary to maintain steady-state operation.

5.3.2 SOURCE INSERTION AND REMOVAL FROM STEADY-STATE REACTOR.

If the source worth effect is dominant at power levels above 0.1 watt source removal during steady-state operation should have the kinetic effect of positive reactivity insertion. Source insertion during steady-state operation should have the kinetic effect of negative reactivity insertion. Below 0.1 watt where the source strength effect is dominant, source insertion and removal from the steady-state reactor should have the kinetic effect of insertion and removal of the source in a sub-critical pile. To substantiate this theory the following experiment is performed. Steady-state operation of the reactor with the source in is achieved at 0.01, 0.05, and 0.10 watts. After assuring steady-state operation the source is removed. The results appear in Figure 5.10. As can be seen the power drops rapidly from 0.01 and 0.05 watts. This is similar to the kinetic behavior after the source is removed from a subcritical pile. From 0.1 watt the power rises slowly. This is similar to the kinetic behavior after a small negative reactivity withdrawal from a critical reactor. In a second set of experiments, steady-state operation of the reactor with the source removed is achieved at 0.01, 0.05, and 0.1 watts. After assuring steady-state operation the source is inserted. The results appear in Figure 5.10. As can be seen, starting from 0.01 and 0.05 watts, the power rises to asymptotically approach a higher power level. From 0.1 watt the power asymptotically approaches a lower power level. It can generally be stated that from

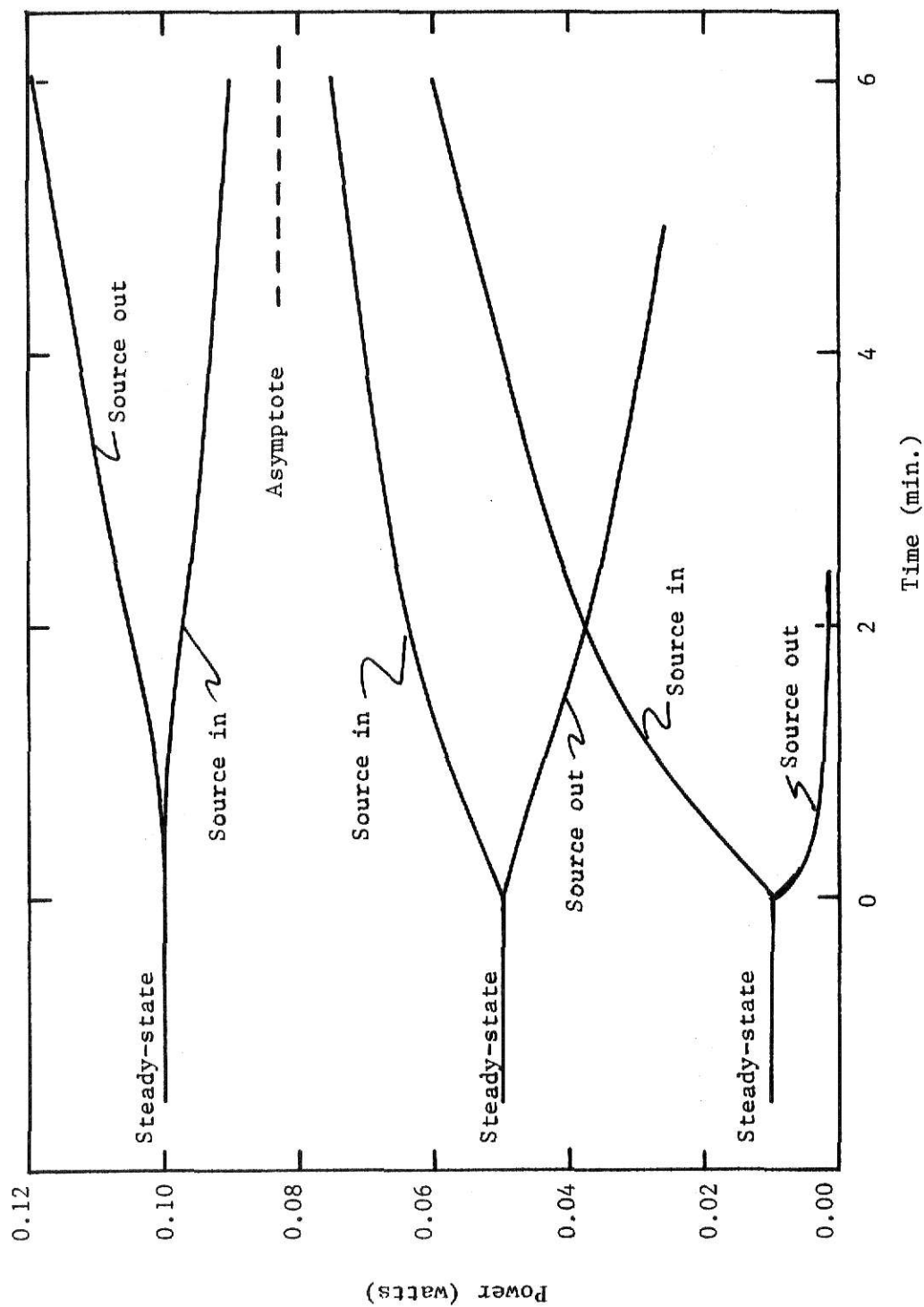


Figure 5.10 Source Insertion and Removal from the Reactor at Steady-State (Data from Operational Tests on the KSUTM II Reactor)

steady-state sourceless operation upon insertion of the source the power will either rise or fall to the same power level. This power level is equivalent to the power level in a subcritical pile with a homogeneous source equal in strength to the reactor source, and $\rho = \rho_S$. The neutron density in such a configuration [9] is

$$n = MS\ell/V ; \quad (5.18)$$

where $M = \text{multiplication} = (\rho_S - 1)\rho_S$,
 $S = \text{source strength (neutrons/sec.)}$,
 and $V = \text{volume of pile}$.

In this case

$$S/V = S_0 = 0.256 \text{ watts/sec.} ,$$

$$\rho_S = 0.0001310 ,$$

$$M = 3.23 \times 10^3 ,$$

and $\ell = 10^{-4} .$

Therefore

$$n = 0.0826 \text{ watts} .$$

This figure compares favorably with that gleaned from the analog solution.

5.4 CONCLUSIONS

Using the analog simulation the source effects are accurately predicted. The model can be utilized to predict and study many other reactor phenomena.

From the effects observed a new start-up technique seems evident. The source does not need to be removed when determining excess reactivity at the beginning of each day. Instead if the determination of criticality is made at about 0.1 watt it will accurately reflect sourceless criticality. This would obviate the need for more than one man during daily reactor check out.

ACKNOWLEDGEMENTS

The author is indebted to Dr. Thomas Hill for his advice on development of the computer codes; to Dr. James Heltshe for help in developing the statistical analysis; and to Professors R. E. Faw, M. J. Robinson and J. O. Mingle for guidance in the preparation of this work.

REFERENCES

1. Argonne National Laboratory, Reactor Physics Constants, ANL-5800 (2nd Edition; Technical Division, U. S. Atomic Energy Commission, 1963), pp. 17-18.
2. Atkins Technical Incorporated, Gainesville, Florida, "Atkins Short Form Catalog and Price List" (1967).
3. Vedat S. Arpacı, Conduction Heat Transfer (Reading Mass.: Addison-Wesley, 1966) pp. 503-15.
4. Charles L. Beeson, "Measurement of the Zero Power Transfer Function of the Kansas State University TRIGA Mark II Nuclear Reactor" (unpublished Master's thesis, Kansas State University, 1966), p. 53.
5. Gary Don Bouchey, "Experimental Neutron Flux Measurements and Power Calibration in the Kansas State University TRIGA Mark II Nuclear Reactor" (unpublished Master's thesis, Kansas State University, 1967).
6. Lincoln L. Chao, Statistics: Methods and Analyses (New York: McGraw-Hill, 1969), chap. 14.
7. M. Copic, "Report on Thermal Power Calibration of KSUTMII Reactor" (Memorandum to W. R. Kimel, August 1, 1966).
8. Electronic Associates Incorporated, Long Branch, New Jersey, "Reactor Kinetics Group Type 2.475" (1963).
9. Harold Etherington (ed.), Nuclear Engineering Handbook (New York: McGraw-Hill, 1961, 1958).
10. Stanley Fifer, Analogue Computation, Vol. 1 (New York: McGraw-Hill, 1961), pp. 13-14.
11. General Atomic, San Diego, California, "Technical Foundations of TRIGA," GA-471 (1958).
12. General Atomic, San Diego, California, "250 kw TRIGA Mark II Pulsing Reactor Mechanical Maintenance and Operating Manual for Kansas State University, Manhattan, Kansas," GA-3399 (1962).
13. P. G. Guest, Numerical Methods of Curve Fitting (Cambridge: Cambridge at the University Press, 1961), p. 108.
14. J. P. Holman, Heat Transfer (New York: McGraw-Hill, 1963), pp. 158-65.
15. Leon Lapidus, Digital Computation for Chemical Engineers (New York: McGraw-Hill, 1962), pp. 254-55.

16. R. F. Loeffler, "Thermocouples, Resistance Temperature Detectors, Thermistors - Which?," Instruments and Control Systems, 40 (May, 1967), pp. 89-93.
17. Henry Margenau and George Moseley Murphey, The Mathematics of Physics and Chemistry (Princeton, N. J.: D. Van Nostrand, 1956), p. 473.
18. Elliott I. Organick, A FORTRAN Primer (Reading, Mass.: Addison-Wesley, 1963), p. 26.
19. Jerry W. Stauder, "An Analysis of the Pulsing Characteristics of the Kansas State University TRIGA Mark II Nuclear Reactor" (unpublished Master's thesis, Kansas State University, 1969).
20. Lynn E. Weaver, Reactor Dynamics and Control (New York: American Elsevier, 1968), pp. 37-42.
21. Walter P. White, The Modern Calorimeter (New York: The Chemical Catalog Co., 1928), p. 19.

APPENDIX A

Analog Simulation of a Reactor

The reactor kinetics equations developed previously are

$$\frac{dn}{dt} = \frac{\rho - \beta}{\ell} n + \sum_{i=1}^m \lambda_i \bar{C}_i + S_o, \quad (\text{neutrons/cm}^3 \text{ sec.}) \quad (\text{A.1})$$

and

$$\frac{d\bar{C}_i}{dt} = \frac{\beta_i}{\ell} n - \lambda_i \bar{C}_i \quad i = 1, 2, \dots, m \quad (\text{neutrons/cm}^3 \text{ sec.}) \quad (\text{A.2})$$

A simple schematic of the analog network used to solve these equations appears in Figure A.1. The voltage output of the operational amplifier simulates the neutron density and is designated as e_n . This voltage is adjusted in the two potentiometers, simulating reactivity changes. The output voltages of the potentiometers are the input voltage, e_n , reduced by a factor Δ_{ρ_R} in one case and by a factor Δ_{ρ_S} in the other case. An external voltage, e_S , simulates the external source. Six RC networks simulate the six delay group approximation of the delayed neutron precursor density. After two summing junctions and an inverter the voltage simulation of source and reactivity becomes

$$e_{in} = -\frac{e_S}{10} - \frac{e_n (\Delta_{\rho_R} + \Delta_{\rho_S})}{10} \quad (\text{volts}) \quad (\text{A.3})$$

Using Kirchoff's law the sum of the currents into node n_o (the input to the operational amplifier) must be zero. The input current from source and reactivity is

$$i_{in} = -\frac{e_S}{10 R_o} - \frac{e_n (\Delta_{\rho_R} + \Delta_{\rho_S})}{10 R_o} \quad (\text{amps}) \quad (\text{A.4})$$

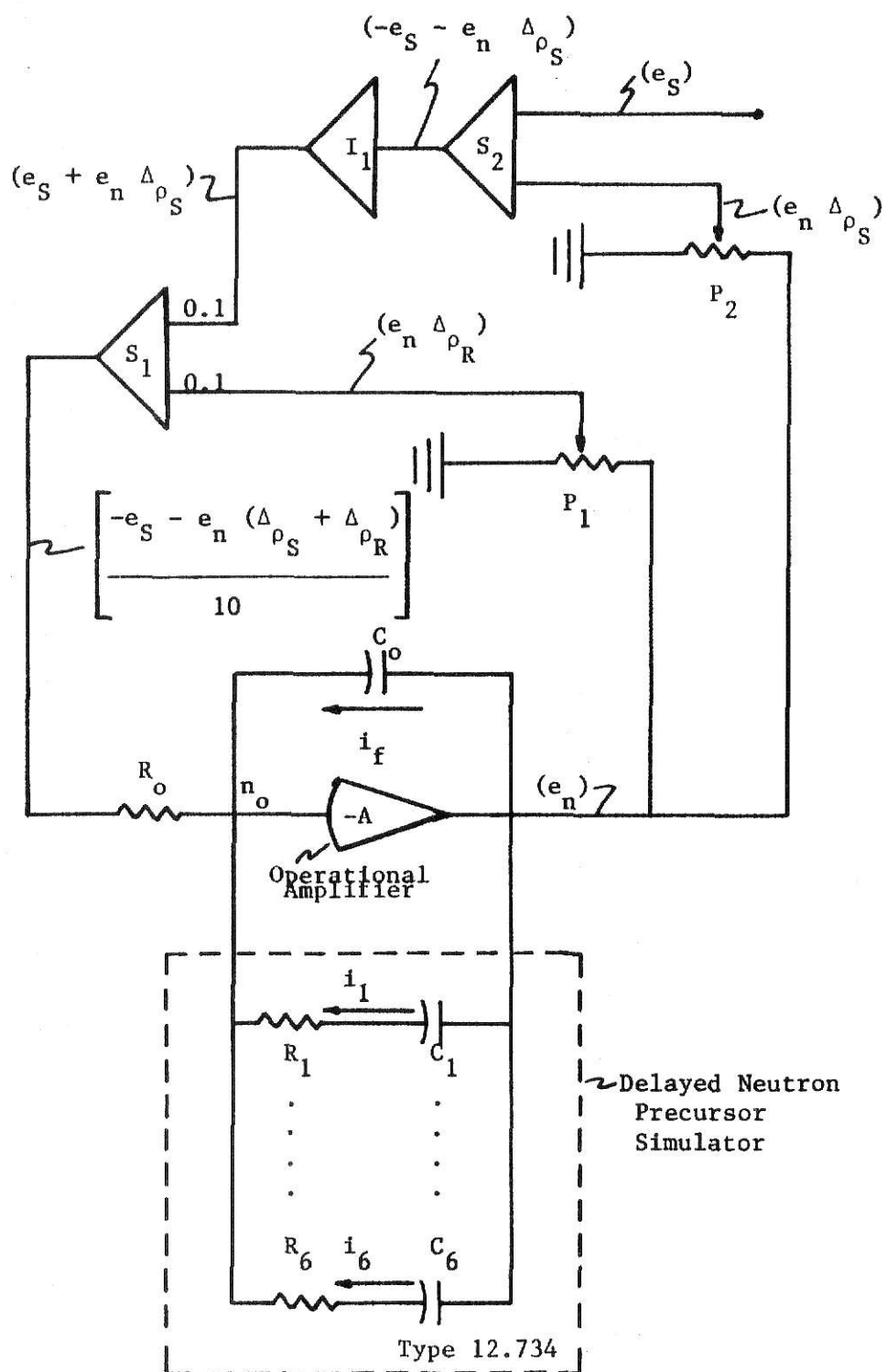


Figure A.1 Analog Simulation of a Reactor with a Removable Source

The feedback current is

$$i_f = C_o \frac{de_n}{dt} \quad (\text{amps}) \quad (\text{A.5})$$

The impedance of the operational amplifier is very high making the nodal voltage near ground. Therefore the sum of the currents at n_o is

$$-\frac{e_S}{10 R_o} - \frac{e_n (\Delta_{\rho_R} + \Delta_{\rho_S})}{10 R_o} + C_o \frac{de_n}{dt} + \sum_{i=1}^6 i_i = 0 \quad (\text{A.6})$$

The current through each precursor network is

$$i_i = \frac{dq_i}{dt} = \frac{e_n}{R_i} - \frac{q_i}{R_i C_i} \quad (\text{amps}) \quad (\text{A.7})$$

Therefore the nodal balance at n_o becomes

$$\frac{de_n}{dt} = \frac{e_n (\Delta_{\rho_R} + \Delta_{\rho_S})}{10 R_o C_o} + \frac{e_S}{10 R_o C_o} - \frac{1}{C_o} \sum_{i=1}^6 \frac{dq_i}{dt} \quad (\text{amps}) \quad (\text{A.8})$$

The voltages and attenuators are made proportional to physical quantities using proportionality factors (b_i 's) as follows:

$$e_n = b_n n \quad (\text{volts})$$

$$\Delta_{\rho_R} = b_{\rho_R} \rho_R \quad ,$$

$$\Delta_{\rho_S} = b_{\rho_S} \rho_S \quad ,$$

and
$$e_S = b_{S_o} S_o \quad (\text{volts})$$

The current through each precursor network then becomes

$$\frac{dq_i}{dt} = \frac{b_n n}{R_i} - \frac{q_i C_i}{R_i} \quad (\text{amps}) \quad (\text{A.9})$$

and the nodal balance at n_o becomes

$$b_n \frac{dn}{dt} = \frac{b_S S_o}{10 R_o C_o} + \frac{b_n n (b_{\rho} \rho_R + b_{\rho} \rho_S)}{10 R_o C_o} - \frac{1}{C_o} \sum_{i=1}^6 \frac{dq_i}{dt} . \quad (A.10)$$

If the precursor densities are defined proportional to the neutron density as:

$$\bar{C}_i = \left[\frac{q_i}{C_o e_n} \right] n \quad \text{or} \quad \bar{C}_i = \frac{q_i}{C_o b_n} ,$$

then

$$\frac{d\bar{C}_i}{dt} = \frac{\frac{dq_i}{dt}}{C_o b_n} . \quad (\text{neutrons/cm}^3 \text{ sec.}) \quad (A.11)$$

and the nodal equation becomes

$$\frac{dn}{dt} = \frac{b_{\rho} \rho_R n}{10 R_o C_o} + \frac{b_{\rho} \rho_S n}{10 R_o C_o} + \frac{b_S S_o}{10 R_o C_o b_n} - \sum_{i=1}^6 \frac{d\bar{C}_i}{dt} ; \quad (A.12)$$

and the precursor currents become

$$\frac{d\bar{C}_i}{dt} = \frac{n}{R_i C_o} - \frac{\bar{C}_i}{R_i C_i} . \quad (A.13)$$

If the passive components are designed such that

$$R_o C_o = \frac{b_{\rho} \ell}{10} , \quad (\text{sec})$$

$$\frac{R_o}{R_i} = \frac{b_{\rho} \beta_i}{10} ,$$

$$R_i C_i = \frac{1}{\lambda_i} , \quad (\text{sec})$$

and

$$b_S = b_{\rho} b_n \ell ;$$

the nodal balance and precursor currents reduce to the kinetics equations, namely:

$$\frac{dn}{dt} = \frac{\rho_R}{\ell} n - \sum_{i=1}^m \frac{d\bar{C}_i}{dt} + S_0 + \rho_S \frac{n}{\ell} \quad (A.14)$$

$$\frac{d\bar{C}_i}{dt} = \frac{\beta_i}{\ell} n - \lambda_i \bar{C}_i \quad (A.15)$$

In the process of defining the voltages and currents in terms of physical quantities the passive components and proportionality factors are determined in terms of physical quantities. Some of these relationships are expressed above and others appear below:

$$b_{\rho} = \frac{\Delta_{\max}}{\rho_{\max}} = \frac{1}{\rho_{\max}},$$

and

$$b_n = \frac{e_{\max}}{n_{\max}}.$$

All the values of the passive elements except C_0 and R_0 are predetermined by the manufacturer of the analog system [8]. The manufacturer's values for the RC precursor networks appear in Table A.1 along with the corresponding delayed neutron parameters from which they are determined.

Table A.2 lists the possible options for the values of R_0 and C_0 and the corresponding values of the neutron generation time and maximum reactivity.

The maximum power level under consideration is 1 watt. The maximum output voltage of the analog unit is 10 volts. The output voltage represents neutron density. The neutron density is directly proportional to the flux which in turn is directly proportional to the power level. Since the quantity monitored at the reactor console is power level, neutron density will be expressed in terms of power. Therefore, when the neutron density

Table A.1 RC Values in Unit Type 2.457 Based on U-235 [8]

Group (i)	R_i (meg Ω)	C_i (mfd)	β_i	λ_i (sec ⁻¹)
1	20.2 \pm 1%	3.89 \pm 1%	0.00027	0.0127
2	3.6 \pm 1%	8.74 \pm 1%	0.00138	0.0317
3	4.09 \pm 1%	2.13 \pm 1%	0.00122	0.111
4	1.88 \pm 1%	1.70 \pm 1%	0.00265	0.311
5	6.01 \pm 1%	0.119 \pm 1%	0.000832	1.40
6	29.6 \pm 1%	0.00873 \pm 1%	0.000169	3.87
$\beta = 0.00652 \quad \sum \frac{\beta_i}{\lambda_i} = 0.0849 \text{ sec.}$				

Table A.2 Options for Neutron Generation Time and Maximum Reactivity [8]

C_o (mfd)	R_o (meg Ω)	ℓ (sec.)	b_ρ	ρ_{\max}
0.02	10.0	10 (-4)	2×10 (-4)	5×10 (-5)
0.02	1.0	10 (-4)	2×10 (-3)	5×10 (-4)
0.02	0.1	10 (-4)	2×10 (-2)	5×10 (-3)
0.002	10.0	10 (-5)	2×10 (-4)	5×10 (-5)
0.002	1.0	10 (-5)	2×10 (-3)	5×10 (-4)
0.002	0.1	10 (-5)	2×10 (-2)	5×10 (-3)

is expressed as 1 watt, what is really meant is the neutron density at 1 watt reactor power. Similarly the external source strength is expressed in units of watt/second whereas the actual units should be neutrons/cm³ sec.

Therefore

$$b_n = \frac{e_{\max}}{n_{\max}} = 10 \quad . \quad (\text{volts/watt})$$

The values of C_o and R_o used in this work were

$$R_o = 0.1 \quad , \quad (\text{megohm})$$

and $C_o = 0.02 \quad . \quad (\text{microfared})$

thus determining the following parameters:

$$\ell = 10^{-4} \quad , \quad (\text{sec.})$$

$$\beta/\ell = 65.2 \quad , \quad (\text{sec}^{-1})$$

$$b_\rho = 2 \times 10^{+2} \quad ,$$

$$\rho_{\max} = 5 \times 10^{-3} \quad ,$$

and $b_S = b_\rho b_n \ell = 2 \times 10^{-1} \quad . \quad (\text{volts/watt/sec})$

A value of 17.9 cps for β/ℓ in the KSU TRIGA MARK II Reactor is reported [4]. This corresponds to 112.5 sec⁻¹. With the available options 65.2 sec⁻¹ is the closest possible value. Also values of reactivity over 5×10^{-3} will probably not be required whereas reactivities greater than 5×10^{-4} probably will be required. Therefore it appears the chosen values of C_o and R_o are the best choice.

Now that all relationships between physical quantities and electrical parameters are determined, it is possible to express physical interpretation of some of the electrical networks. First, the feedback loop through

potentiometer #1 (see Figure A.1) represents rod withdrawal and insertion. The magnitude of the reactivity involved in the rod movement is directly proportional to $\Delta \rho_R$ (the setting of potentiometer #1). The proportionality constant, b_ρ , has already been determined. Therefore Table A.3, potentiometer settings and corresponding reactivity values, is constructed.

Reactivity in dollars is reactivity ($\delta k/k$) divided by the total delayed neutron fraction (β). A negative feedback into node n_o represents a positive reactivity insertion. The signal must be inverted to represent a negative reactivity insertion.

The feedback loop through potentiometer #2 is identical to that through potentiometer #1 except that it is added to the source signal such that the source effects can be isolated from the system. Again the magnitude of the reactivity is determined from Table A.3. However, because of the summing junction the signal must be inverted to represent positive reactivity. If it is not inverted the signal is positive at node n_o and thus simulates a negative reactivity insertion.

The external voltage e_s applied to summing junction #2 represents the effective neutron density contribution from the external source. Since the proportionality constant, b_s , has been determined a table of values of e_s and corresponding effective neutron density from the source is constructed. (See Table A.4). Obviously, the feedback loops through the RC networks in unit 2.475 (Figure A.2) represent the six delay group precursor densities. The relationship between the electrical and physical quantities are graphically exhibited in Table A.1. As is explained earlier the input resistance, R_o , and the feedback through capacitor C_o determine the neutron generation time and the maximum reactivity.

Table A.3 Relationship between Potentiometer Settings and Reactivity for Potentiometers #1 and #2

Potentiometer Setting	Reactivity (ρ)	
	$\delta k/k$	(ρ)
1.0	0.0050	0.767
0.5	0.0025	0.383
0.1	0.0005	0.077

Table A.4 Relationship between External Voltage and Effective Neutron Density of the External Source

e_s	Effective Neutron Density
(volts)	(watts/sec.)
10	50
1	5
0.1	0.5

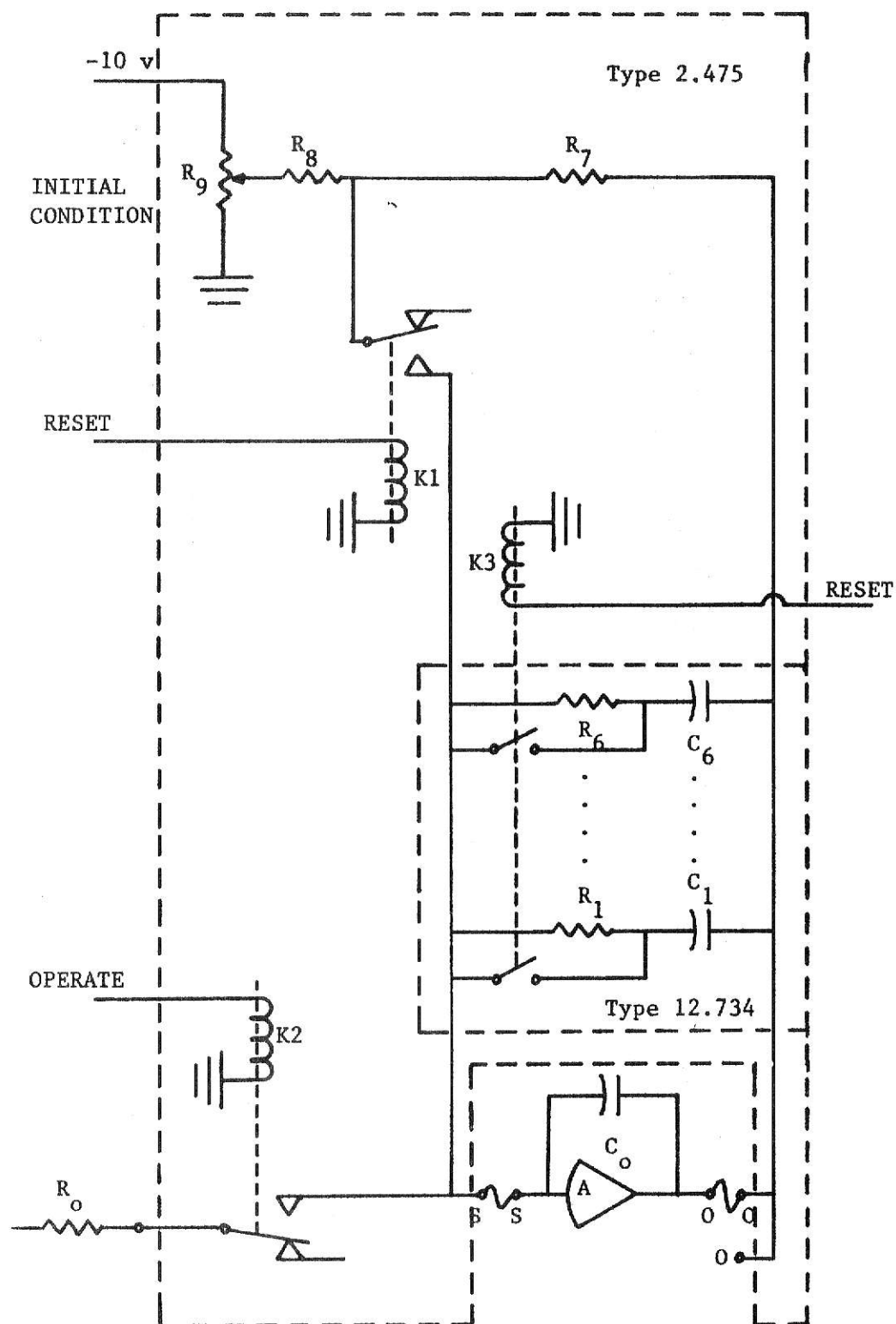


Figure A.2 Operational Relays on the Reactor Simulator Unit

So far the circuit theory simulating the kinetics equations has been described. Also the relationship between the electrical components and the physical quantities they represent has been explained. What remains is to describe briefly how the whole analog unit operates. In doing this, reference will be made to Figure A.2. There are three relays in the reactor simulator (K1, K2, and K3 in Figure A.2). These relays are controlled by the computer mode switch. In Figure A.2 all three relays are shown de-energized. Normally the computer is in the RESET mode, before operation. While in the RESET mode, relays K1 and K3 are energized. This shorts out the six precursor resistors and permits the initial voltage, which is controlled by the INITIAL CONDITION potentiometer, to be applied across all six precursor capacitors. This charges all the capacitors to the selected initial voltage. This operation represents setting the steady-state neutron density and corresponding steady-state precursor densities. When the computer is switched to the HOLD mode all the relays are de-energized. This switches the initial condition voltage out of the circuit and opens the shorts around the precursor resistors. In the HOLD mode, node n_o (S in Figure A.2) is at the same potential as the output of the operational amplifier (O in Figure A.2). The input from the source and reactivity feedback are out of the circuit because relay K2 is de-energized. Since the potential across the precursor RC networks is zero the current through them is zero. Looking back at the nodal balance at node n_o , the only input left is the feedback through C_o . Kirchoff's Law requires the sum of the currents to be zero, therefore

$$C_o \frac{de_n}{dt} , \quad \text{or} \quad \frac{de_n}{dt} = 0 .$$

Thus the HOLD position is representative of steady-state operation.

When the computer is switched to the OPERATE mode relay K2 is energized. This applies the currents from the source and reactivity feedback to node n_o . Since the voltage across the precursor networks is no longer zero the currents from these networks and the feedback through C_o all are summed at n_o . The result is the solution to the kinetics equations at the output of the operational amplifier.

In summary, the circuit theory involved in the analog simulation of the reactor kinetics equations has been described. Also an attempt has been made to relate the operation of the electrical components and networks to the physical quantities they were intended to represent. A complete discussion of the physical problems solved by the equipment described in this section can be found in Section 5 of this paper.

APPENDIX B

Least Squares Fitting of Data to a Straight Line

Chao [6] discusses simple linear regression and the application of least squares to determine the regression relation. The following discussion uses this general development to establish relationships for the specific problems encountered in this paper. When discussing linear bivariate distributions the following are assumed:

1. The values of the independent variable, X , are fixed in advance. They have no observation errors associated with them.
2. The values of the dependent variable, Y , are dependent on the corresponding X values. The Y values are considered random and are left free to take any value associated with X .
3. The true relationship between X and Y can be described by the equation:

$$Y_i = \alpha + \beta X_i + \epsilon_i \quad (\text{B.1})$$

where ϵ_i is the difference between Y_i , the observed value of Y , and the expected value of Y , $\mu_{Y/X}$. Therefore $\mu_{Y/X} = \alpha + \beta X$ represents the average relationship between X and Y .

4. The distribution of the Y values corresponding to a given X value is normal.

5. The normal distribution of Y values is considered to have the same variance, $\sigma_{Y/X}^2$, for all possible values of X .

Since α , the intercept, and β , the slope, completely determine the regression relationship the relationship can be estimated by estimating α and β . If a and b are the estimate for α and β respectively, the following relation defines the computed value of Y , Y_c .

$$Y_c = a + b X \quad (B.2)$$

The deviation of Y_i from Y_c is:

$$e_i = Y_i - Y_c = Y_i - (a + b X_i) \quad (B.3)$$

The least square line is the line that minimizes the sum of the squares of these deviations. To determine the values of the parameters that minimize a function, the derivatives of the function with respect to each parameter is set equal to zero. Therefore

$$\partial F / \partial a = 0, \quad \text{and} \quad \partial F / \partial b = 0;$$

where

$$F = \sum_{i=1}^n e_i^2 = \sum_{i=1}^n (Y_i - (a + b X_i))^2.$$

Performing this differentiation yields the following two normal equations:

$$\sum_{i=1}^n Y_i = n a + b \sum_{i=1}^n X_i \quad (B.4)$$

$$\sum_{i=1}^n X_i Y_i = a \sum_{i=1}^n X_i + b \sum_{i=1}^n X_i^2 \quad (B.5)$$

These two equations can be solved simultaneously yielding the following expressions for a and b :

$$a = \frac{\sum_{i=1}^n X_i^2 \sum_{i=1}^n Y_i - \sum_{i=1}^n X_i \sum_{i=1}^n (X_i Y_i)}{D}, \quad (B.6)$$

$$\text{and} \quad b = \frac{n \sum_{i=1}^n (X_i Y_i) - \sum_{i=1}^n X_i \sum_{i=1}^n Y_i}{D}; \quad (B.7)$$

$$\text{where} \quad D = n \sum_{i=1}^n X_i^2 - \left(\sum_{i=1}^n X_i \right)^2.$$

An indication of the degree of precision with which the computed line estimates the population regression line is σ_{Y_c} . Since σ_{Y_c} is not known it must be estimated. The conditional standard deviation, $\sigma_{Y/X}$, is also not known but its unbiased estimator, $\hat{s}_{Y/X}$, is known and

$$\hat{s}_{Y/X} = \sqrt{\sum_{i=1}^n e_i^2 / (n - 2)} . \quad (B.8)$$

The estimators of σ_a and σ_b are:

$$\hat{s}_a = \hat{s}_{Y/X} \sqrt{\sum_{i=1}^n X_i^2 / D} , \quad (B.9)$$

and

$$\hat{s}_b = \hat{s}_{Y/X} \sqrt{n/D} . \quad (B.10)$$

From these relationships \hat{s}_{Y_c} can be determined and

$$\hat{s}_{Y_c}(X_i) = \hat{s}_{Y/X} \sqrt{(1/n + n(X_i - \bar{X})^2/D)} . \quad (B.11)$$

The confidence interval for the population regression line can be established.

The function $(Y_c - \mu_{Y/X})/\hat{s}_{Y_c}$ follows the t distribution with $n - 2$ degrees of freedom. Therefore the following relation holds:

$$P(Y_c - t(i,j) \hat{s}_{Y_c} < \mu_{Y/X} < Y_c + t(i,j) \hat{s}_{Y_c}) = 1 - \alpha ; \quad (B.12)$$

where

$$i = \alpha/2 ,$$

and

$$j = n - 2 = \text{degrees of freedom.}$$

To test for homogeneity of the slope [13] for a large number of observations, the data can be divided into r subsets. There are n_j

observations in the j th subset. A straight line is fitted to the data from each subset such that

$$Y_{cj} = a_j + b_j X_i, \quad j = 1, 2, \dots, r;$$

and

$$e_{ij} = Y_i - Y_{cj} = Y_i - (a_j + b_j X_i).$$

It is assumed that the variance ($\sigma_{Y/X}^2$) and the true slope ($\mu_{Y/X}$) are the same in each subset. The variance of the slope in each subset is

$$\sigma_{b_j}^2 = \sigma_{Y/X}^2 / D_j / n_j, \quad (B.13)$$

where

$$D_j = n_j \sum_{i=1}^{n_j} X_i^2 - \left(\sum_{i=1}^{n_j} X_i \right)^2.$$

The weighted mean of the slopes is

$$\bar{b} = \frac{\sum_{j=1}^r W_j b_j}{\sum_{j=1}^r W_j}, \quad (B.14)$$

where

$$W_j = \sigma_{Y/X}^2 / \sigma_{b_j}^2 = D_j / n_j. \quad (B.15)$$

If the slopes are homogeneous (i.e. $\sigma_{Y/X}^2$ and $\mu_{Y/X}$ equal), the following expression will be distributed as F with $r - 1$ and $n - 2r$ degrees of freedom:

$$F = \frac{\sum_{j=1}^r W_j (b_j - \bar{b})^2}{r - 1} / \frac{\sum_{j=1}^r \sum_{i=1}^{n_j} e_{ij}^2}{n - 2r}. \quad (B.16)$$

If F is less than $F(\alpha)$ the slope is considered homogeneous for a significance level of α . Also the average slope, \bar{b} , is an estimate of $\mu_{Y/X}$ with variance equal to

$$\sigma_{\bar{b}}^2 = \sigma_{Y/X}^2 / \sum_{j=1}^r W_j.$$

An unbiased estimate of the standard deviation of \bar{b} is

$$\hat{s}_{\bar{b}} = \hat{s}_{X/Y} / \sqrt{\sum_{j=1}^r w_j} . \quad (\text{B.17})$$

APPENDIX C

Numerical Solution of the Time and Space Dependent Temperature

Distribution in the Fuel and Cladding

Following the procedure described in Arpaci [3] and using the assumptions outlined on pages 13 and 14 of this paper, a numerical solution to the temperature distribution in the fuel and cladding of a TRIGA fuel element is developed.

The fuel is divided into control volumes Δx high and Δr_f thick. Each Δx section of fuel has NL concentric control volumes. Since the cladding is very thin (30 mils), it is divided into control volumes Δx high and r_c thick, where r_c is the thickness of the cladding. Figure C.1 depicts a typical Δx section of fuel and cladding. A solution to the temperature distribution is accomplished by making a heat balance at each node. The heat generation is considered constant within each control volume.

The net heat change in each control volume is equal to the heat generated within the volume, plus the heat flow into the control volume, plus the heat flow out of the control volume, or

$$q_{\text{net}} = q_G + q_I + q_O \quad . \quad (\text{watts}) \quad (\text{C.1})$$

At the central node (node 1) the heat generation in the control volume is

$$q_G = Q(x) \Delta x \pi r_1^2 \quad . \quad (\text{watts}) \quad (\text{C.2})$$

The net heat change in the control volume is

$$q_{\text{net}} = \rho_f \Delta x \pi r_1^2 \quad dT/dt \quad . \quad (\text{watts}) \quad (\text{C.3})$$

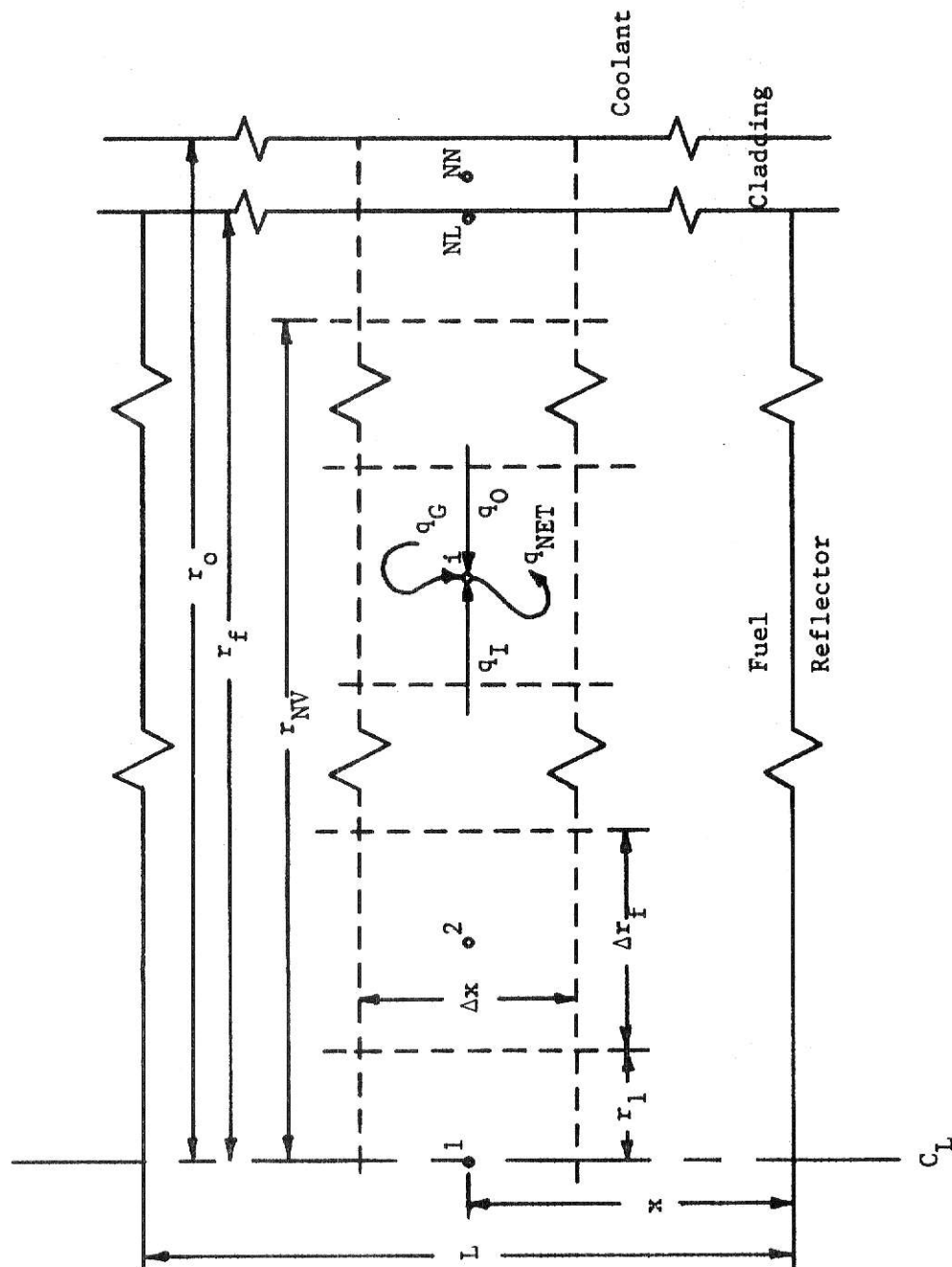


Figure C.1 Typical Control Volumes for Numerical Solution of Temperatures in the Fuel and Cladding

If the temperature distribution is assumed to have radial symmetry and since there is assumed to be no axial heat flow, heat can only flow outward from node 1. The outward heat flow is

$$q_0 = k_f 2\pi r_1 \Delta x \left. \frac{dT}{dr} \right|_{r_1} . \quad (\text{watts}) \quad (\text{C.4})$$

In fuel nodes 2 through NV, designated as node (i), the heat generation is

$$q_G = Q(x) \Delta x (\pi r_i^2 - \pi r_{i-1}^2) . \quad (\text{watts}) \quad (\text{C.5})$$

The net heat change is

$$q_{\text{NET}} = \rho_f c_f \Delta x (\pi r_i^2 - \pi r_{i-1}^2) \frac{dT}{dt} . \quad (\text{watts}) \quad (\text{C.6})$$

The heat flow inward is

$$q_I = -k_f 2\pi r_{i-1} \Delta x \left. \frac{dT}{dr} \right|_{r_{i-1}} . \quad (\text{watts}) \quad (\text{C.7})$$

The heat flow outward is

$$q_0 = k_f 2\pi r_i \Delta x \left. \frac{dT}{dr} \right|_{r_i} . \quad (\text{watts}) \quad (\text{C.8})$$

In node NL the heat generation is

$$q_G = Q(x) \Delta x (\pi r_f^2 - \pi r_{\text{NV}}^2) . \quad (\text{watts}) \quad (\text{C.9})$$

The net heat change is

$$q_{\text{NET}} = \rho_f c_f \Delta x (\pi r_f^2 - \pi r_{\text{NV}}^2) \frac{dT}{dt} . \quad (\text{watts}) \quad (\text{C.10})$$

The heat flow inward is

$$q_I = -k_f 2\pi r_{\text{NV}} \Delta x \left. \frac{dT}{dr} \right|_{r_{\text{NV}}} . \quad (\text{watts}) \quad (\text{C.11})$$

The heat flow outward is

$$q_0 = -h_{\text{gap}} 2\pi r_f \Delta x (T_{\text{NL}} - T_{\text{NN}}) . \quad (\text{watts}) \quad (\text{C.12})$$

There is no heat generation in the cladding in the control volume around node NN. The net heat change is

$$q_{\text{NET}} = \rho_c c_c \Delta x (\pi r_o^2 - \pi r_f^2) \frac{dT}{dt} . \quad (\text{watts}) \quad (\text{C.13})$$

The heat flow inward is

$$q_I = h_{\text{gap}} 2\pi r_f \Delta x (T_{\text{NL}} - T_{\text{NN}}) . \quad (\text{watts}) \quad (\text{C.14})$$

The heat flow outward is

$$q_O = -h_w 2\pi r_o (T_{\text{NN}} - T_O) \Delta x . \quad (\text{watts}) \quad (\text{C.15})$$

Note that since there is only one node in the cladding all the cladding will be at the same temperature. Therefore the wall temperature (T_w) is identical to the internal temperature (T_{NN}).

In order to solve the system of equations numerically the differentials must be linearized. This is done by utilizing the forward difference approximation. The differentials become

$$\left. \frac{dT}{dr} \right|_{r_i} = \frac{T_i^n - T_{i+1}^n}{\Delta r} , \quad (^\circ\text{C/cm}) \quad (\text{C.16})$$

and

$$\frac{dT}{dt} = \frac{T_i^{n+1} - T_i^n}{\Delta t} . \quad (^\circ\text{C/sec}) \quad (\text{C.17})$$

The heat balance at node 1 becomes

$$k_f 2\pi r_1 \Delta x \frac{(T_2^n - T_1^n)}{\Delta r_f} + Q(x) \Delta x r_1^2 = \rho_f c_f \pi r_1^2 \Delta x \frac{(T_1^{n+1} - T_1^n)}{\Delta r_f} . \quad (\text{C.18})$$

The heat balance at node i (i=2 through NV) becomes

$$\begin{aligned} k_f 2\pi r_1 \Delta x \frac{(T_{i+1}^n - T_i^n)}{\Delta r_f} + k_f 2\pi r_{i-1} \Delta x \frac{(T_{i-1}^n - T_i^n)}{\Delta r_f} \\ + Q(x) \Delta x (\pi r_i^2 - \pi r_{i-1}^2) = \rho_f c_f \Delta x (\pi r_i^2 - \pi r_{i-1}^2) \frac{(T_i^{n+1} - T_i^n)}{\Delta t} . \end{aligned} \quad (\text{C.19})$$

The heat balance at node NL becomes

$$\begin{aligned}
 h_{\text{gap}} 2\pi r_f \Delta x (T_{\text{NN}}^n - T_{\text{NL}}^n) + k_f 2\pi r_{\text{NV}} \Delta x \frac{(T_{\text{NV}}^n - T_{\text{NL}}^n)}{\Delta r_f} \\
 + Q(x) \Delta x (\pi r_f^2 - \pi r_{\text{NV}}^2) = \rho_f c_f \Delta x (\pi r_f^2 - \pi r_{\text{NV}}^2) \frac{(T_{\text{NL}}^{n+1} - T_{\text{NL}}^n)}{\Delta t} .
 \end{aligned}
 \tag{C.20}$$

The heat balance at node NN becomes

$$h_{\text{gap}} 2\pi r_f (T_{\text{NL}}^n - T_{\text{NN}}^n) + h_w 2\pi r_o (T_o - T_{\text{NN}}^n) = \rho_c c_c (\pi r_o^2 - \pi r_f^2) \frac{(T_{\text{NN}}^{n+1} - T_{\text{NN}}^n)}{\Delta t} .
 \tag{C.21}$$

In order to facilitate later computations the following factors are defined:

$$\text{HW} = 2 h_w r_o ; \quad (\text{watts/cm-}^\circ\text{C})$$

$$\text{HG} = 2 h_{\text{gap}} r_f ; \quad (\text{watts/cm-}^\circ\text{C})$$

$$K(i) = \frac{2 k_f r_i}{\Delta r_f} , \quad (i=1, \text{NV}) ; \quad (\text{watts/cm-}^\circ\text{C})$$

$$Q(1) = Q(x) r_1^2 ; \quad (\text{watts/cm})$$

$$Q(i) = Q(x) (r_i^2 - r_{i-1}^2) , \quad (i=2, \text{NV}) ; \quad (\text{watts/cm})$$

$$Q(\text{NL}) = Q(x) (r_f^2 - r_{\text{NV}}^2) ; \quad (\text{watts/cm})$$

$$P(1) = \frac{\rho_f c_f r_1^2}{\Delta t} ; \quad (\text{watts/cm-}^\circ\text{C})$$

$$P(i) = \frac{\rho_f c_f (r_i^2 - r_{i-1}^2)}{\Delta t} ; \quad (\text{watts/cm-}^\circ\text{C})$$

$$P(\text{NL}) = \frac{\rho_f c_f (r_f^2 - r_{\text{NV}}^2)}{\Delta t} ; \quad (\text{watts/cm-}^\circ\text{C})$$

and

$$P(NN) = \frac{\rho_c c_c (r_o^2 - r_f^2)}{\Delta t} \quad (\text{watts/cm-}^\circ\text{C})$$

Using the previously derived heat balances the temperatures at each node can be solved explicitly as

$$T_1^{n+1} = \frac{K(1) T_2^n}{P(1)} + \frac{Q(1)}{P(1)} + [1 - \frac{K(1)}{P(1)}] T_1^n ; \quad (^\circ\text{C}) \quad (C.22)$$

$$T_i^{n+1} = \frac{K(i) T_{i+1}^n}{P(i)} + \frac{K(i-1) T_{i-1}^n}{P(i)} + \frac{Q(i)}{P(i)} + [1 - \frac{K(i) + K(i-1)}{P(i)}] T_i^n , \quad (i=2, NV) \quad (C.23)$$

$$T_{NL}^{n+1} = \frac{HG T_{NN}^n}{P(NL)} + \frac{K(NV) T_{NV}^n}{P(NL)} + \frac{Q(NL)}{P(NL)} + [1 - \frac{HG + K(NV)}{P(NL)}] T_{NL}^n , \quad (C.24)$$

and

$$T_{NN}^{n+1} = \frac{HG T_{NL}^n}{P(NN)} + \frac{HW T_0}{P(NN)} + [1 - \frac{HG + HW}{P(NN)}] T_{NN}^n . \quad (C.25)$$

Starting with all temperatures at the ambient temperature, T_0 , the temperatures at each node can be solved explicitly at later times in Δt increments.

The temperatures at each node can also be solved implicitly as follows:

$$[1 + \frac{K(1)}{P(1)}] T_1^{n+1} - \frac{K(1)}{P(1)} T_2^{n+1} = T_1^n + \frac{Q(1)}{P(1)} , \quad (C.26)$$

$$\frac{-K(i-1)}{P(i)} T_{i-1}^{n+1} + [1 + \frac{K(i)}{P(i)} + \frac{K(i-1)}{P(i)}] T_i^{n+1} - \frac{K(i)}{P(i)} T_{i+1}^{n+1} = T_i^n + \frac{Q(i)}{P(i)} , \quad (C.27)$$

$$\frac{-K(NV)}{P(NL)} T_{NV}^{n+1} + [1 + \frac{K(NV)}{P(NL)} + \frac{HG}{P(NL)}] T_{NL}^{n+1} - \frac{HG}{P(NL)} T_{NN}^{n+1} = T_{NL}^n + \frac{Q(NL)}{P(NL)} , \quad (C.28)$$

and

$$\frac{-HG}{P(NN)} T_{NL}^{n+1} + [1 + \frac{HG}{P(NN)} + \frac{HW}{P(NN)}] T_{NN}^{n+1} = T_{NN}^n + \frac{HW T_0}{P(NN)} . \quad (C.29)$$

Again starting with all the temperatures at the ambient temperature, T_0 , the temperatures at all the nodes can be solved simultaneously at later times in Δt increments.

Eventually the system will reach a steady-state condition. At such a time all time differentials become identically equal to zero. The nodal heat balances then become:

node 1 -

$$k_f 2\pi r_1 \frac{(T_2 - T_1)}{\Delta r_f} + Q(x) \pi r_1^2 = 0, \quad (C.30)$$

node i ($i = 2, NV$) -

$$k_f 2\pi r_i \frac{(T_{i+1} - T_i)}{\Delta r_f} + k_f 2\pi r_{i-1} \frac{(T_{i-1} - T_i)}{\Delta r_f} + Q(x) (\pi r_i^2 - \pi r_{i-1}^2) = 0, \quad (C.31)$$

node NL -

$$h_{gap} 2\pi r_f (T_{NN} - T_{NL}) + k_f 2\pi r_{NV} \frac{(T_{NV} - T_{NL})}{\Delta r_f} + Q(x) (\pi r_f^2 - \pi r_{NV}^2) = 0, \quad (C.32)$$

node NN -

$$h_{gap} 2\pi r_f (T_{NL} - T_{NN}) + h_w 2\pi r_o (T_o - T_{NN}) = 0. \quad (C.33)$$

At steady-state all the heat generated in the fuel must be deposited in the coolant. Therefore

$$Q(x) \Delta x \pi r_f^2 = 2\pi r_o \Delta x h_w (T_{NN} - T_o), \quad (\text{watts}) \quad (C.34)$$

and

$$h_w = \frac{Q(x) r_f^2}{2r_o (T_{NN} - T_o)}. \quad (\text{watts/cm}^2\text{-}^\circ\text{C}) \quad (C.35)$$

If one more factor is defined as

$$QF = Q(x) r_f^2, \quad (\text{watts/cm})$$

then

$$T_{NN} = \frac{HW}{QF} + T_o \quad (^\circ\text{C}) \quad (\text{C.36})$$

The nodal balances become;

node 1 -

$$K(1) T_1 - K(1) T_2 = Q(1), \quad (\text{C.37})$$

node i (i = 2, NV) -

$$-K(i-1) T_{i-1} + [K(i) + K(i-1)] T_i - K(i) T_{i+1} = Q(i), \quad (\text{C.38})$$

node NL -

$$-K(NV) T_{NV} + [HG + K(NV)] T_{NL} = \frac{HG HW}{QF} + HG T_o + Q(NL). \quad (\text{C.39})$$

Once the steady-state heat transfer coefficient is determined, the steady-state cladding temperature is solved explicitly using equation C.36. The steady-state fuel temperature can be determined simultaneously from the nodal balances.

APPENDIX D

Natural Convection Heat Transfer from a Vertical Cylinder

A derivation of the natural convection from a flat plate is worked out by J. P. Holman [14]. In natural convection all the heat is deposited in a film layer in the coolant surrounding the heated plate. The liquid in this film has a vertical and horizontal velocity and temperature distribution.

Holman determined the horizontal temperature profile to be

$$\frac{T(y,x) - T_o}{T_w(x) - T_o} = \left[1 - \frac{y}{\delta(x)}\right]^2 ; \quad (D.1)$$

where T_o = the ambient coolant temperature,
 $T_w(x)$ = the cladding wall temperature at height x , and
 $\delta(x)$ = the film thickness at x .

The horizontal velocity profile was determined to be

$$\frac{u(y,x)}{U(x)} = \frac{y}{\delta(x)} \left[1 - \frac{y}{\delta(x)}\right]^2 ; \quad (D.2)$$

$$\text{where } U(x) = \frac{g\beta \delta(x)^2 (T_w(x) - T_o)}{4\nu} , \quad (D.3)$$

g = the acceleration of gravity,

β = the coefficient of expansion,

and ν = the kinematic viscosity.

These equations can be applied directly to the film around a large cylinder if the horizontal distance from the plate, y , is replaced by the radial distance from the cylinder, $r-r_o$. The temperature profile then becomes

$$\frac{T(r,x) - T_o}{T_w(x) - T_o} = \left[\frac{r_o - r + \delta(x)}{\delta(x)} \right]^2 ; \quad (D.4)$$

and the velocity profile becomes

$$\frac{u(r,x)}{U(x)} = \frac{r-r_o}{\delta(x)} \left[\frac{r_o - r + \delta(x)}{\delta(x)} \right]^2 . \quad (D.5)$$

If $\delta(x)$ can be determined then $U(x)$, $u(r,x)$, and $T(r,x)$ are all determined. Instead of trying to find a continuous solution for $\delta(x)$, the film is divided in Δx sections as is done for the fuel and cladding (see Appendix C). The film is then represented by a series of control volumes Δx high and $\delta(x_i)$ wide. Inside each control volume the temperature distribution is $T(r,x_i)$ and the velocity distribution is $u(r,x_i)$. Thus within each control volume the temperature and velocity are only radially dependent. In order to determine the relationship between temperatures in adjacent film control volumes and between adjacent film and cladding control volumes a heat flow balance is performed. Referring to Figure D.1, a heat flow balance on the film control volume at x_i requires that the heat flow out of the element (q_3) be equal to the heat flow into the element from the film element below (q_1) plus the heat flow into the element from the fuel (q_2). Heat is transferred out of the fuel element by conductive heat transfer through the water-cladding interface. The heat flow out of a fuel element section, Δx , can be expressed as

$$q_2 = -k_w 2\pi r_o \Delta x \left. \frac{dT}{dr} (r,x_i) \right|_{r_o} . \quad (\text{watts}) \quad (D.6)$$

Heat is transferred into a film element and out of the film element by the mass transfer of the heated fluid. The total heat flow in an incremental volume Δx by dr in the film control volume at x_i is

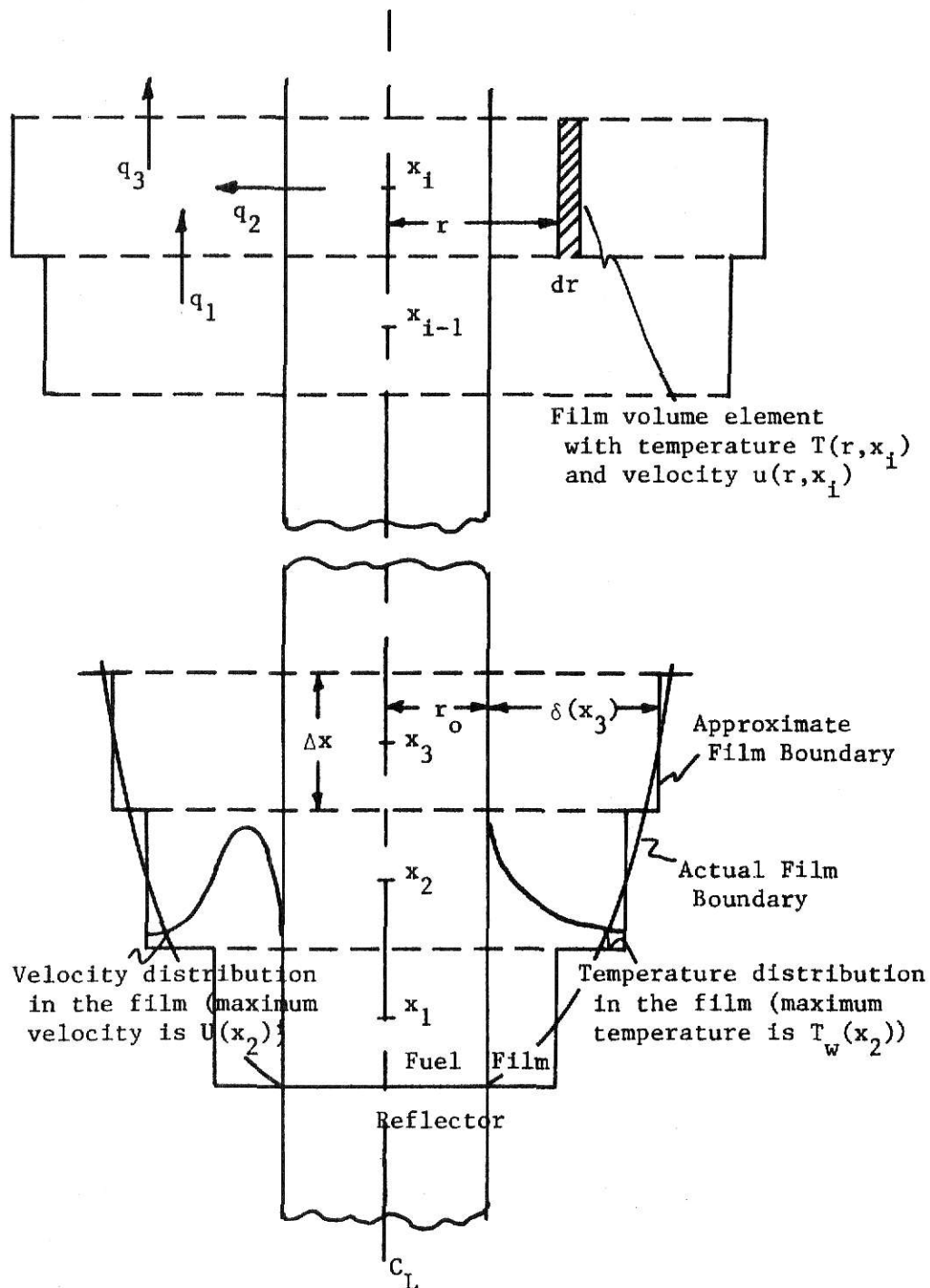


Figure D.1 Typical Natural Convection Film around a Fuel Element

$$dq = \rho c_p u(r, x_1) (T(r, x_1) - T_0) 2\pi r dr . \quad (\text{watts})$$

The total heat flow in the element is

$$q = \int_{r_0}^{r_0 + \delta(x_1)} \rho c_p u(r, x_1) (T(r, x_1) - T_0) 2\pi r dr . \quad (\text{watts}) \quad (\text{D.7})$$

The velocity and temperature distributions have already been determined as

$$u(r, x_1) = U(x_1) \frac{(r-r_0)}{\delta(x_1)} \left[\frac{r_0 - r + \delta(x_1)}{\delta(x_1)} \right]^2 , \quad (\text{cm/sec}) \quad (\text{D.8})$$

$$\text{and} \quad T(r, x_1) - T_0 = (T_w(x_1) - T_0) \left[\frac{r_0 - r + \delta(x_1)}{\delta(x_1)} \right]^2 . \quad (^\circ\text{C}) \quad (\text{D.9})$$

The total heat flow in the element can then be expressed as

$$q = \int_{r_0}^{r_0 + \delta(x_1)} \rho U(x_1) 2\pi (T_w(x_1) - T_0) r \frac{(r-r_0)}{\delta(x_1)} \left[\frac{r_0 - r + \delta(x_1)}{\delta(x_1)} \right]^4 dr ,$$

or

$$q = \rho c_p 2\pi (T_w(x_1) - T_0) \frac{U(x_1) \delta(x_1)}{30} \left[r_0 + \frac{2}{7} \delta(x_1) \right] . \quad (\text{watts}) \quad (\text{D.10})$$

The velocity normalization was defined as

$$U(x_1) = \frac{g\beta (T_w(x_1) - T_0)}{4\nu} \delta(x_1)^2 . \quad (\text{cm/sec}) \quad (\text{D.11})$$

The total heat flow in the film element at x_1 then becomes

$$q = \rho c_p 2\pi (T_w(x_1) - T_0)^2 \frac{g\beta \delta(x_1)^3}{120\nu} \left[r_0 + \frac{2}{7} \delta(x_1) \right] . \quad (\text{watts}) \quad (\text{D.12})$$

The temperature gradient at the water-cladding interface at x_1 is

$$\left. \frac{dT}{dr} \right|_{r=r_0} = (T_w(x_i) - T_0) \frac{d}{dr} \left[\frac{r_0 - r + \delta(x_i)}{\delta(x_i)} \right]^2 \Big|_{r_0}, \quad (^\circ\text{C}/\text{cm})$$

$$\text{or} \quad \left. \frac{dT}{dr} \right|_{r=r_0} = -2 \frac{(T_w(x_i) - T_0)}{\delta(x_i)}. \quad (^\circ\text{C}/\text{cm}) \quad (\text{D.13})$$

Therefore the heat flow into the film element at x_i from the fuel control volume at x_i is

$$q_2 = k_w 4\pi r_0 \Delta x \frac{(T_w(x_i) - T_0)}{\delta(x_i)}. \quad (\text{watts}) \quad (\text{D.14})$$

The heat flow balance on the fuel element at x_i becomes

$$\begin{aligned} \rho c_p 2\pi (T_w(x_i) - T_0)^2 \frac{g\beta \delta(x_i)^3}{120\nu} \left[r_0 + \frac{2}{7} \delta(x_i) \right] &= k \frac{4\pi (T_w(x_i) - T_0)}{\delta(x_i)} r_0 \Delta x \\ &+ \rho c_p 2\pi (T_w(x_{i-1}) - T_0)^2 \frac{g\beta \delta(x_{i-1})^3}{120\nu} \left[r_0 + \frac{2}{7} \delta(x_{i-1}) \right]. \quad (\text{watts}) \end{aligned} \quad (\text{D.15})$$

From this heat flow balance comes a transcendental solution for the film thickness

$$\delta(x_i) = \frac{\delta(x_i)^4 (T_w(x_i) - T_0)^2 \left[r_0 + \frac{2}{7} \delta(x_i) \right] - \frac{k_w 240\nu r_0 \Delta x (T_w(x_i) - T_0)}{\rho c_p \beta g}}{\delta(x_{i-1})^3 (T_w(x_{i-1}) - T_0)^2 \left[r_0 + \frac{2}{7} \delta(x_{i-1}) \right]}. \quad (\text{cm}) \quad (\text{D.17})$$

If all the parameters determined from the previous control volume are lumped into one factor namely

$$B(x_i) = \delta(x_{i-1})^3 (T_w(x_{i-1}) - T_0)^2 \left[r_0 + \frac{2}{7} \delta(x_{i-1}) \right]. \quad (\text{cm}^4 \text{ } ^\circ\text{C}^2) \quad (\text{D.18})$$

The film thickness at x_1 can be written as

$$\delta(x_1) = \left[\frac{\frac{\delta(x_1) B(x_1)}{(T_w(x_1) - T_0)^2} + \frac{240 r_o \Delta x x_1^3}{Pr Gw}}{r_o + \frac{2}{7} \delta(x_1)} \right]^{1/4} \quad (\text{cm}) \quad (\text{D.18})$$

Since there is no heat flow from the film control volume below into the control volume at x_1 the expression for the film thickness at x_1 becomes

$$\delta(x_1) = \left[\frac{\frac{240 r_o \Delta x x_1^3}{Pr Gw}}{r_o + \frac{2}{7} \delta(x_1)} \right]^{1/4} \quad (\text{cm}) \quad (\text{D.19})$$

At steady-state the total heat generated in the fuel control volume must be deposited in the adjacent film control volume. Therefore,

$$Q(x_1) \Delta x \pi r_f^2 = \frac{k_w 4\pi r_o \Delta x (T_w(x_1) - T_0)}{\delta(x_1)}, \quad (\text{watts})$$

or

$$T_w(x_1) - T_0 = \frac{\delta(x_1) Q(x_1) r_f^2}{4 k_w r_o} \quad (^\circ\text{C}) \quad (\text{D.20})$$

The film thickness in the first control volume at steady-state is the same as in equation D.19. In subsequent control volumes the film thickness is

$$\delta(x_1) = \left[\frac{\frac{16 k_w^2 r_o^2 B(x_1)}{Q(x_1)^2 r_f^4 \delta(x_1)} + \frac{240 k_w r_o \Delta x x_1^3}{Pr Gw}}{r_o + \frac{2}{7} \delta(x_1)} \right]^{1/4} \quad (\text{cm}) \quad (\text{D.21})$$

Using these equation the film thickness can be determined in each control volume at any time. Once the film thickness is determined the coolant temperature and velocity distributions are found using equations D.4 and D.5.

APPENDIX E

Experimental Temperature Distribution in the Pool

In order to gain insight into the flow patterns and heat transfer within the reactor pool, this experiment is designed to map the temperature profiles within the pool during steady-state operation. A grid of 33 points throughout the pool is established. Figure E.1 depicts the location of these grid points. Using the temperature sensing equipment described in Section 4 of this paper, the temperatures are recorded at all grid points during three hours of steady-state 100 kw operation.

Only six thermistors are available therefore not all the grid points can be monitored during a single operation. Seven separate runs are made at approximately the same operating power. Data for each run appears in Table E.1. During each run temperatures from a reference thermistor located at the same position for all runs are recorded. At all times the central thimble is out, the pool covers are closed, and the primary cooling is off.

The procedure during each run is identical. First the grid thermistors and the reference thermistor are positioned. The ambient temperatures are recorded and the temperatures are monitored for the duration of the experiment. The reactor is brought to steady-state zero power (1 watt). The reactor is then brought to 100 kw on about a 30 second period and held at 100 kw with as little rod movement as possible. Both the time for the start to 100 kw and the time 100 kw is reached are recorded. From the start to 100 kw until the end of the experiment all temperatures are recorded approximately every 1.5 minutes. The reactor is scrammed after three hours of 100 kw operation and temperatures are no longer monitored.

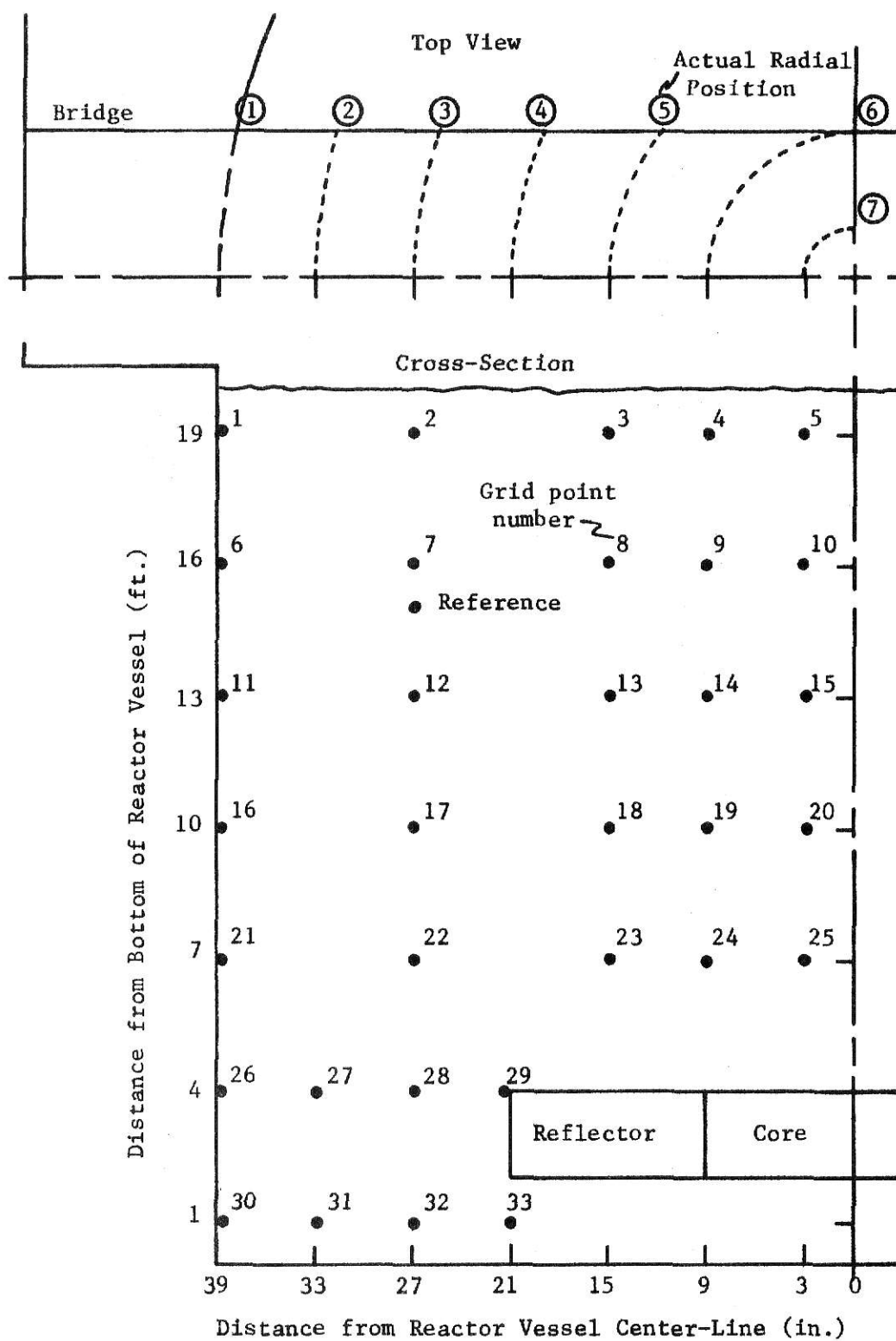


Figure E.1 Grid Positions for Temperature Distribution Experiment

Table E.1 Parameters for Pool Temperature Distribution Experiment

Run #	Power		Ambient Reference Temperature (deg C)	Time Start to Power (min)	Probe Locations					
	Indicated	Actual*			1	2	3	4	5	6
1	100.0	108.1	20.79	-6.10	30/31/32/33/ref/air					
2	100.0	104.4	21.23	-6.00	26/27/28/29/ref/air					
3	100.0	102.4	24.01	-5.75	21/22/23/24/25/ref					
4	100.0	103.5	22.92	-7.00	16/17/18/19/20/ref					
5	100.0	109.9	18.38	-5.85	11/12/13/14/15/ref					
6	100.0	106.3	20.88	-5.03	6/ 7/ 8/ 9/10/ref					
7	100.0	104.0	22.73	-5.80	1/ 2/ 3/ 4/ 5/ref					

*From the analysis in Section 4.33, using a total heat capacity of
20 kw hr/deg C.

The resulting data is analyzed with the aid of a computer program. All time is measured from the time 100 kw is reached. All temperatures are computed as temperature differences from the temperatures at the time of start to 100 kw. The computer program (DATAFIX) prints out a temperature grid of all 33 points plus the temperatures of the reference thermistors for various times. DATAFIX also computes a normalized grid. The normalization is the temperature of reference 1 divided by the temperature of reference i. Some typical results from DATAFIX appear in Table E.2.

The results from DATAFIX can be displayed more graphically in the form of isothermal charts. The isothermal lines are computed by rough linear interpolation between grid temperatures. Isothermal charts for various times appear in Figures E.2, E.3, and E.4. From these charts several general characteristics of the heat transfer in the pool can be surmised.

Initially it appears the warmed water leaving the core forms a column of rising water within the pool. This column is approximately the radius of the core. The height varies with time. As can be seen in Figure E.2, the column has risen well up the pool by the time the reactor reaches 100 kw. The temperature gradient is very steep at the outer edge of the column. The temperature gradient within the column in the direction of flow is much less steep. This column continues to rise until it hits the upper water level in the pool. At this time a chimney of warmer water from the core to the upper water level is established within the pool. Also at this point a second stage in the development of the flow begins.

It appears that when the velocity of the rising water is deaccelerated and changed in direction as a result of its collision with the water surface some mixing occurs. This can be seen in Figure E.2. After operating for two minutes at 100 kw the column appears to have reached the water surface.

Table E.2 Typical Results from DATAFIX

Time from T-100 kw = 60.0 min.					
Grid pt./Temperature Rise (deg C)					
<hr/>					
Unnormalized Data					
1/5.74	2/5.67	3/5.68	4/5.73	5/ 5.82	ref 1/5.57
6/5.56	6/5.68	8/5.77	9/5.81	10/ 6.19	ref 2/5.59
11/5.75	12/5.92	13/6.00	14/6.23	15/ 6.78	ref 3/5.88
16/5.15	17/5.34	18/5.39	19/5.58	20/ 7.70	ref 4/5.46
21/4.85	22/4.81	23/4.81	24/4.97	25/11.12	ref 5/5.48
26/4.05	27/4.05	28/4.07	29/4.07	XXXXXXXX	ref 6/5.40
30/0.93	31/0.99	32/1.00	33/0.96	XXXXXXXX	ref 7/5.71
Normalized Data					
1/5.74	2/5.67	3/5.68	4/5.73	5/ 5.82	ref 1/5.57
6/5.55	7/5.66	8/5.76	9/5.80	10/ 6.18	ref 2/5.57
11/5.44	12/5.61	13/5.69	14/5.91	15/ 6.42	ref 3/5.57
16/5.26	17/5.45	18/5.50	19/5.70	20/ 7.85	ref 4/5.57
21/4.93	22/4.89	23/4.90	24/5.05	25/11.31	ref 5/5.57
26/4.19	27/4.19	28/4.20	29/4.20	XXXXXXXX	ref 6/5.57
30/0.91	31/0.97	32/0.98	33/0.94	XXXXXXXX	ref 7/5.57

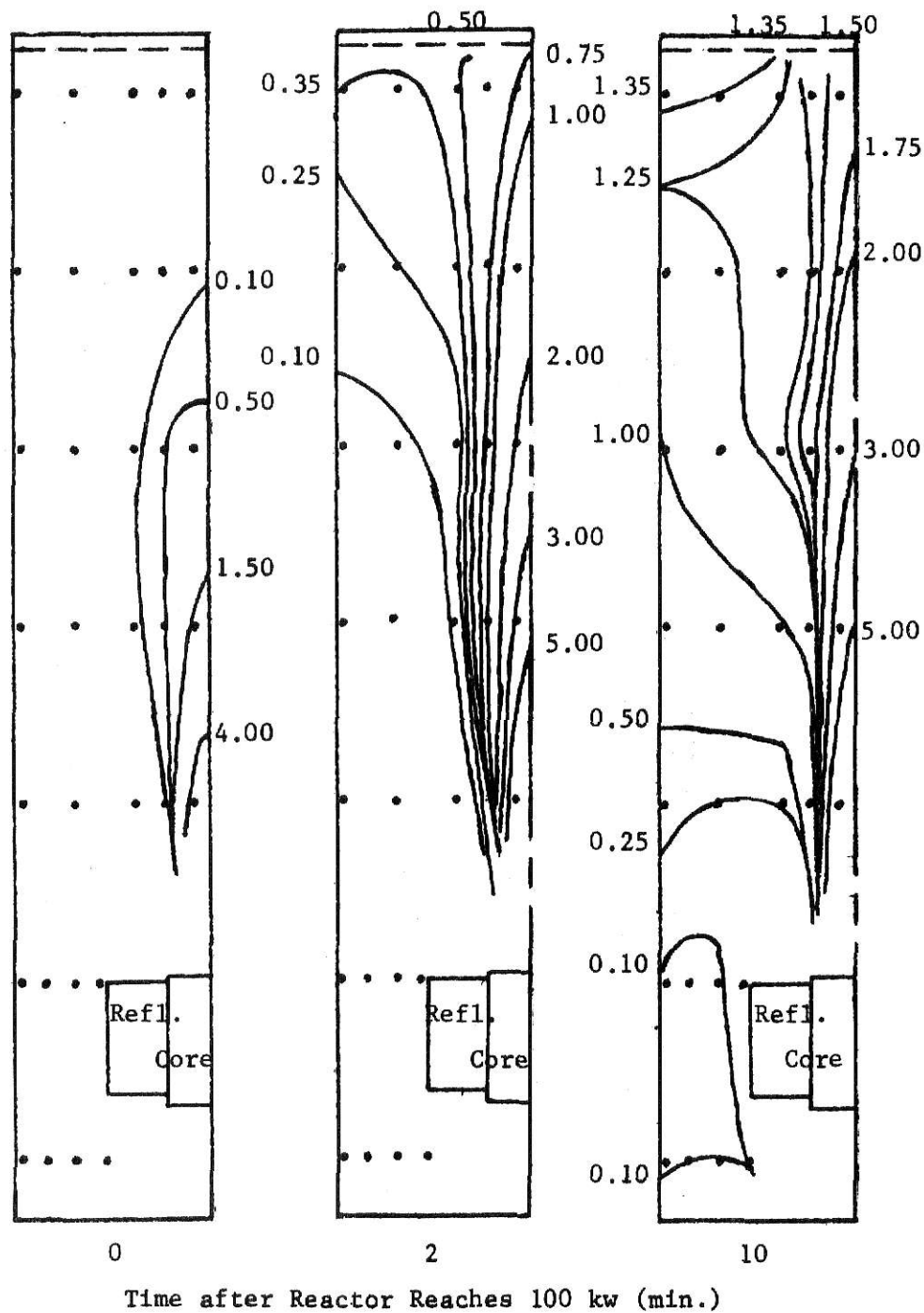


Figure E.2 Temperature Distribution in the Reactor Pool during 100 kw Steady-State Operation (isothermal lines in degrees C above ambient)

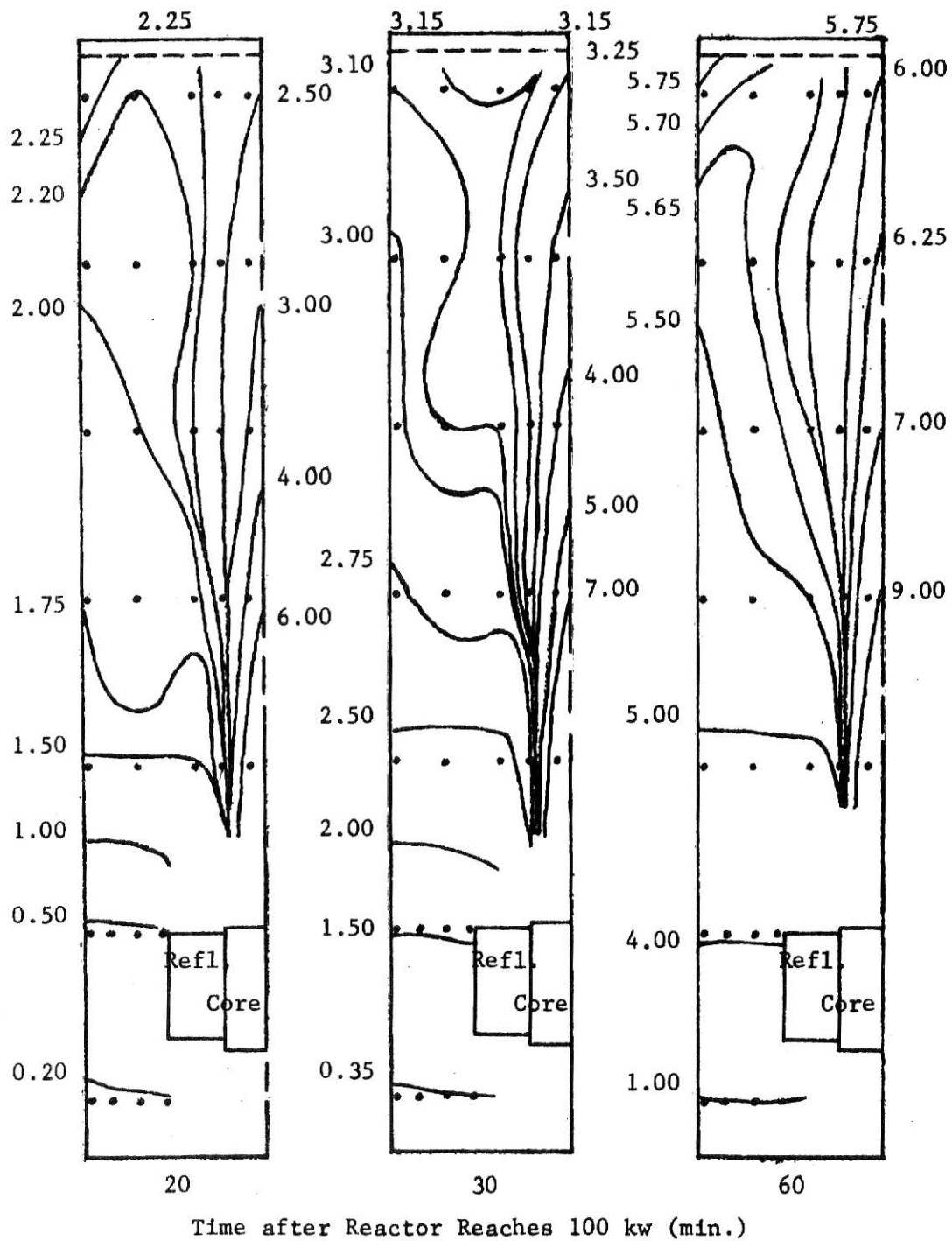


Figure E.3 Temperature Distribution in the Reactor Pool during 100 kw Steady-State Operation (isothermal lines in degrees C above ambient)

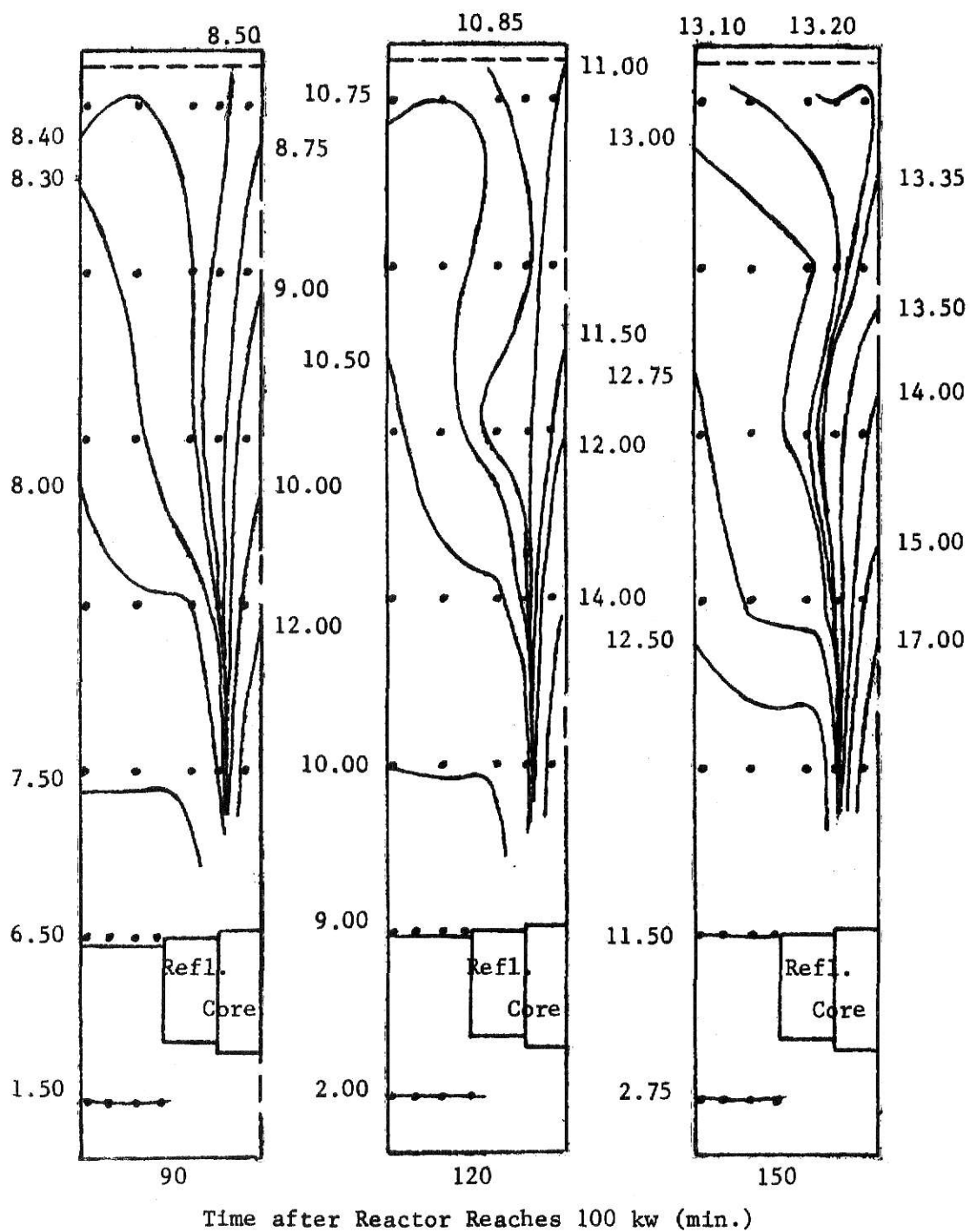


Figure E.4 Temperature Distribution in the Reactor Pool during 100 kw Steady-State Operation (isothermal lines in degrees C above ambient)

From the much less steep gradient at the top of the pool it appears the water from the column is becoming more well mixed after it reaches the surface of the water. After ten minutes the outer edge of the column at the top of the pool is no longer well defined. Also another stage in the flow has started.

The warmed water is being forced down the outside of the established central chimney. The flow of the water, after mixing and flowing fairly randomly at the top the pool, once again becomes well established. This time the direction of flow is opposite to the flow in the chimney. The temperature gradient in the direction of flow in the downward flowing water is much less than in the chimney. Also the radial temperature gradient is almost flat.

As time progresses the chimney remains and the flow down the sides continues. Once this pattern is established it appears most of the water in the pool is heating at approximately the same rate.

The obvious exception to this constant heating is the region below the core. Even after three hours this region is heating more slowly than the rest of the pool. It appears that the suction created by the water rising through the core pulls the downward flowing water into the core as soon as it passes the reflector. Thus less warmed water is available for heating the water below the core.

Simultaneously with the mass transfer process, heat is being conducted throughout the pool. In most cases it is not obvious because the mass transport process is occurring more rapidly than the conduction. It is obvious heat is being conducted out of the chimney because the temperature gradient at the outer edge of the chimney becomes less pronounced with time.

There is certainly some heat lost at the boundaries of the pool. However because of the construction of the pool these losses are small. The trapped air pocket between the pool surface and the pool covers provides

a good insulator. The contact resistance between the metal can and the concrete shielding provides a better insulator than if the pool had been constructed of concrete only. After a long enough period of time, as the temperatures in the pool become appreciably larger than the ambient air temperature, these heat losses become significant.

The observations made from the data from this experiment are used to construct a model of the heat flow in the pool. This development is in Section 3 of this paper.

Appendix F

POWCAL

```

C
C   POWCAL ACCOMPLISHES A LEAST SQUARES ANALYSIS OF POWER
C   CALIBRATION DATA. THE RESULTS ARE TEMPERATURE GRADIENT,
C   ACTUAL POWER, AND ASSOCIATED STATISTICS.
C
1   DIMENSION X(200),Y(200),T(200)
C
C   READ IN TOTAL HEAT CAPACITY DATA
C
C   THC IS THE TOTAL HEAT CAPACITY IN KWHR/DEG C
C   SDTHC IS THE STD DEV OF THE HEAT CAPACITY IN KWHR/DEG C
C
2   READ(5,1)THC,SDTHC
3   1 FORMAT(2F7.4)
C
C   READ IN TEMPERATURE GRADIENT DATA
C
C   IDATE AND NP ARE DATA SET IDENTIFICATION
C   NT IS THE NUMBER OF DATA POINTS
C   TO IS THE AMBIENT TEMPERATURE
C   TMO IS THE TIME FOR THE FIRST DATA POINT
C   DELTM IS THE TIME INTERVAL BETWEEN DATA
C   TMS IS THE TIME THE ASYMPTOTIC SLOPE STARTS
C   TME IS THE TIME THE ASYMPTOTIC SLOPE ENDS
C   T(N) IS THE NTH TEMPERATURE (NOTE, ENTER 999 FOR ANY
C   TEMPERATURE DATA MISSING OR CONSIDERED BAD)
C   TEMPERATURES ARE IN DEGRES CENTIGRAD AND TIMES ARE IN
C   MINUTES
C
4   51 READ(5,2)IDATE,NP,NT,TO,TMO,DELT,M,TMS,TME
5   2 FORMAT(A4,I3,I4,F6.2,F7.2,F7.4,2F7.2)
6   IF(NP.EQ.0) GO TO 50
7   ASSIGN 61 TO KANSAS
8   READ(5,3)(T(N),N=1,NT)
9   3 FORMAT(16F5.2)
10  WRITE(6,4)IDATE,NP
11  4 FORMAT(1H1////////15X,'LEAST SQUARE FIT TO POWER CALIBRATION DATA'/
11  1/5X,23X,'DATE',2X,A4,5X,'PROBE NO. -',I2//)
C
C   REDUCE DATA
C
12  DO 6 N=1,NT
13  Y(N)=T(N)-TO
14  X(N)=TMO+DELT*M*(N-1)
15  GO TO KANSAS, (61,62,6)
16  61 IF(X(N).LT.TMS) GO TO 6
17  NS = N
18  ASSIGN 62 TO KANSAS
19  62 IF(X(N).GT.TME) GO TO 63
20  GO TO 6
21  63 NE = N-1
22  ASSIGN 6 TO KANSAS
23  6 CONTINUE
C
C   INITIALIZE WORKING PARAMETERS
C
24  SXY=0.0
25  SX1=0.0
26  SX2=0.0

```

```

27      SY1=0.0
28      SY2=0.0
      C
      C      COMPUTE ASYMPTOTIC SLOPE
      C      X(N) IS THE TIME IN MINUTES AND Y(N) IS THE CORRESPONDING
      C      TEMPERATURE RISE IN DEGREES CENTIGRAD
      C
29      L = 0
30      DO 10 N=NS,NE
31      TEST = T(N)
32      IF (TEST.GT.99.0) GO TO 10
33      L = L+1
34      SX1=SX1+X(N)
35      SX2=SX2+X(N)*X(N)
36      SY1=SY1+Y(N)
37      SY2=SY2+Y(N)*Y(N)
38      SXY=SXY+X(N)*Y(N)
39      10 CONTINUE
40      SDELS=0.0
      C
      C      B IS THE SLOPE
      C      C IS THE INTERCEPT
      C      SIGY IS THE CONDITIONAL STANDARD DEVIATION
      C      SIGB IS THE STANDARD DEVIATION OF THE SLOPE
      C
41      D = L*SX2-SX1*SX1
42      B=(L*SXY-SX1*SY1)/D
43      C=(SX2*SY1-SX1*SXY)/D
44      DO 12 I=NS,NE
45      TEST = T(I)
46      IF (TEST.GT.99.0) GO TO 12
47      DEL=Y(I)-C-B*X(I)
48      DELS=DEL*DEL
49      SDELS=SDELS+DEL*DEL
50      12 CONTINUE
51      SIGY=SQRT(SDELS/(N-2))
52      BB=L/D
53      SIGB=(SQRT(BB))*SIGY
      C
      C      COMPUTE ACTUAL POWER AND PRINT RESULTS
      C
54      P = B*THC*60.0
55      PP = 3600.0*THC*THC*SIGB*SIGB+SDTHC*SDTHC*3600.0*B*B
56      SIGP = SQRT(PP)
57      WRITE(6,13) L,B,SIGY,SIGB,THC,SDTHC,P,SIGP
58      13 FORMAT(1H,5X,'TEMPERATURE GRADIENT INFORMATION'//10X,
1'NUMBER OF DATA POINTS ON ASYMPTOTE',2X,'-',2X,I3/10X,
2'ASYMPTOTIC SLOPE',6X,'-',2X,1PE11.3,5X,'DEG. C/MIN.'//10X,
3'CONDITIONAL STD. DEV.',2X,'-',2X,1PE11.3,5X,'DEG. C'/10X,
4'STD. DEV. OF SLOPE',5X,'-',2X,1PE11.3,5X,'DEG.C/MIN.'//5X,
5'TOTAL HEAT CAPACITY INFORMATION'//10X,
6'TOTAL HEAT CAPACITY',9X,'-',2X,1PE11.3,5X,'KWHR/DEG. C'/10X,
7'STD. DEV. OF HEAT CAPACITY',2X,'-',2X,L11.3,5X,'KWHR/DEG. C'//5X,
8'POWER INFORMATION'//10X,
9'ACTUAL POWER',8X,'-',2X,1PE11.3,5X,'KW'/10X,
A'STD. DEV. OF POWER',2X,'-',2X,1PE11.3,5X,'KW')
      C
      C      PRINT DATA
      C
59      WRITE(6,14) IDATE,NP

```

```

60      14 FORMAT(1H1,15X,'LEAST SQUARE FIT TO POWER CALIBRATION DATA'//5X,
        123X,'DATE',2X,A4,5X,'PROBE NO. ',12//
        233X,'DATA'//15X,'POINT',5X,'TIME',5X,'TEMPERATURE'/
        315X,' NO. ',17X,'RISE'//)
61      DO 20 I=1,NT
62      IF(I.EQ.NS) GO TO 25
63      GO TO 26
64      25 WRITE(6,15)
65      15 FORMAT(1HJ,14X,'START ASYMPTOTIC DATA'//)
66      26 IF(I.EQ.NE) GO TO 27
67      GO TO 21
68      27 WRITE(6,5)I, X(I),Y(I)
69      WRITE(6,16)
70      16 FORMAT(1HJ,14X,'END ASYMPTOTIC DATA'//)
71      GO TO 20
72      21 WRITE(6,5)I, X(I),Y(I)
73      5 FORMAT(1H ,14X,I3,6X,F6.2,6X,F5.2)
74      20 CONTINUE
C
C      START NEXT DATA SET
C      NOTE, END DATA WITH BLANK CARD
C
75      GO TO 51
76      50 WRITE(6,30)
77      30 FORMAT(1H1)
78      STOP
79      END

```

CALORIMETRIC POWER CALIBRATION AND SOURCE EFFECTS IN
THE KANSAS STATE UNIVERSITY TRIGA MARK II NUCLEAR REACTOR

by

EDWARD ALBERT HECKMAN, JR.

B.S., Pennsylvania State University, 1966

AN ABSTRACT OF A MASTER'S THESIS

submitted in partial fulfillment of the

requirements for the degree

MASTER OF SCIENCE

Department of Nuclear Engineering

KANSAS STATE UNIVERSITY
Manhattan, Kansas

1973

ABSTRACT

A study of two facets in the operation of the Kansas State University Triga Mark II nuclear reactor is undertaken. The first study involves the calorimetric power calibration of the reactor. The second study deals with kinetic effects of the removable neutron source.

In the calibration study a mathematical model of the heating in the reactor is developed. The model predicts the heat transfer out of the fuel and into the coolant and thus the temperature and heat content of the coolant leaving the core during 100 kw steady-state operation. An experimental mapping of the temperature profiles in the pool during 100 kw steady-state operation is utilized to calibrate the model. The transient temperatures throughout the fuel, cladding and coolant during 100 kw steady-state operation are then predicted. The model shows that after a period of stabilization the majority of the pool water is heating at a constant rate and leads to the possibility of determining the operating power from this asymptotic temperature gradient. A calorimetry type technique, where the power is determined from the temperature gradient and total heat capacity, is shown to be an applicable procedure for determining the reactor operating power.

A sophisticated system for measuring the temperature gradient utilizing thermistors is developed. Operating procedures for the temperature gradient measuring system are tested and formalized. A "best" region of the pool in which to measure the temperature gradient for a power calibration experiment is defined as 6 to 18 inches from the outer radius of the pool and 5 to 15 feet from the bottom of the pool. Using the procedure developed the asymptotic temperature gradient is easily and precisely measured.

The latter study involves simulating the transient neutronic response with the point reactor kinetics equation and an analog network. The removable concentrated neutron source is separated into two components; an equivalent homogeneous source and a uniform poison. The source worth as a poison is experimentally determined to be -4.75 ± 0.37 cents of reactivity. The equivalent source strength is experimentally determined to be 0.256 ± 0.007 watts/second. At higher power levels the effect of the source is predominantly that of a poison. At low power levels the effect of the source is predominantly that of a source of neutrons. The analog simulation predicts the two effects nullify each other at a reactor power of 0.083 watts. Thus the configuration required to achieve steady-state operation at 0.083 watts with the source present is equivalent to the critical configuration with the source not present.